

คุณลักษณะและสมบัติในการเร่งปฏิกิริยาของตัวเร่งปฏิกิริยา Pd/TiO₂ ขนาดนาโน
ที่เตรียมโดยวิธีเฟลมสเปรย์ไฟโรไลซิส



นายทรงพล โพธาขวัญประชา

วิทยานิพนธ์นี้เป็นส่วนหนึ่งของการศึกษาตามหลักสูตรปริญญาวิทยาศาสตรมหาบัณฑิต

สาขาวิชาวิศวกรรมเคมี ภาควิชาวิศวกรรมเคมี

คณะวิศวกรรมศาสตร์ จุฬาลงกรณ์มหาวิทยาลัย

ปีการศึกษา 2550

ลิขสิทธิ์ของจุฬาลงกรณ์มหาวิทยาลัย

CHARACTERISTICS AND CATALYTIC PROPERTIES OF NANO-Pd/TiO₂
CATALYST PREPARED BY FLAME SPRAY PYROLYSIS



Mr. Songphon Phothakwanpracha

A Thesis Submitted in Partial Fulfillment of the Requirements
for the Degree of Master of Engineering Program in Chemical Engineering
Department of Chemical Engineering

Faculty of Engineering
Chulalongkorn University

Academic Year 2007

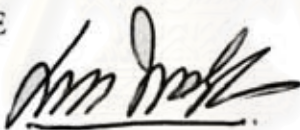
Copyright of Chulalongkorn University

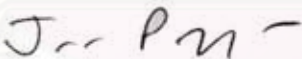
Thesis Title CHARACTERISTICS AND CATALYTIC PROPERTIES OF
 NANO-Pd/TiO₂ CATALYST PREPARED BY FLAME
 SPRAY PYROLYSIS
By Mr. Songphon Phothakwanpracha
Field of study Chemical Engineering
Thesis Advisor Assistant Professor Joongjai Panpranot, Ph.D.
Thesis Co-Advisor Assistant Professor Okorn Mekasuwandamrong, Ph.D.

Accepted by the Faculty of Engineering, Chulalongkorn University in Partial
Fulfillment of the Requirements for the Master's Degree



..... Dean of the Faculty of Engineering
(Associate Professor Boonsom Lerdkhirunwong, Dr.Ing)

THESIS COMMITTEE


..... Chairman
(Associate Professor ML. Supakanok Thongyai, Ph.D.)


..... Thesis Advisor
(Assistant Professor Joongjai Panpranot, Ph.D.)


..... Thesis Co-Advisor
(Assistant Professor Okorn Mekasuwandamrong, Ph.D.)


..... Member
(Assistant Professor Bunjerd Jongsomjit, Ph.D.)


..... External Member
(Assistant Professor Worapon Kiatkittipong, Ph.D.)

ทรงพล โพธาขวัญประชา: คุณสมบัติและสมบัติในการเร่งปฏิกิริยาของตัวเร่งปฏิกิริยา Pd/TiO₂ ขนาดนาโน ที่เตรียมโดยวิธีเฟลมสเปรย์ไพโรไลซิส (CHARACTERISTICS AND CATALYTIC PROPERTIES OF NANO-Pd/TiO₂ CATALYST PREPARED BY FLAME SPRAY PYROLYSIS) อ. ที่ปรึกษา: ผศ. ดร. จุงใจ ปั้นประณต, อ. ที่ปรึกษาร่วม: ผศ. ดร. โอกร เมฆาสุวรรณดำรง, 116 หน้า

งานวิจัยนี้ศึกษาคุณสมบัติและสมบัติของตัวเร่งปฏิกิริยาแพลเลเดียมบนไทเทเนียมไดออกไซด์ขนาดนาโนที่สังเคราะห์ในขั้นตอนเดียวโดยวิธีเฟลมสเปรย์ไพโรไลซิสที่มีปริมาณแพลเลเดียม 0.5-10 เปอร์เซ็นต์โดยน้ำหนัก และขนาดไทเทเนียมไดออกไซด์ต่างๆ กันในช่วง 9.7-24.6 นาโนเมตร โดยทำการเปรียบเทียบกับตัวเร่งปฏิกิริยาแพลเลเดียมบนไทเทเนียมไดออกไซด์ที่เตรียมโดยวิธีการเคลือบฝั่ม และไทเทเนียมไดออกไซด์ทางการค้า จากการวิเคราะห์ด้วยเครื่องกระเจิงรังสีเอ็กซ์ กล้องจุลทรรศน์อิเล็กตรอนแบบส่องผ่าน การดูดซับด้วยแก๊สไนโตรเจนและคาร์บอนมอนอกไซด์ และเอ็กซ์เรย์โฟโตอิเล็กตรอนสเปกโทรสโกปี พบว่าเมื่อเพิ่มปริมาณแพลเลเดียมในระหว่างการเตรียมด้วยวิธีเฟลมสเปรย์ไพโรไลซิสขนาดผลึกของไทเทเนียมไดออกไซด์ลดลงและมีปริมาณของเฟสรูไทล์ต่ออนุภาคสูงขึ้น แสดงว่าแพลเลเดียมยับยั้งการโตของผลึกไทเทเนียมไดออกไซด์ในระหว่างการสังเคราะห์ด้วยวิธีเฟลมสเปรย์ไพโรไลซิส นอกจากนี้ตัวเร่งปฏิกิริยาที่เตรียมในขั้นตอนเดียวพบปริมาณแพลเลเดียมที่พื้นผิวน้อยกว่าตัวเร่งปฏิกิริยาที่เตรียมโดยวิธีการเคลือบฝั่มมาก ซึ่งอาจเกิดจากการที่แพลเลเดียมถูกปกคลุมด้วยชั้นของไทเทเนียมไดออกไซด์ อย่างไรก็ตามเมื่อนำไปทดสอบในปฏิกิริยาไฮโดรจิเนชันของ 1-เฮปไทน์ ในวัฏภาคของเหลวพบว่าที่ปริมาณแพลเลเดียมเท่ากันตัวเร่งปฏิกิริยาแพลเลเดียมบนไทเทเนียมไดออกไซด์ที่สังเคราะห์โดยวิธีเฟลมสเปรย์ไพโรไลซิสในขั้นตอนเดียวให้ค่าความว่องไว (TOF) สูงกว่าโดยไม่มีความแตกต่างของค่าการเลือกเกิดของ 1-เฮปทีน และค่า TOF ลดลงเมื่อปริมาณแพลเลเดียมเพิ่มขึ้น เมื่อเปรียบเทียบกับตัวเร่งปฏิกิริยาที่เตรียมบนไทเทเนียมไดออกไซด์ขนาดต่างๆ พบว่าค่า TOF ของตัวเร่งปฏิกิริยาที่เตรียมโดยวิธีเฟลมสเปรย์ลดลงจาก 102-23 ต่อวินาที เมื่อขนาดไทเทเนียมไดออกไซด์เพิ่มขึ้นจาก 9.7 เป็น 24.6 นาโนเมตร ในขณะที่ตัวเร่งปฏิกิริยาที่เตรียมโดยวิธีการเคลือบฝั่ม และตัวเร่งปฏิกิริยาบนไทเทเนียมไดออกไซด์ทางการค้าให้ค่า TOF ใกล้เคียงกันประมาณ 6-12 ต่อวินาที ทั้งนี้แสดงว่า การเตรียมตัวเร่งปฏิกิริยาในขั้นตอนเดียวโดยวิธีเฟลมสเปรย์ไพโรไลซิสทำให้สมบัติในการเร่งปฏิกิริยาของตัวเร่งปฏิกิริยาแพลเลเดียมเปลี่ยนแปลงไปโดยมีค่าสูงขึ้น โดยจะส่งผลกระทบต่อปริมาณแพลเลเดียมต่ำ และผลึกไทเทเนียมไดออกไซด์ขนาดเล็ก

ภาควิชา วิศวกรรมเคมี ลายมือชื่อนิสิต ทรงพล โพธาขวัญประชา
 สาขาวิชา วิศวกรรมเคมี ลายมือชื่ออาจารย์ที่ปรึกษา ผศ. ดร. จุงใจ ปั้นประณต
 ปีการศึกษา 2550 ลายมือชื่ออาจารย์ที่ปรึกษาร่วม โอกร เมฆาสุวรรณดำรง

4970331121: MAJOR CHEMICAL ENGINEERING

KEYWORDS: FLAME SPRAY PYROLYSIS / TITANIA SUPPORTED
PALLADIUM CATALYSTS / LIQUID-PHASE HYDROGENATION /
1-HEPTYNE HYDROGENATION

SONGPHON PHOTHAKWANPRACHA: CHARACTERISTICS AND
CATALYTIC PROPERTIES OF NANO-Pd/TiO₂ CATALYST PREPARED
BY FLAME SPRAY PYROLYSIS THISIS ADVISOR: ASST. PROF.
JOONGJAI PANPRANOT Ph.D., THESIS CO-ADVISOR : ASST. PROF.
OKORN MEKASUWANDUMRONG Ph.D., 116 pp.

The characteristics and catalytic properties of nano-Pd/TiO₂ catalysts prepared by one-step flame spray pyrolysis with various Pd loadings 0.5-10 wt% and various TiO₂ crystallite sizes of 9.7 to 24.6 nm were studied. Pd/TiO₂ catalysts prepared by impregnation method and commercial TiO₂ were used for comparison. Based on characterization results from various techniques such as XRD, TEM, N₂ physisorption, CO-pulse chemisorption, and XPS, addition of Pd during one-step flame spray synthesis of Pd/TiO₂ catalysts resulted in smaller crystallite size of TiO₂ and higher amount of rutile phase in the TiO₂. It is indicated that Pd particles inhibited the crystal growth of TiO₂ during the flame spray synthesis. Moreover, the single-step flame spray catalysts had much lower amount of Pd on surface than those prepared by conventional impregnation method: this was probably due to that Pd particles were covered by Ti-O groups. However, for a similar Pd loading, the FSP-derived Pd/TiO₂ catalysts exhibited higher specific activities (TOF) than the impregnated ones in liquid-phase hydrogenation of 1-heptyne with no difference in 1-heptene selectivity. However, the TOFs decreased with increasing amount of Pd loading. The TOFs of FSP-Pd/TiO₂ catalysts also decreased from 102-23 s⁻¹ when TiO₂ crystallite size increased from 9.7 to 24.6 nm whereas the impregnated catalysts and the catalysts prepared on commercial TiO₂ exhibited similar TOF of around 6-12 s⁻¹. It is considered that the single-step flame spray pyrolysis modified and improved the catalytic properties of Pd/TiO₂ catalysts especially when the catalysts were prepared with low Pd loading and small TiO₂ crystallite size.

Department Chemical Engineering. Student's signature *Songphon Phothakwanpracha*
Field of Study .. Chemical Engineering Advisor's signature *Jongjai Panpranot*
Academic year 2007 Co-advisor's signature *Okorn Mekasuwandumrong*

ACKNOWLEDGEMENTS

The author would like to express his greatest gratitude to his advisor, Associate Professor Joongjai Panpranot, and co-advisor, Assistant Professor Okorn Mekasuwamdamong from Department of Chemical Engineering, Silpakorn University, for their invaluable suggestion and guidance throughout this study. In addition, I would also grateful to thank to Associate Professor ML. Supakanok Thongyai who has been the chairman of the committee for this thesis, Associate Professor Bunjerd Jongsomjit and Assistant Professor Worapon Kiatkittipong, members of the thesis committee for their kind cooperation.

Most of all, the author would like to express his highest gratitude to his parents, Mr.Sompong and Mrs.Nattawan Phothakwanpracha who always pay attention to his all the times for suggestion and encouragement. The most success of graduation is devoted to my parents.

Moreover, the author wishes to thank all my friends, especially Mr.Tanakorn Suksri and all members of the Center of Excellent on Catalysis & Catalytic Reaction Engineering (Petrochemical Engineering Research Laboratory), Department of Chemical Engineering, Chulalongkorn University for their assistance and friendly encouragement.

Finally, the author would like to thank the Thailand Research Fund (TRF), as well as the Graduate School of Chulalongkorn University for their financial supports.

CONTENTS

	Page
ABSTRACT (IN THAI)	iv
ABSTRACT (IN ENGLISH)	v
ACKNOWLEDGMENTS	vi
CONTENTS	vii
LIST OF TABLES	x
LIST OF FIGURES	xii
CHAPTER	
I INTRODUCTION	1
II THEORY	5
2.1 Flame Spray Pyrolysis (FSP)	5
2.2 Liquid-Phase Hydrogenation	7
2.3 Hydrogenation of Alkynes	8
2.4 Palladium-Based Catalysts	9
2.4 Titanium (IV) Oxide.....	9
III LITERATURE REVIEWS	14
3.1 Flame Spray Pyrolysis (FSP)	14
3.2 Role of Titania in the Selective Hydrogenation on Pd Catalysts.	22
3.3 Comments on the previous studies	23
IV EXPERIMENTAL	25
4.1 Catalyst Preparation	25
4.1.1 Materials	25
4.1.2 Synthesis of Flame-Made TiO ₂ supports and Pd/TiO ₂ Catalysts (Part I-study).....	25
4.1.3 Synthesis of Flame-Made Pd/TiO ₂ Catalysts with Various Crystalline Sizes (Part II-study).....	26
4.1.4 Palladium Loading by Incipient Wetness Impregnation Method.....	27

CHAPTER

4.2	The Reaction Study in Liquid-Phase Hydrogenation	27
4.2.1	Chemicals and Reagents	27
4.2.2	Instrument and Apparatus	28
4.2.3	Liquid-Phase Hydrogenation Procedure	29
4.3	Catalyst Characterization	29
4.3.1	Atomic Absorption Spectroscopy (AAS)	29
4.3.2	N ₂ Physisorption	29
4.3.3	X-ray Diffraction (XRD)	30
4.3.4	Transmission Electron Microscopy (TEM)	30
4.3.5	CO-Pulse Chemisorption	30
4.3.6	X-ray Photoelectron Spectroscopy (XPS)	31
4.4	Catalyst Nomenclature	31
V	RESULTS AND DISCUSSIONS	32
5.1	The Effect of Palladium Loading on the Properties of Pd/TiO ₂ Catalysts	32
5.1.1	Characterization of the Catalysts	32
5.1.1.1	X-ray Diffraction (XRD).....	32
5.1.1.2	Transmission Electron Microscopy	35
5.1.1.3	N ₂ Physisorption.....	46
5.1.1.4	CO-Pulse Chemisorptions	52
5.1.1.5	X-ray Photoelectron Spectroscopy	54
5.1.2	Selective 1-Heptyne Hydrogenation Study.....	58
5.2	The Effects of TiO ₂ Crystallite Size on the Properties of Pd/TiO ₂ Catalysts	65
5.2.1	Characterization of the Catalysts	65
5.2.1.1	X-ray Diffraction (XRD).....	65
5.2.1.2	Transmission Electron Microscopy	69
5.2.1.3	N ₂ Physisorption.....	80
5.2.1.4	CO-Pulse Chemisorptions	85
5.2.1.5	X-ray Photoelectron Spectroscopy.....	86

CHAPTER

5.2.2 Selective 1-Heptyne Hydrogenation Study.....	90
VI CONCLUSIONS AND RECOMMENDATIONS	97
6.1 Conclusions	97
6.2 Recommendations	98
REFERENCES	99
APENDICES	103
APPENDIX A: CALCULATION FOR CATALYST PREPARATION ..	104
APPENDIX B: CALCULATION FOR METAL ACTIVE SITES AND DISPERSION	107
APPENDIX C: CALIBRATION CURVES	108
APPENDIX D: CALCULATION OF 1-HEPYNE CONVERSION AND 1-HEPTENE SELECTIVITY.....	111
APPENDIX E: CALCULATION OF RUTILE PHASE COMPOSITION.....	113
APPENDIX F: CALCULATION OF TURNOVER OF FREQUENCY ..	114
APPENDIX G: LIST OF PUBLICATION	115
VITA	116

LIST OF TABLES

TABLE	Page
2.1	Crystallographic properties of anatase, brookite, and rutile 10
3.1	Example of oxide/mixed-oxides obtained from flame spray pyrolysis method. 20
3.2	Example of metal loaded catalysts obtained from flame spray pyrolysis method 21
4.1	Chemicals used in the synthesis of flame-made catalysts 25
4.2	Commercial TiO ₂ used for the synthesis of Pd/TiO ₂ reference catalysts..... 25
4.3	Preparation conditions of the flame-made Pd/TiO ₂ catalysts with various crystalline sizes 27
4.4	The chemicals and reagents used in the reaction 28
4.5	Operating condition for gas chromatograph 28
5.1	XRD analysis results and TiO ₂ phase composition of various Pd loading of flame-made and impregnated catalysts 34
5.2	Primary particle size of TiO ₂ and Pd/PdO from TEM micrographs of flame-made and impregnated catalysts with various Pd loading 37
5.3	N ₂ physisorption properties of flame-made and impregnated catalysts with various Pd loading..... 47
5.4	The amounts of CO chemisorption of flame-made and impregnated catalysts with of various Pd loading 54
5.5	Binding energies and surface composition from XPS of flame-made and impregnated catalysts with various Pd loading 57
5.6	Specific activity (TOFs, s ⁻¹) on the various Pd loading flame-made and impregnated catalysts..... 60

TABLE

Page

5.7	XRD analysis results and phase composition of flame-made and impregnated catalysts with various TiO ₂ crystallite sizes	67
5.8	Primary particle size of TiO ₂ and Pd/PdO from TEM micrographs of flame-made and impregnated catalysts with on various TiO ₂ crystallite sizes	70
5.9	N ₂ physisorption properties of the flame and impregnated-made 5 wt% Pd/TiO ₂ catalysts with various TiO ₂ crystallite sizes	81
5.10	The amounts of CO chemisorption of flame-made and impregnated catalysts with various TiO ₂ crystallite size.....	86
5.11	Binding energies and surface composition from XPS on various crystallite sizes of flame-made and impregnated catalysts.....	89
5.12	Specific activity (TOFs, s ⁻¹) on the various TiO ₂ crystallite size flame-made and impregnated catalysts.....	91
C.1	Conditions uses in Shimadzu modal GC-14B	109

LIST OF FIGURES

FIGURE		Page
2.1	Skecth of the flame spray pyrolysis unit.....	5
2.2	Experimental set-up for Pd/TiO ₂ catalyts synthesis by flame spray pyrolysis	7
2.3	Free-energy diagrams for the hydrogenation of an alkene in the presence of a catalyst and the hypothetical reaction in the absence of a catalyst.....	8
2.4	Crystal structure of TiO ₂	11
5.1	XRD patterns of the flame-made Pd/TiO ₂ catalyts with Pd loading between 0.5 and 10 wt%	33
5.2	XRD patterns of all impregnated Pd/TiO ₂ catalyts with Pd loading 1-5 wt% after reduction in H ₂ at 30°C for 2 h.....	35
5.3	TEM micrographs of 0.5 wt% Pd/TiO ₂ catalyts prepared by single-step flame synthesis (0.5FSP)	38
5.4	TEM micrographs of 1 wt% Pd/TiO ₂ catalyts prepared by single-step flame synthesis (1FSP)	39
5.5	TEM micrographs of 2 wt% Pd/TiO ₂ catalyts prepared by single-step flame synthesis (2FSP)	40
5.6	TEM micrographs of 5 wt% Pd/TiO ₂ catalyts prepared by single-step flame synthesis (5FSP)	41
5.7	TEM micrographs of 10 wt% Pd/TiO ₂ catalyts prepared by single-step flame synthesis (10FSP)	42
5.8	TEM micrographs of 1 wt% Pd/TiO ₂ prepared by incipient wetness impregnation with flame-made TiO ₂ supports (1Im-FSP)	43
5.9	TEM micrographs of 2 wt% Pd/TiO ₂ prepared by incipient wetness impregnation with flame-made TiO ₂ supports (2Im-FSP).....	44
5.10	TEM micrographs of 5 wt% Pd/TiO ₂ prepared by incipient wetness impregnation with flame-made TiO ₂ supports (5Im-FSP)	45

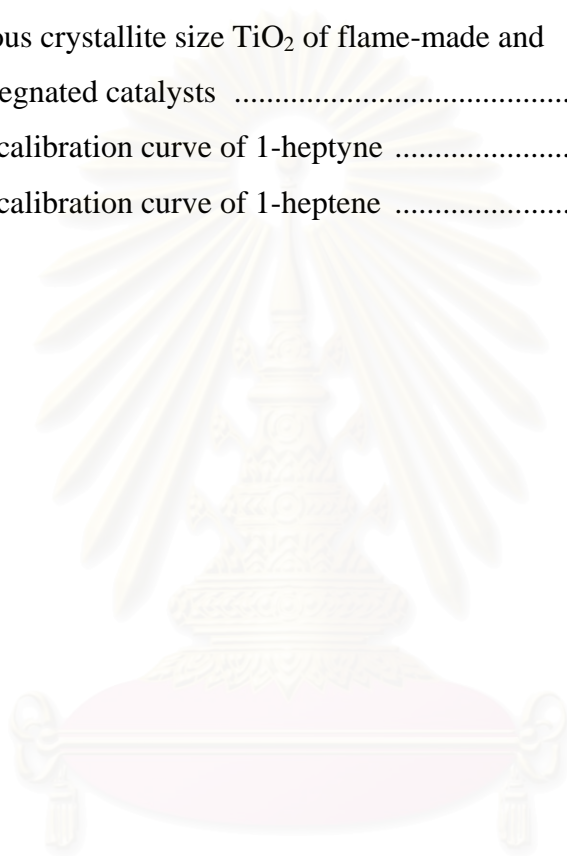
FIGURE	Page
5.11 N ₂ adsorption – desorption isotherms of TiO ₂ FSP (26 nm)	48
5.12 N ₂ adsorption – desorption isotherms of 0.5 wt% Pd/TiO ₂ catalysts prepared by single-step flame synthesis (0.5FSP)	48
5.13 N ₂ adsorption – desorption isotherms of 1 wt% Pd/TiO ₂ catalysts prepared by single-step flame synthesis (1FSP)	49
5.14 N ₂ adsorption – desorption isotherms of 2 wt% Pd/TiO ₂ catalysts prepared by single-step flame synthesis (2FSP)	49
5.15 N ₂ adsorption – desorption isotherms of 5 wt% Pd/TiO ₂ catalysts prepared by single-step flame synthesis (5FSP)	50
5.16 N ₂ adsorption – desorption isotherms of 10 wt% Pd/TiO ₂ catalysts prepared by single-step flame synthesis (10FSP)	50
5.17 N ₂ adsorption – desorption isotherms of 1 wt% Pd/TiO ₂ prepared by incipient wetness impregnation with flame-made TiO ₂ supports (1Im-FSP)	51
5.18 N ₂ adsorption – desorption isotherms of 2 wt% Pd/TiO ₂ prepared by incipient wetness impregnation with flame-made TiO ₂ supports (2Im-FSP)	51
5.19 N ₂ adsorption – desorption isotherms of 5 wt% Pd/TiO ₂ prepared by incipient wetness impregnation with flame-made TiO ₂ supports (5Im-FSP)	52
5.20 Binding energies of various Pd loading flame-made catalysts	56
5.21 Binding energies of various Pd loading impregnated catalysts	56
5.22 Suggested model for Pd/TiO ₂	57
5.23 Time on stream with concentration of 1-heptyne on flame-made Pd/TiO ₂ catalysts prepared in single-step with Pd loading 0.5, 1, 2, 5, and 10 wt%	60
5.24 Time on stream with concentration of 1-heptene on flame-made Pd/TiO ₂ catalysts prepared in single-step with Pd loading 0.5, 1, 2, 5, and 10 wt%	61

FIGURE	Page
5.25 Time on stream with concentration of 1-heptane on flame-made Pd/TiO ₂ catalysts prepared in single-step with Pd loading 0.5, 1, 2, 5, and 10 wt%	61
5.26 Time on stream with concentration of 1-heptyne on Pd catalysts prepared on flame-made TiO ₂ supports by incipient wetness impregnation with Pd loading 1, 2, and 5 wt%....	62
5.27 Time on stream with concentration of 1-heptene on Pd catalysts prepared on flame-made TiO ₂ supports by incipient wetness impregnation with Pd loading 1, 2, and 5 wt% ...	62
5.28 Time on stream with concentration of 1-heptane on Pd catalysts prepared on flame-made TiO ₂ supports by incipient wetness impregnation with Pd loading 1, 2, and 5 wt% ...	63
5.29 Time on stream with concentration of 1-heptyne on various Pd loading of flame-made and impregnated catalysts	63
5.30 Time on stream with concentration of 1-heptene on various Pd loading of flame-made and impregnated catalysts	64
5.31 Time on stream with concentration of 1-heptane on various Pd loading of flame-made and impregnated catalysts	64
5.32 XRD patterns of 5 wt% Pd/TiO ₂ catalysts prepared by single-step flame synthesis with average crystallite sizes of 9.7, 15.7, and 24.6 nm	65
5.33 XRD patterns of 5 wt% Pd/TiO ₂ catalysts prepared by incipient wetness impregnation with flame-made TiO ₂ supports average crystallite sizes of 9.8, 15, and 26 nm after reduction in H ₂ at 30°C for 2 h.....	68
5.34 TEM micrographs of 5 wt% Pd/TiO ₂ catalysts prepared by single-step flame synthesis with average crystallite sizes of 9.7 nm (5FSP-9.7)	71
5.35 TEM micrographs of 5 wt% Pd/TiO ₂ catalysts prepared by single-step flame synthesis with average crystallite sizes of 15.7 nm (5FSP-15.7)	72

FIGURE	Page
5.36 TEM micrographs of 5 wt% Pd/TiO ₂ catalysts prepared by single-step flame synthesis with average crystallite sizes of 24.6 nm (5FSP-24.6)	73
5.37 TEM micrographs of 5 wt% Pd/TiO ₂ catalysts prepared by incipient wetness impregnation with flame-made TiO ₂ supports average crystallite sizes of 9.8 nm (5Im-FSP-9.8).....	74
5.38 TEM micrographs of 5 wt% Pd/TiO ₂ catalysts prepared by incipient wetness impregnation with flame-made TiO ₂ supports average crystallite sizes of 15 nm (5Im-FSP-15).....	75
5.39 TEM micrographs of 5 wt% Pd/TiO ₂ catalysts prepared by incipient wetness impregnation with flame-made TiO ₂ supports average crystallite sizes of 26 nm (5Im-FSP-26).....	76
5.40 TEM micrographs of references catalysts (5Im-nano)	77
5.41 TEM micrographs of references catalysts (5Im-P25).....	78
5.42 TEM micrographs of references catalysts (5Im-micron).....	79
5.43 N ₂ adsorption – desorption isotherms of 5 wt% Pd/TiO ₂ catalysts prepared by single-step flame synthesis with average crystallite sizes of 9.7 nm (5FSP-9.7)	82
5.44 N ₂ adsorption – desorption isotherms of 5 wt% Pd/TiO ₂ catalysts prepared by single-step flame synthesis with average crystallite sizes of 15.7 nm (5FSP-15.7)	82
5.45 N ₂ adsorption – desorption isotherms of 5 wt% Pd/TiO ₂ catalysts prepared by single-step flame synthesis with average crystallite sizes of 24.6 nm (5FSP-24.6)	83
5.46 N ₂ adsorption – desorption isotherms of 5 wt% Pd/TiO ₂ catalysts prepared by incipient wetness impregnation with flame-made TiO ₂ supports average crystallite sizes of 9.8 nm (5Im-FSP-9.8)	83
5.47 N ₂ adsorption – desorption isotherms of 5 wt% Pd/TiO ₂ catalysts prepared by incipient wetness impregnation with flame-made TiO ₂ supports average crystallite sizes of 15 nm (5Im-FSP-15)	84

FIGURE	Page
5.48 N ₂ adsorption – desorption isotherms of 5 wt% Pd/TiO ₂ catalysts prepared by incipient wetness impregnation with flame-made TiO ₂ supports average crystallite sizes of 26 nm (5Im-FSP-26)	84
5.49 Binding energies of various crystallite size flame-made catalysts	88
5.50 Binding energies of various crystallite size impregnated catalysts	88
5.51 Binding energies of reference catalysts	89
5.52 Time on stream with concentration of 1-heptyne on 5 wt% Pd/TiO ₂ catalysts prepared by single-step flame synthesis with average crystallite sizes of 9.7, 15.7, and 24.6 nm.....	92
5.53 Time on stream with concentration of 1-heptene on 5 wt% Pd/TiO ₂ catalysts prepared by single-step flame synthesis with average crystallite sizes of 9.7, 15.7, and 24.6 nm.....	92
5.54 Time on stream with concentration of 1-heptane on 5 wt% Pd/TiO ₂ catalysts prepared by single-step flame synthesis with average crystallite sizes of 9.7, 15.7, and 24.6 nm.....	93
5.55 Time on stream with concentration of 1-heptyne on 5 wt% Pd/TiO ₂ catalysts prepared by incipient wetness impregnation with flame-made TiO ₂ supports average crystallite sizes of 9.8, 15, and 26 nm.....	93
5.56 Time on stream with concentration of 1-heptene on 5 wt% Pd/TiO ₂ catalysts prepared by incipient wetness impregnation with flame-made TiO ₂ supports average crystallite sizes of 9.8, 15, and 26 nm.....	94
5.57 Time on stream with concentration of 1-heptane on 5 wt% Pd/TiO ₂ catalysts prepared by incipient wetness impregnation with flame-made TiO ₂ supports average crystallite sizes of 9.8, 15, and 26 nm.....	94
5.58 Time on stream with concentration of 1-heptyne on various crystallite size TiO ₂ of flame-made and impregnated catalysts	95

FIGURE		Page
5.59	Time on stream with concentration of 1-heptene on various crystallite size TiO ₂ of flame-made and impregnated catalysts	95
5.60	Time on stream with concentration of 1-heptane on various crystallite size TiO ₂ of flame-made and impregnated catalysts	96
C.1	The calibration curve of 1-heptyne	110
C.2	The calibration curve of 1-heptene	110



สถาบันวิทยบริการ
จุฬาลงกรณ์มหาวิทยาลัย

CHAPTER I

INTRODUCTION

1.1 Rationale

Nanotechnology has become a key area in the development of science and engineering. Nanotechnology basically involves the production and application of materials that have unit sizes of about 10–100 nm. Various methods can be used for preparation of nanoparticles and nanocrystalline metal/metal-oxides including sol-gel, solvothermal, and flame spray pyrolysis methods [1].

Flame synthesis, especially flame spray pyrolysis (FSP) has been used to produce various nanoparticles with good control of particle size and particle crystal structure.

It is employed widely for large-scale manufacture of carbon blacks and ceramic commodities such as fumed silica and titania and to a lesser extent, for specialty chemicals such as zinc oxide and alumina powders [2, 3]. This method can also produce highly pure particles continuously without further subsequent process, for example, drying, calcinations, and milling in the wet chemical processes. The sizes of flame-made particles range from a few to several hundreds nanometers in diameter depending

on process conditions. In this process a flame is used to drive chemical reactions of precursor compounds, resulting in the formation of clusters, which grow to nanometer-sized products by coagulation and sintering [2, 4].

Flame spray pyrolysis, is a relatively new process for one-step synthesis of supported metal catalysts. The conventional technique for preparation of supported metal catalysts involves impregnation of a solution of metal precursor into the supports followed by drying, calcination, and reduction steps in order to obtain the high dispersion of the catalytically active components. Some other techniques for direct deposition of metals onto high surface area supports such as physical or chemical vapor deposition (PVD/CVD) or electrochemical methods are more

complicated and may not be suitable for the preparation of commercial catalysts. Moreover, they include a liquid phase at some stage during the catalyst deposition and make it difficult to obtain the metal particle in nano-scale. Flame spray pyrolysis gives the opportunity to prepare conveniently high surface area supported metal catalysts in a single step at relatively low cost. The applications of supported metal catalysts synthesized via one-step flame spray pyrolysis in catalytic reaction have been reported. For examples, flame-made Pt-Ba/Al₂O₃ and Pt/Ba/Ce_xZr_{1-x}O₂ have been investigated in lean-NO_x storage-reduction [5, 6]. High surface area Ag/ZnO prepared by flame spray pyrolysis has been reported to exhibit high photocatalytic performance in UV-photodegradation of methylene blue [7]. Recently, Baiker et al. successfully applied the FSP method for syntheses of various Al₂O₃ supported noble metal catalysts [8]. The flame-made Pt/Al₂O₃ showed an improved turnover frequency in the hydrogenation of ethyl pyruvate compared to a conventional porous catalyst. The structural differences of the flame-made and conventionally prepared catalysts have often been explained as the reasons for their differences in catalytic behaviors [4].

Supported Pd catalysts are preferred for the selective hydrogenation of alkynes to alkenes. It is one of the most useful, versatile, and environmentally acceptable reaction routes available for organic syntheses. Many products obtained through this kind

of reactions are useful in the synthesis of natural products, such as biologically active compounds. However, the catalysts are usually used with a variety of modifiers to improve reaction selectivity. Metal salts, amines, amine oxides, sulfur compounds, hydroxides and carbon monoxide are among the modifiers used. Several supports have been employed for Pd catalysts including silica, alumina, carbon, and titania. Titania

is of particular interest as a support for Pd catalysts in hydrogenation reactions because

it exhibits a strong metal-support interaction (SMSI) effect. It was found that noble metal supported on reducible oxides such as titania exhibits differences in catalytic activity

and selectivity in hydrogenation reaction when reduced at high temperature, compared with the one reduced at lower temperature or the corresponding noble metal supported

on un-reducible supports. The Pd/TiO₂ catalysts with SMSI were found to exhibit higher selectivities for anatase titnia supported palladium catalyst than rutile titania supported palladium catalyst in selective hydrogenation of long chain alkadienes [9].

To the best of our knowledge, Pd/TiO₂ synthesized by flame spray pyrolysis has never been reported so far. It is thus the aims of this thesis to synthesize Pd/TiO₂ by FSP method and investigate their characteristics and catalytic properties in liquid phase selective hydrogenation of alkynes. The effects of palladium loading and TiO₂ crystallite size on the properties of Pd/TiO₂ Catalysts were focused in this study.

1.2 Objective

The objective of this research is to investigate the characteristics and catalytic properties of titania-supported palladium catalysts prepared by flame spray pyrolysis in liquid-phase selective hydrogenation of 1-heptyne.

1.3 Research Scopes

Part I

1. Preparation of titania-supported palladium catalysts (Pd/TiO₂) with 0.5 – 10 wt% Pd loadings and titania supports by flame spray pyrolysis method (FSP).
2. Loading 1 – 5 wt% Pd on the flame-made titania supports using incipient wetness impregnation method.
3. Catalyst pretreatment by reduction in H₂ at 30°C.
4. Characterization of the titania-supported palladium catalysts using several techniques such as Atomic Absorption Spectroscopy (AAS), X-ray diffraction (XRD), transmission electron microscopy (TEM), N₂ physisorption, X-ray Photoelectron Spectroscopy (XPS), and CO-pulse chemisorption.
5. Reaction study of titania-supported palladium catalysts in liquid-phase hydrogenation of 1-heptyne using stirring batch reactor (stainless steel autoclave 50 ml).

Part II

1. Preparation of titania-supported palladium catalysts (Pd/TiO₂) with 5 wt% Pd loading and titania supports by flame spray pyrolysis method (FSP) from different conditions such as concentration of solution, feed flow rate and O₂-dispersion.
2. Loading 5 wt% Pd on the flame-made titania supports and commercial titania supports using incipient wetness impregnation method.
3. Catalyst pretreatment by reduction in H₂ at 30°C.
4. Characterization of the titania-supported palladium catalysts using several techniques such as atomic absorption spectroscopy (AAS), X-ray diffraction (XRD), transmission electron microscopy (TEM), N₂ physisorption, X-ray Photoelectron Spectroscopy (XPS), and CO-pulse chemisorption.
5. Reaction study of titania-supported palladium catalysts in liquid-phase hydrogenation of an 1-heptyne using stirring batch reactor (stainless steel autoclave 50 ml).

CHAPTER II

THEORY

2.1 Flame Spray Pyrolysis (FSP)

Flame synthesis is a relatively new method for the one-step production of supported noble metal catalysts and catalysts in general. Flame aerosol synthesis is a cost-effective and versatile process for the controlled production of nanoparticles. In flame reactors, the energy of a flame is used to drive chemical reactions of precursor compounds that result in the formation of clusters which further grow by coagulation and sintering in the hot flame environment to nanometer-sized product particles [2, 4].

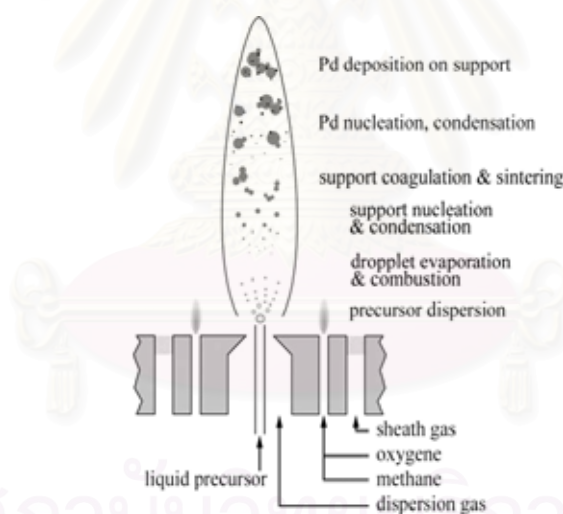


Figure 2.1 Skecth of the flame spray pyrolysis unit [2]

There are two primary types of the flame aerosol process for the synthesis of those nanoparticles. One is a flame assisted vapor-to-particle conversion process that is called as flame vapor synthesis (FVS). The other is a flame assisted liquid droplet-to-particle conversion process called as flame spray pyrolysis (FSP). The FVS process is the best choice for the synthesis of solid nanoparticles of single-component and binary systems such as metals, semiconductors, simple oxide, nitrides, etc.

However, the FVS process requires the use of volatile precursors. High production rate is possible when highly volatile precursors are available, and because the vapor phase precursors can be purified more easily than solid or liquid precursors, the FVS process allows the generation of materials with ultrahigh purities. Unfortunately, a disadvantage of the FVS process is that the synthesis of high-purity volatile precursors is complicated and expensive.

In general, the FVS is more complex to design and operate than the FSP because the FVS requires a gas-handling subsystem for the controlled introduction of vapor phase reactants. In contrast, the FSP systems require only an atomizer. The FSP has the major advantages that can handle materials containing a large number of elements and that aqueous solution of precursors can be used to produce multi-components oxide nanoparticles [3].

In conventional spray pyrolysis, the solution is atomized into a hot wall reactor where the aerosol droplets undergo evaporation and solute concentration within the droplet, drying, thermolysis of the precipitate particle at higher temperature to form a microporous particle, and, eventually a dense one by sintering. The advantages of FSP include the ability to dissolve the precursor directly in the fuel, simplicity of introduction of the precursor into the hot reaction zone (e.g. a flame), and flexibility in using the high-velocity spray jet for rapid quenching of aerosol formation [10].

When producing nano-catalyst using a high temperature flame, the particle collection technique has to be chosen. One solution is to collect the material directly on the substrate either inside the flame or very close to it. The variety of operational details includes several physical parameters such as e.g. particle size of the material. When nanosized particles are deposited on the substrate, it is assumed that coarsening of the material may take place, including partial sintering, neck formation and even full coalescence of the particles, especially if the temperature is sufficiently high.

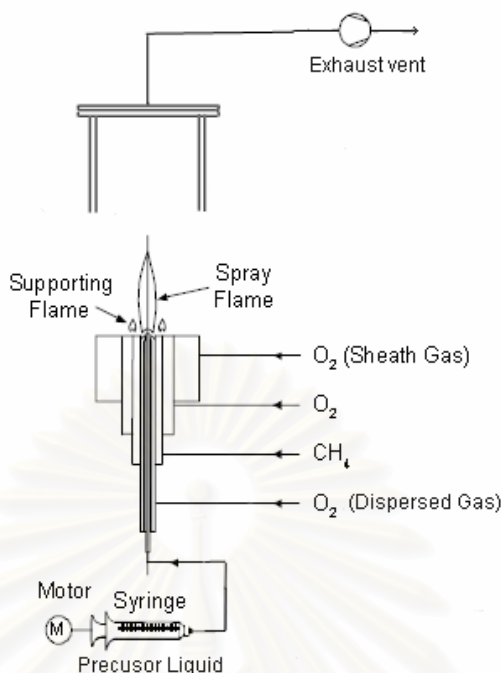


Figure 2.2 Experimental set-up for Pd/TiO₂ catalysts synthesis by flame spray pyrolysis

2.2 Liquid-Phase Hydrogenation

Liquid phase hydrogenation covers a huge range of processes, from the hydrogenation of vegetable oils and various sweeteners to hydrocarbons within the petrochemical industry. Even though classified as hydrogenation, all are very different processes, with their own characteristic process solutions. They possess some common features nevertheless, such as mass transfer and reliance on a catalyst. Indeed there are more hydrogenation catalysts available commercially than any other type, and for good reason, because hydrogenation is one of the most useful, versatile and environmentally acceptable reaction routes for organic synthesis. Typically the catalyst is powdered and slurried with reactant; a solvent is usually present to influence product selectivity and to adsorb the reaction heat liberated by the reaction. Since most hydrogenations are highly exothermic, careful temperature control is required to achieve the desired selectivity and to prevent temperature runaway.

2.3 Hydrogenation of Alkynes

Addition of hydrogen to a carbon-carbon double bond or triple bond is called hydrogenation. The overall effect of such an addition is the reductive removal of the double bond functional group. Regioselectivity is not an issue, since the same group (a hydrogen atom) is bonded to each of the double bond carbons. The simplest source of two hydrogen atoms is molecular hydrogen (H_2), but mixing alkenes or alkynes with hydrogen does not result in any discernable reaction. Although the overall hydrogenation reaction is exothermic, a high activation energy prevents it from taking place under normal conditions. This restriction may be circumvented by the use of a catalyst, as shown in the following diagram.

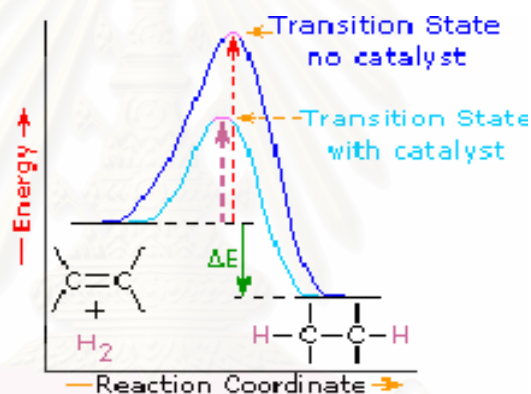


Figure 2.3 Free-energy diagrams for the hydrogenation of an alkene in the presence of a catalyst and the hypothetical reaction in the absence of a catalyst

As shown in the energy diagram, the hydrogenation of alkenes is exothermic, and heat is released corresponding to the ΔE in the diagram. This heat of reaction can be used to evaluate the thermodynamic stability of alkenes having different numbers of alkyl substituent on the double bond.

2.4 Palladium-Based Catalysts

Palladium, the preferred metal of choice for alkyne semi-hydrogenation, is normally used as a supported heterogeneous catalyst and frequently in presence of some form of additive to promote selectivity. For heterogeneous system in particular catalyst performance is strongly influenced by, firstly, the ability to get reactants to the active sites, then to establish the optimum hydrogen-to-hydrocarbon surface coverage, and, finally, the rapid removal of the hydrogenated products. These constitute the 'mass transfer limitations' and can have an overriding impact on the ability to achieve selective hydrogenation. In this respect, the nature of the support (inertness, surface area, pore size distribution) controls molecular access to the active sites and can also participate in unwanted side reaction through so-called 'spillover' effects.

2.5 Titanium (IV) Oxide [11]

Physical and chemical properties

Titanium (IV) oxide occurs naturally in three crystalline forms:

1. Rutile, which tends to be more stable at high temperatures. The application of almost rutile type is used in industrial products such as paints, cosmetics foodstuffs and sometimes found in igneous rocks.
2. Anatase, which tends to be more stable at lower temperatures. This type generally shows a higher photoactivity than other types of titanium dioxide.
3. Brookite, which is usually found only in minerals and has a structure belonging to orthorhombic crystal system.

A summary of the crystallographic properties of the three varieties is given in Table 2.1

Table 2.1 Crystallographic properties of anatase, brookite, and rutile.

Properties	Anatase	Brookite	Rutile
Crystal structure	Tetragonal	Orthorhombic	Tetragonal
Optical	Uniaxial, negative	Biaxial, positive	Uniaxial, negative
Density, g/cm ³	3.9	4.0	4.23
Hardness, Mohs scale	5 ^{1/2} – 6	5 ^{1/2} – 6	7 – 7 ^{1/2}
Unit cell	D _{4h} ¹⁹ .4TiO ₂	D _{2h} ¹⁵ .8TiO ₂	D _{4h} ¹² .3TiO ₂
Dimension, nm			
a	0.3758	0.9166	0.4584
b		0.5436	
c	0.9514	0.5135	2.953

Both of rutile and anatase type have a structure belonging to tetragonal crystal system but they are not isomorphous (Figure 2.4). The two tetragonal crystal types are more common because they are easy to make. Anatase occurs usually in near-regular octahedral, and rutile forms slender prismatic crystal, which are frequently twinned. Rutile is the thermally stable form and is one of the two most important ores of titanium.

The three allotropic forms of titanium dioxide have been prepared artificially but only rutile, the thermally stable form, has been obtained in the form of transparent large single crystal. The transformation from anatase to rutile is accompanied by the evolution of ca. 12.6 kJ/mol (3.01 kcal/mol), but the rate of transformation is greatly affected by temperature and by the presence of other substance which may either catalyze or inhibit the reaction. The lowest temperature at which conversion of anatase to rutile takes place at a measurable rate is ca. 700°C, but this is not a transition temperature. The change is not reversible; ΔG for the change from anatase to rutile is always negative.

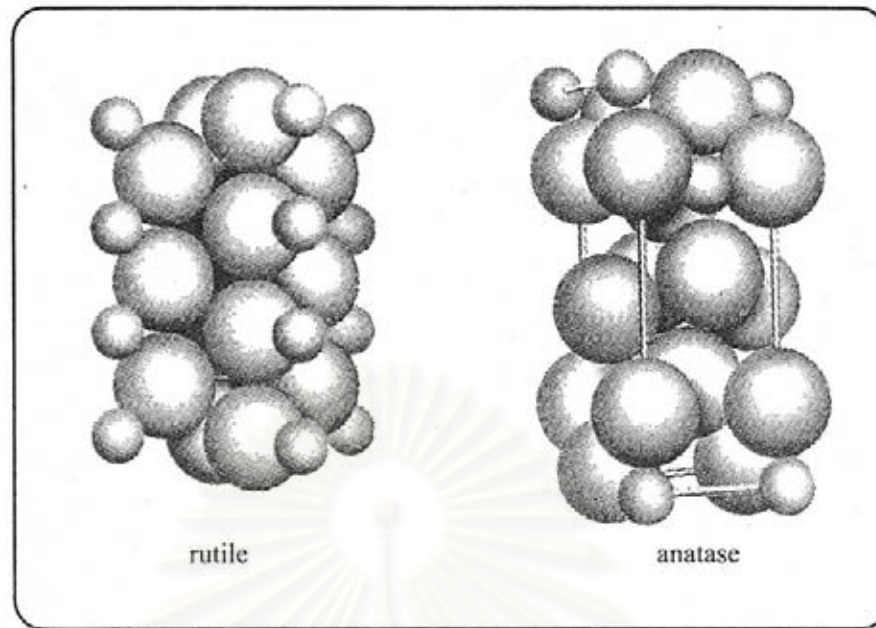


Figure 2.4 Crystal structure of TiO_2 [11]

Brookite has been produced by heating amorphous titanium (IV) oxide, prepared from an alkyl titanates of sodium titanate with sodium or potassium hydroxide in an autoclave at 200 to 600 °C for several days. The important commercial forms of titanium (IV) oxide are anatase and rutile, and these can readily be distinguished by X-ray diffraction spectrometry.

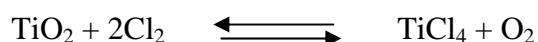
Since both anatase and rutile are tetragonal, they are both anisotropic, and their physical properties, e.g. refractive index, vary according to the direction relative to the crystal axes. In most applications of these substances, the distinction between crystallographic direction is lost because of the random orientation of large numbers of small particles, and it is mean value of the property that is significant.

Measurement of physical properties, in which the crystallographic directions are taken into account, may be made of both natural and synthetic rutile, natural anatase crystals, and natural brookite crystals. Measurements of the refractive index of titanium dioxide must be made by using a crystal that is suitably orientated with respect to the crystallographic axis as a prism in a spectrometer. Crystals of suitable size of all three modifications occur naturally and have been studied. However, rutile is the only form that can be obtained in large artificial crystals from melts.

The refractive index of rutile is 2.75. The dielectric constant of rutile varies with direction in the crystal and with any variation from the stoichiometric formula, TiO_2 ; an average value for rutile in powder form is 114. The dielectric constant of anatase powder is 48.

Titanium dioxide is thermally stable (mp 1855°C) and very resistant to chemical attack. When it is heated strongly under vacuum, there is a slight loss of oxygen corresponding to a change in composition to $\text{TiO}_{1.97}$. The product is dark blue but reverts to the original white color when it is heated in air.

Hydrogen and carbon monoxide reduce it only partially at high temperatures, yielding lower oxides or mixtures of carbide and lower oxides. At ca. 2000°C and under vacuum, carbon reduces it to titanium carbide. Reduction by metal, e.g., Na, K, Ca, and Mg, is not complete. Chlorination is only possible if a reducing agent is present; the position of equilibrium in the system is The reactivity of titanium dioxide towards acids is very dependent on the temperature to which it has been heated. For example, titanium dioxide that has been prepared by precipitation from a titanium (IV) solution and gently heated to remove water is soluble in concentrated hydrochloric acid. If the titanium dioxide is heated to ca. 900°C , then its solubility in acids is considerably reduced. It is slowly dissolved by hot concentrated sulfuric acid, the rate of salvation being increased by the addition of ammonium sulfate, which raises the boiling point of the acid. The only other acid in which it is soluble is hydrofluoric acid, which is used extensively in the analysis of titanium dioxide for trace elements. Aqueous alkalis have virtually no effect, but molten sodium and potassium hydroxides, carbonates, and borates dissolve titanium dioxide readily. An equimolar molten mixture of sodium carbonate and sodium borate is particularly effective as is molten potassium pyrosulfate.



The reactivity of titanium dioxide towards acids is very dependent on the temperature to which it has been heated. For example, titanium dioxide that has been prepared by precipitation from a titanium (IV) solution and gently heated to remove water is soluble in concentrated hydrochloric acid. If the titanium dioxide is heated to ca.

900°C, then its solubility in acids is considerably reduced. It is slowly dissolved by hot concentrate sulfuric acid, the rate of salvation being increased by the addition of ammonium sulfate, which raises the boiling point of the acid. The only other acid in which it is soluble is hydrofluoric acid, which is used extensively in the analysis of titanium dioxide for trace elements. Aqueous alkalies have virtually no effect, but molten sodium and potassium hydroxides, carbonates, and borates dissolve titanium dioxide readily. An equimolar molten mixture of sodium carbonate and sodium borate is particularly effective as is molten potassium pyrosulfate.



สถาบันวิทยบริการ
จุฬาลงกรณ์มหาวิทยาลัย

CHAPTER III

LITERATURE REVIEWS

3.1 Flame Spray Pyrolysis (FSP)

R. Mueller et al. [12] investigated continuous FSP synthesis of nanostructured silica particles with closely controlled characteristics at high production rates (up to 1.1 kg/d) in a pilot plant using baghouse filters. The influence of silica powder production rate, precursor concentration and oxidant dispersion gas flow rate was investigated on the product primary particle diameter, morphology and carbon content using HMDSO in EtOH at 1.26 and 3.0 M as well as pure HMDSO (4.7 M). The average product primary particle size was controlled from 10 to 75 nm independent of precursor concentration confirming that particle formation can take place during FSP in the gas phase following rapid evaporation of precursor droplets. The control of primary particle size using FSP is similar to that by the well-established vapor-fed aerosol reactors through the oxidant or precursor delivery rates. Limited variation of the product particle size was obtained when using air instead O₂ as dispersion gas (at constant pressure drop across the nozzle) or by providing additional sheath O₂ gas.

R. Stobel et al. [2] studied flame spray synthesis of Pd/Al₂O₃ catalysts and their behavior in enantioselective hydrogenation. They prepared 1 - 7.5 wt% Pd using flame spray pyrolysis (FSP). The result showed that palladium dispersion depended on the metal loading and decreased for higher amounts of Pd and then tested for the enantioselective hydrogenation of 4-methoxy-6-methyl-2-pyrone. Rate and enantioselectivity decreased with higher Pd dispersion. However, hydrogen pretreatment of the flame-made catalysts at 500°C improved rate and enantioselectivity strongly. Enantiomeric excess in the formation of (*R*)-4-methoxy-6-methyl-5,6-dihydro-2-pyrone reached 80% for flame-made catalysts after

pretreatment in hydrogen. Hydrogen pretreatment temperatures above 600°C led to sintering of the Pd particles and drastic loss in activity and enantioselectivity.

W. Y. Teoh et al. [13] studied TiO₂ and Pt/TiO₂ nanoparticles that were made by a one-step flame spray pyrolysis (FSP) process that resulted in mostly anatase (69–85 wt%) powders with controlled specific surface area and crystallite size. These particles resulted in shorter half-lives for sucrose photomineralisation, up to 50% lower than Degussa P25. Co-precipitation of Pt on TiO₂ during FSP increased the rutile content and slightly increased the specific surface area. Close control over Pt deposit size during this process was possible by varying the Pt concentration in the feed precursor. The dispersion of the Pt was high, 45–77% (at 4.0–0.1 atom% Pt) and corresponded to metal deposit size of 2.5–1.4 nm, respectively. An optimum photocatalytic activity was observed at 0.5 atom % Pt loading. At low Pt loading (0.1 atom% Pt), the activity was lower than that of FSP-made TiO₂ since the high photocurrent density of the Pt deposits increased the electron-hole recombination. The deposit size was also too small to establish sufficient electrical contact for efficient interfacial charge transfer between the photocatalysts and sucrose. Additional studies on the photocatalytic mineralisation of sucrose under oxygen enriched conditions reaffirmed the postulation that both FSP-made TiO₂ and improved Pt/TiO₂ photocatalysts favoured a reductive pathway which was different and faster than the pathway followed when using Degussa P25 TiO₂. The intricate relationship between photocatalyst characteristics and its performance is highlighted.

H. D. Jang et al. [3] studied synthesis of SiO₂ nanoparticles from sprayed droplets of tetraethylorthosilicate by the flame spray pyrolysis. TEOS concentration, maximum flame temperature, and residence time of reactants in the flame were chosen as key experimental variables for the control of the particle morphology, and average particle diameter. Larger particles were produced with decrease of the maximum flame temperature by controlling of hydrogen flow rate and oxygen in the burner. Average particle diameter increased with the increase of residence time by controlling the carrier gas flow rate.

A.I.Y. Tok et al. [1] studied novel synthesis of Al_2O_3 nano-particles by flame spray pyrolysis. The novel flame spray pyrolysis method has successfully produced nano-sized Al_2O_3 of about 10–30 nm (α -phase + γ -phase), and 80–100 nm (α -phase, calcined) from AlCl_3 vapour. Based on XRD results, the as-sprayed nano-particles consisted of α -phase and γ -phase Al_2O_3 , which can be converted to α -phase by calcination at 1100°C for 2 h. The particle size of calcined powders was about 80–100 nm. Although this work focused on the synthesis of Al_2O_3 nanoparticles, it can be seen that this method has the flexibility of easily producing other nano-particles by flame spraying other metal chlorides that have a low boiling point.

A. Teleki et al. [14] studied nanostructured anatase TiO_2 which was produced by flame spray pyrolysis (FSP) and tested for sensing of volatile organic compounds and CO at 500°C . The as-prepared powders were characterized by transmission/scanning electron microscopy, X-ray diffraction and nitrogen adsorption. Titania films about 30 μm thick on alumina substrates interdigitated with gold electrodes were prepared by drop-coating a heptanol suspension of these powders. The films showed a high signal of n-type sensor to isoprene, acetone and ethanol at concentrations ranging from 1 to 75 ppm in dry N_2/O_2 at 500°C . The response (within seconds) and recovery (within minutes) times were very fast. Heat-treatment at 900°C caused a nearly complete anatase to rutile transformation and a transition to p-type sensing behavior. That resulted in a poor sensor signal to all hydrocarbons tested and considerably longer recovery times than that of the anatase sensor. That rutile sensor could detect CO that the original, anatase sensor could not. For ethanol the sensor response changed back to n-type.

M. J. Height et al. [7] studied Ag-ZnO catalysts. High specific surface area and crystalline Ag-ZnO photocatalysts were made by one-step flame spray pyrolysis. The photocatalyst powders consist of monocrystalline zinc oxide primary particles of 8–25 nm supporting nanocrystals of silver metal around 5–20 nm for Ag loadings of 1–5 at.%. Flame-made Ag-ZnO showed higher photocatalytic activity than wet-made and reference titania powders. An Ag loading between 1 and 3 at.% gave the fastest photodegradation of MB and the reaction rate decreased at higher

Ag loadings. This is consistent with the presence of discrete Ag clusters leading to retarded recombination of the photoinduced electron–hole pairs. Decreasing activity at higher loadings is likely to arise from decreasing surface availability on the particles for reactant adsorption and light absorption. The photocatalytic performance was improved for flame-made materials made at longer high-temperature residence times in the flame. The latter particles exhibited improved crystallinity, as measured by UV–vis absorption and XRD.

W. Y. Teoh et al. [15] studied visible light-active Fe-doped TiO₂ that was prepared by a one-step flame spray pyrolysis (FSP) technique. Introduction of Fe into TiO₂ matrix by flame synthesis was effective in extending the particle photoresponse to the visible regime ($\lambda > 400$ nm). At the same time, it also enhances transformation to rutile. Being a bottom-up approach, the short residence time coupled with a high quenching rate during the FSP process was found to be an excellent method in synthesising homogeneous Fe-doped TiO₂ solid solutions with high Fe solubility. The reported solubility of up to Fe/Ti = 0.05 in this work is significantly higher than the Fe/Ti \sim 0.01 commonly found for particles synthesised by wet techniques followed by high temperature calcination. Doping Fe above its solubility limit was accompanied by formation of amorphous structure and a UV–vis optical band centred at 490 nm. A slight shift in the XRD rutile (1 1 0) peak and a decrease in specific surface area were also observed at high Fe loadings. The Fe-TiO₂ sample was able to mineralise oxalic acid under visible light. This is also accompanied by a unique Fe-leaching and re-adsorption properties. Extraction of Fe (III) from photocatalyst surface was found to take place even in the dark to form an Fe (III)-oxalate complex. The complex is photolysed under visible light irradiation leaving behind Fe (II) ions. Here, the presence of visible light-active Fe-TiO₂ is important to reoxidise the adsorbed Fe (II) to Fe (III) to sustain the photoreaction under visible light. A high extent of oxalic acid mineralisation (70%) for 10 ppm (as carbon) of oxalic acid was observed for Fe-doped TiO₂ with Fe/Ti ratio of 0.05 compared to just 50% for the same bulk amount of aqueous Fe (III) and TiO₂. In addition, most dissolved Fe ions are re-adsorbed back on the Fe-TiO₂ particles at the end of the oxalic acid oxidation reaction, thereby minimizing the loss of Fe and rendering its re-usability. On the other hand, a mixture of dissolved Fe (III) and bare TiO₂ resulted in significant loss of

unadsorbed Fe after each run. Hence it is not surprising that the Fe-doped TiO₂ particles exhibited reproducible mineralization rates even after 5 repeated runs whereas the latter saw deteriorating rates after every run. The UV–vis absorption spectrum of Fe-doped TiO₂ was also found to be unchanged despite repeated photocatalytic runs.

R. Jossen et al. [16] studied Vanadia (0.9 or 2 wt.%) and silica (0–5 wt.%) doping of flame-made tungsten oxide–titania nanostructured catalyst powders (anatase, 100 m²/g, 10 wt.% WO₃). The characteristics and thermal stability of silica–vanadia–tungsten oxide–titania powder depend strongly on its composition. Pure TiO₂ has very low thermal stability and during calcination most anatase is converted to rutile with large loss of its SSA. Addition of 10 wt.% tungsten oxide slightly improves its thermal and crystalline stability. In contrast, adding even up to 2 wt.% vanadia deteriorates both while adding silica improves both drastically: 90% of the initial SSA remained after calcination at 700°C for 20 h upon adding 5 wt.% silica to the 2V10WTi. Additionally the anatase content remains above 95 wt.%. Microscopic analysis shows that the vanadia and tungsten oxide are well distributed on the surface of the titania support. After calcination, crystalline tungsten oxide was only formed in the presence of vanadia and at low silica contents (≤ 1 wt.%). Adding silica prevents the crystallization of tungsten oxide. For all samples before and after calcination no crystalline vanadia is found. TPR analysis shows that vanadia has a very good accessibility as between 80 and 100 % of the V⁵⁺ is reduced to V³⁺. It is shown that by adding silica (1–2 wt.%) the reducibility of vanadia is decreased while when adding 5 wt.% silica the reducibility is again increased. The 5Si2V10WTi powder has the lowest reduction peak as it is most easily reduced. For 0.9 wt.% vanadia content the catalytic conversion and reaction rate were increased for increasing silica content as silica improves the thermal stability of the powder even at higher reactor temperature. For 2 wt.% vanadia catalysts and low reactor temperature the conversion and the reaction time were decreased by adding silica. At higher reactor temperature, however, silica increases the catalytic activity by increasing the thermal and crystal stability of the catalyst. Therefore, adding silica can prevent this thermal deactivation and can again increase the conversion as well as the reaction rate at higher reactor temperatures.

S. Hannemann et al. [8] studied Mono and multi-noble metal particles on Al_2O_3 . The combination of FSP with high-throughput testing has been shown to be an attractive approach for rapid preparation and testing of various supported multi-metallic (Rh, Ru, Pt, Pd) noble metal catalysts. Precursor solutions based on $\text{Al}(\text{acac})_3$ and methanol-acetic acid showed the best stability and were less sensitive to air/moisture than precursor solutions based on xylene. In addition, they were advantageous in case of volatile metal oxides probably due to a lower flame temperature. The noble metal particles (0.1–2.5 wt% on Al_2O_3) of 1–2 nm in diameter were found to be mostly alloyed after reduction. Exceptions were alloys containing noble metals prone to surface segregation. The CPO is an alternative way of exploiting methane or natural gas in chemical industry. In the CPO of methane to CO and H_2 between 300 and 500°C, extinction and ignition temperatures rates and selectivities were identified for various combinations of supported noble metals. HTE testing routines enabled a fast, comprehensive and parallel testing procedure including longterm stability tests. In situ spectroscopy on selected samples indicated a correlation between the oxidation state of the noble metals and the ignition/extinction of the partial oxidation towards CO and H_2 . As long as only the total combustion reaction to CO_2 and H_2O took place they remained at least in partially oxidized state. Flame-spray pyrolysis in combination with high-throughput experimentation is thus a promising route to scrutinize new catalyst materials by a combination of both high-throughput preparation and testing. A fully robot-controlled synthesis would further speed up the preparation routine. A careful characterization of selected catalyst samples, including in situ characterization, remains important for a targeted catalyst preparation.

Up till now a variety of products have been synthesized by FSP as shown in table 3.1.and 3.2

Table 3.1 Example of oxide/mixed-oxides obtained from flame spray pyrolysis method.

Product	Particle/ Crystallite size (nm.)	Applications	Comments	Reference
CeO ₂	n/a*	n/a	Good thermal stability	L. Mädler et al. [17]
LiCoO ₂	11-35	n/a	n/a	H. D. Jang et al. [18]
SnO ₂	17-20	Gas sensing.	High sensitivity and fast responses to NO ₂ and propanal.	T. Sahma et al. [19]
ZnO	20	Photocatalytic degradation of methylene blue	Photoactivity of the ZnO nanoparticles of 20 nm in the average diameter was higher than that of the ZnO nano-crystalline of 20 nm.	Y. J. Jang et al. [20]
SiO ₂	12-47	n/a	n/a	H. D. Jang et al. [3]
Al ₂ O ₃	10-30	n/a	n/a	A.I.Y. Tok et al. [1]
TiO ₂	15	Sensing of organic vapors	High signal of n-type sensor to isoprene, acetone and ethanol at 500°C.	A. Teleki et al. [14]

* n/a = data not available

Table 3.2 Example of metal loaded catalysts obtained from flame spray pyrolysis method.

Product	Applications	Comments	Reference
Pt/Al ₂ O ₃	Enantioselective hydrogenation	Turnover frequency increased with higher platinum loading.	R. Strobel et al. [4]
Pd/La ₂ O ₃ /Al ₂ O ₃	Catalytic combustion of methane	Excellent thermal stability in terms of specific surface area up to 1200°C and retarded γ - to α -alumina transformation.	R. Strobel et al. [21]
Pt/TiO ₂	Photocatalytic mineralisation of sucrose	Both FSP-made TiO ₂ and improved Pt/TiO ₂ photocatalysts favoured a reductive pathway which was different and faster than the pathway followed when using Degussa P25 TiO ₂ .	W. Y. Teoh et al. [13]
V ₂ O ₅ /TiO ₂	Synthesis of phthalic anhydride	Flame coated foams (V ₂ O ₅ /TiO ₂) showed superior catalytic activity and selectivity at high conversions than classic, wet-made V ₂ O ₅ /TiO ₂ catalysts.	B.Schimmoeller et al. [22]
Ag/ZnO	UV-photodegradation of methylene blue	Flame-made Ag-ZnO showed higher photocatalytic activity than wet-made and reference titania powders.	M. J. Height et al. [7]
Fe/TiO ₂	Photomineralisation of oxalic acid	The FSP Fe-doped TiO ₂ photocatalyst was found to be stable and reusable after each run with minimal loss of Fe from the surface.	W. Y. Teoh et al. [15]

3.2 Role of Titania in the Selective Hydrogenation on Pd Catalysts

J. H. Kang et al. [23] investigated the performance of TiO₂-modified Pd catalysts, containing TiO₂ either as an additive or as a support, in the selective hydrogenation of acetylene was investigated using a steady-state reaction test. They reported that the TiO₂ added Pd catalyst reduced at 500°C (Pd–Ti/SiO₂/500°C) showed a higher selectivity for ethylene production than either the Pd/TiO₂ or Pd/SiO₂ catalyst. The amounts of chemisorbed H₂ and CO were significantly reduced and, in particular, the adsorption of multiply coordinated CO species was suppressed on Pd–Ti/SiO₂/500°C, which is characteristic of the well-known strong-metal-support-interaction (SMSI) phenomenon that has been observed with the TiO₂-supported Pd catalyst reduced at 500°C, Pd/TiO₂/500°C. Moreover, XPS analyses of Pd–Ti/SiO₂/500°C suggested an electronic modification of Pd by TiO₂, and the TPD of ethylene from the catalyst showed the weakening in ethylene adsorption on the Pd surface. The 1,3-Butadiene was produced in smaller amounts when using Pd–Ti/SiO₂/500°C than when using Pd/SiO₂/500°C, indicating that the polymerization of C₂ species leading to catalyst deactivation proceeds at slower rates on the former catalyst than on the latter. They also suggested that the enhanced ethylene selectivity on Pd–Ti/SiO₂/500°C may be explained by correlating the catalyst surface properties with the mechanism of acetylene hydrogenation.

Y. Li. et al. [9] investigated in situ EPR and IR by using CO as probe molecules show that even pre-reduced by H₂ at lower temperature results in SMSI for anatase titania supported palladium catalyst, but not for rutile titania supported palladium catalyst. This difference is attributed that the Ti³⁺ ions produced by reduction of Ti⁴⁺ are fixed in the surface lattice of TiO₂, as rutile titania is more thermodynamically and structurally stable than anatase titania so that the Ti³⁺ ions fixed in the surface lattice of anatase TiO₂ is easier to diffuse to surface of palladium particle than one in the surface lattice of rutile TiO₂. The reason why the pre-reduction of both anatase and rutile supported palladium catalyst at higher temperature results in SMSI between Ti³⁺ and Pd is attributed that the thermal diffusion of produced Ti³⁺ ion at higher temperature is much easier than at lower temperature so that it could overcome the binding of surface lattice of both anatase and rutile titania to move to the surface or surrounding of palladium particle.

The anatase titania supported palladium catalyst 0.075%Pd/TiO₂ (A) reduced at lower temperature has higher selectivity of alkenes than rutile titania supported palladium catalysts 0.075%Pd/TiO₂ (R). For titania (rutile or anatase) supported palladium catalysts, the elevation of pre-reduction temperature from 200 to 450°C gives rise to sharp change of catalytic properties, especially for selectivity of alkenes. The very different catalytic properties between 0.075%Pd/TiO₂ (R) and 0.075%Pd/TiO₂ (A) catalyst pre-reduced at lower temperature, and the rapid change of conversion and selectivity of 0.075%Pd/TiO₂ (A) and 0.075%Pd/TiO₂ (R) with the elevation of pre-reduction temperature are reasonably explained by the presence of SMSI both for anatase titania supported palladium catalyst pre-reduced at lower temperature, and titania (rutile and anatase) supported palladium catalyst pre-reduced at higher temperature.

L. Nakkararuang et al., [24] prepared nanocrystalline titanias by thermal decomposition of titanium (IV) *n*-butoxide in two different solvents (toluene and 1,4-butanediol) at 320°C and employed as supports for Pd and Pd-Ag catalysts for selective acetylene hydrogenation. The titania products obtained from both solvents showed only anatase phase with similar crystallite sizes and BET surface areas. However, due probably to the different crystallization pathways, the number of Ti³⁺ defective sites as shown by ESR results of the titania prepared in toluene were much higher than the ones prepared in 1,4-butanediol. It was found that the use of anatase titania with higher Ti³⁺ defective sites as a support for Pd catalysts resulted in lower activity and ethylene selectivity in selective acetylene hydrogenation. However, this effect was suppressed by Ag promotion.

3.3 Comments on the previous studies

From the previous studies, FSP process is a promising method to produce highly crystalline nano-particles using high synthesis temperature and rapid cooling rate. Depending on the synthesis conditions, specific surface area and size of metal on the catalysts can be controlled. Pd/TiO₂ is one of the most useful catalysts used in liquid-phase hydrogenation reaction. Their catalytic performances strongly depend on the TiO₂ crystal structure. For example, anatase TiO₂ is the favorable phase for selective hydrogenation of long chain alkadienes. However, the properties

of flame-made palladium/titania catalysts in catalytic liquid-phase hydrogenation have never been studied so far. Thus, it is the aims of this study to synthesize titania-supported palladium by flame spray pyrolysis and investigate their catalytic behavior in liquid-phase selective hydrogenation.



สถาบันวิทยบริการ
จุฬาลงกรณ์มหาวิทยาลัย

CHAPTER IV

EXPERIMENTAL

4.1 Catalyst Preparation

4.1.1 Materials

The chemical used in the synthesis of flame-made catalysts are specified as follows in Table 4.1. Table 4.2 presents the commercial TiO₂ used of preparation of Pd/TiO₂ reference catalysts.

Table 4.1 Chemicals used in the synthesis of flame-made catalysts

Chemical	Supplier
Palladium acetylacetonate	Aldrich
Titanium(IV)tert-butoxide	Aldrich
Xylene (99.8 vol.%)	MERCK
Acetonitrile (99.5 vol.%)	Fluka

Table 4.2 Commercial TiO₂ used for the synthesis of Pd/TiO₂ reference catalysts

Chemical	Supplier
TiO ₂ -nano	Aldrich
P-25	Aldrich
TiO ₂ -micron	Aldrich

4.1.2 Synthesis of Flame-Made TiO₂ supports and Pd/TiO₂ Catalysts (Part I-study)

The synthesis of titania-supported palladium catalysts was carried out by flame spray pyrolysis. Palladium acetylacetonate (Pd(acac)₂) and titanium (IV) tert-butoxide were chosen as raw materials for preparation of a liquid-phase precursor.

The precursors were prepared by dissolving in xylene/acetonitrile mixtures (70/30 vol%). The total concentration was always 0.5 M. During particle synthesis, 5 ml/min of liquid precursor are fed to the flame by a syringe pump and disperse with 5 l/min oxygen forming fine spray droplets. The pressure drop at the capillary tip was maintained at 1.5 bar by adjusting the orifice gap area at the nozzle. The spray was ignited by supporting flamelets feed with oxygen (3 l/min) and methane (1.5 l/min) which were positioned in a ring around the nozzle outlet. A sintered metal plate ring (8 mm wide, starting at a radius of 8 mm) provided additional 25 l/min of oxygen as sheath for the supporting flame. The product particles were collected on a glass fiber filter (Whatman GF/D, 25.7 cm in diameter) with the aid of a vacuum pump.

The titania supports were prepared by the flame spray pyrolysis method using the same conditions as those for the preparation of titania supported palladium catalysts prepared in single step flame synthesis. These TiO₂ supports were used in Part I study (preparation of 1-5 wt% Pd/TiO₂ by impregnation method).

4.1.3 Synthesis of Flame-Made Pd/TiO₂ Catalysts with Various Crystallite Sizes (Part II-study)

Flame-made Pd/TiO₂ catalysts with various crystallite sizes were prepared using the same chemicals and reactor as titania-supported palladium catalysts in section 4.1.2 with 5 wt% Pd loadings. The concentration of solution, feed flow rate and O₂-dispersion were varied as shown in Table 4.3.

สถาบันวิทยบริการ
จุฬาลงกรณ์มหาวิทยาลัย

Table 4.3 Preparation conditions of the flame-made Pd/TiO₂ catalysts with various crystallite sizes

Catalyst	Conditions		
	Concentration (mol/dm ³)	Feed flow rate (ml/min)	O ₂ -dispersion (l/min)
5FSP-9.7 nm*	0.3	3	5
5FSP-15.7 nm	0.5	5	5
5FSP-24.6 nm	0.5	8	3

* d_{XRD} crystallite size of TiO₂

4.1.4 Palladium Loading by Incipient Wetness Impregnation Method

In this experiment, incipient wetness impregnation was used for loading palladium into flame-made titania. Palladium acetylacetonate was used as precursor. The certain amount of palladium precursor (from 1 to 5 wt% loading) was introduced into the acetonitrile which its volume equals to pore volume of catalyst. The titania support was impregnated with a palladium solution. The palladium solution was dropped slowly to the titania support, then dried overnight in the oven at 100°C and calcined in air at 450°C for 3 h.

4.2 The Reaction Study in Liquid-Phase Hydrogenation

The liquid-phase hydrogenation was used to study the properties of these prepared catalysts. 1-heptyne was used as reactant in an organic solvent (toluene) as reaction medium.

4.2.1 Chemicals and Reagents

The chemicals and reagents used in the reaction are shown in Table 4.4

Table 4.4 The chemicals and reagents used in the reaction

The chemicals and reagents	Supplier
High purity grade Hydrogen (99.99 vol.%)	Thai Industrial Gases Limited
1-heptyne	Aldrich
1-heptene	TRADE TCI MARK
n-heptane	Wako
Toluene	Fluka

4.2.2 Instrument and Apparatus

The main instruments and apparatus are explained as follow:

The autoclave reactor

The 50 ml stainless steel autoclave was used as reactor. Hot plate stirrer with magnetic bar was used to heat up the reactant and to ensure that the reactant and the catalyst were well mixed.

Gas chromatography

A gas chromatography equipped with flame ionization detector (FID) with GS-alumina capillary column was used to analyze the feed and product.

Table 4.5 Operating condition for gas chromatograph

Gas Chromatograph	Shimadzu GC-14A
Detector	FID
Packed column	GS-alumina (length =30 m, I.D. =0.53 mm)
Carrier gas	Helium (99.99 vol.%)
Make-up gas	Nitrogen (99.99 vol.%)
Column temperature	200°C
Injector Temperature	250°C
Detector Temperature	280°C

4.2.3 Liquid-Phase Hydrogenation Procedure

The reaction study of liquid-phase hydrogenation of 1-heptyne in toluene is consisted of two steps:

1. Reduction step

Approximately 20 mg of supported palladium catalyst was placed into the glass tube. Then the catalyst was reduced by hydrogen gas at the volumetric flow rate of 50 ml/min at room temperature for 2 h.

2. Reaction step

0.2 ml of 1-heptyne, 9.8 ml of toluene and 20 mg of catalyst were introduced into the autoclave reactor. The reaction was carried out under hydrogen atmosphere at 1 bar and 30°C for 3-40 min. After the reaction, the vent valve was slowly opened to prevent the loss of product. Then, the product mixture was analyzed by gas chromatography with flame ionization detector (FID).

4.3 Catalyst Characterization

The catalysts were characterized by several techniques as follow:

4.3.1 Atomic Absorption Spectroscopy (AAS)

The bulk composition of palladium was determined using a Varian Spectra A800 atomic adsorption Spectrometer at the Department of Science Service Ministry of Science and Technology.

4.3.2 N₂ Physisorption

The surface area of solid, average pore size diameters and pore size distribution were determined by physisorption of nitrogen (N₂) using Micromeritics ASAP 2020 (surface area and porosity analyzer).

4.3.3 X-ray Diffraction (XRD)

The bulk crystal structure and chemical phase composition are determined by diffraction of an X-ray beam as a function of the angle of the incident beam. The XRD spectrum of the catalyst was measured by using a SIEMENS D500 X-ray diffractometer and Cu $K\alpha$ radiation. The crystallite size is calculated from Scherrer's equation.

4.3.4 Transmission Electron Microscopy (TEM) with Electron Diffraction Mode

Catalyst crystallite size and the diffraction pattern of titania support were observed using JEOL-JEM 200CX transmission electron microscope operated at 100kV at National Metal and Materials Technology Center.

4.3.5 CO-Pulse Chemisorption

The active sites and the relative percentages dispersion of palladium catalyst was determined by CO-pulse chemisorption technique using Micromeritics ChemiSorb 2750 (pulse chemisorption system)

Approximately 0.2 g of catalyst was filled in a quartz tube, incorporated in a temperature-controlled oven and connected to a thermal conductivity detector (TCD). He was introduced into the reactor at the flow rate of 30ml/min in order to remove remaining air. Prior to chemisorp, the samples were reduced in a H_2 flow rate at 50 ml/min with heated from room temperature to 30°C and held at this temperature for 2 h. Carbon monoxide that was not adsorbed was measured using thermal conductivity detector. Pulsing was continued until no further carbon monoxide adsorption was observed. Calculation details of %metal dispersion are given in Appendix B.

4.3.6 X-ray Photoelectron Spectroscopy (XPS)

The XPS analysis was performed originally using an AMICUS spectrometer equipped with a Mg K_{α} X-ray radiation. For a typical analysis, the source was operated at voltage of 20 kV and current of 10 mA. The pressure in the analysis chamber was less than 10^{-5} Pa. The AMICUS system is computer controlled using the AMICUS “VISION2” software.

4.4 Catalyst Nomenclature

- The flame-made Pd/TiO₂ Catalysts prepared in single-step with Pd loading 0.5, 1, 2, 5, and 10 wt% are denoted as 0.5FSP, 1FSP, 2FSP, 5FSP, and 10FSP, respectively.
- The Pd catalysts prepared on flame-made TiO₂ supports by incipient wetness impregnation with Pd loading 1, 2, and 5 wt% are referred to as 1Im-FSP, 2Im-FSP, and 5Im-FSP, respectively.
- The 5 wt% Pd/TiO₂ catalysts prepared by single-step flame synthesis with average crystallite sizes of 9.7, 15.7, and 24.6 nm are referred to as 5FSP-9.7, 5FSP-15.7, and 5FSP-24.6, respectively.
- The 5 wt% Pd/TiO₂ catalysts prepared by incipient wetness impregnation of palladium on the flame-made TiO₂ supports with average crystallite sizes of 9.8, 15, and 26 nm are referred to as 5Im-FSP-9.8, 5Im-FSP-15, and 5Im-FSP-26, respectively.
- Reference catalysts prepared by incipient wetness impregnation of palladium on TiO₂-nano, P-25, and TiO₂-micron from Aldrich are referred to as 5Im-nano, 5Im-P25, and 5Im-micron, respectively.

CHAPTER V

RESULTS AND DISCUSSION

Supported Pd catalysts are preferred for the selective hydrogenation of alkynes to alkenes. It is one of the most useful, versatile, and environmentally acceptable reaction routes available for organic syntheses. The flame-made catalysts with Pd loading 0.5-10 wt%, impregnated catalysts with Pd loading 1-5 wt% and the reference catalysts were used in this study. Reference catalysts prepared with 5 wt% Pd loading by impregnation method were Pd/TiO₂-nano, Pd/TiO₂-P25, and Pd/TiO₂-micron (all commercial TiO₂ were obtained from Aldrich). This chapter is divided into two sections: 5.1) the effect of palladium loading and 5.2) the effect of TiO₂ crystallite size on the properties of Pd/TiO₂ catalysts. Each section consists of catalyst characterization and selective 1-heptyne hydrogenation study.

For catalyst characterization, the catalysts were characterized by several techniques such as XRD, TEM, N₂ physisorption, AAS, CO-pulse chemisorption, and XPS. For selective 1-heptyne hydrogenation, the reaction was carried out at 30°C and 1 bar of H₂ pressure.

5.1 The Effect of Palladium Loading on the Properties of Pd/TiO₂ Catalysts

5.1.1 Characterization of the Catalysts

5.1.1.1 X-ray Diffraction (XRD)

The XRD patterns of flame-made Pd/TiO₂ catalysts with Pd loading 0.5 - 10 wt% were collected at the diffraction angle (2θ) between 20° and 80°, the XRD patterns are shown in Figure 5.1. All the samples exhibited XRD characteristic peaks of anatase titania at 25°(major), 37°, 48°, 55°, 56°, 62°, 71°, and 75° 2θ . XRD peaks for rutile titania also appeared at 28°(major), 36°, 42°, 57° 2θ . The major peak of PdO was shown at 33° 2θ .

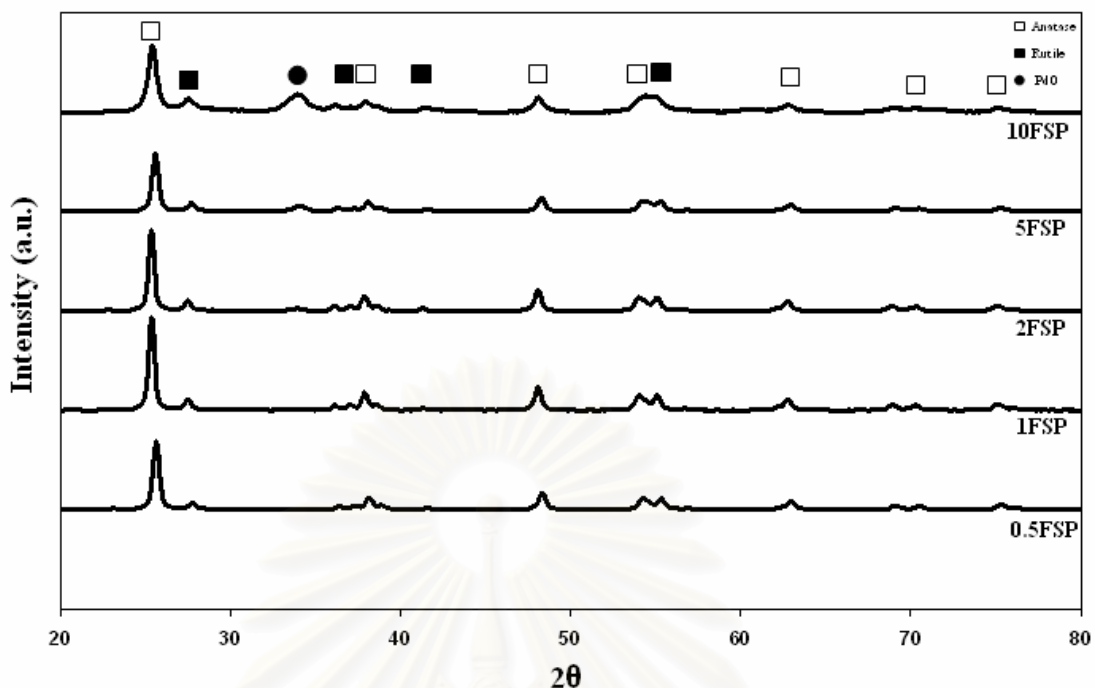


Figure 5.1 XRD patterns of the flame-made Pd/TiO₂ catalysts with Pd loading between 0.5 and 10 wt%

The results of XRD analysis such as diameter of anatase TiO₂ from flame-made and impregnated catalysts, diameter of PdO, and composition of anatase and rutile titania are shown in Table 5.1. Without Pd addition, the crystallite size of the flame-made TiO₂ was 26 nm. Addition of Pd during flame synthesis 0.5-10 wt% resulted in smaller TiO₂ crystallite size with the 10 wt% sample (10FSP) had the smallest TiO₂ crystallite size (14.6 nm).

It has been suggested by W.Y. Teoh et al. [13] that increasing Pt loading from 0.25 to 10 wt% during the synthesis of Pt/TiO₂ by flame spray pyrolysis suppressed sintering and crystal growth of TiO₂. So similar results were observed for our Pd/TiO₂ catalysts. The effect, however, was more pronounced for 10 wt% loading of Pd.

The percentages of anatase and rutile phase TiO₂ were also presented in Table 5.1. It was found that %anatase decreased with increasing Pd loading while %rutile phase increased especially at high Pd loading. W.Y. Teoh et al. [15] also reported that doping TiO₂ with Fe greatly promotes the formation of rutile. Calculation of anatase and rutile phase TiO₂ composition is given in Appendix E.

Preparation of Pd/TiO₂ by one-step flame spray pyrolysis with Pd loading 5-10 wt% resulted in the formation of PdO as seen from XRD results in Figure 5.1.

The calculated PdO crystallite sizes for 5 and 10 wt% Pd/TiO₂ catalysts were 5.9 and 6.3 nm, respectively. For the catalysts with lower Pd loadings (0.5-2 wt%), the XRD peaks for PdO or Pd⁰ metal were not observed due probably to the low amount of Pd present and/or their crystallite sizes were smaller than XRD detectable limit.

It should be noted that preparation of supported Pd catalysts on other supports such as Pd/SiO₂ [30] and Pd/Al₂O₃ [2] by flame spray pyrolysis under similar conditions can result in formation of Pd⁰ metal phase not the PdO.

Compared to the one-step synthesis catalysts, the crystallite size of TiO₂ of the impregnated catalysts was relatively constant. There was also no significant transformation of anatase to rutile phase TiO₂ for the impregnated catalysts with 1-5 wt% Pd loading. It indicates that flame-made TiO₂ is stable during calcination at 450°C.

Table 5.1 XRD analysis results and TiO₂ phase composition of various Pd loading of flame-made and impregnated catalysts

Catalyst	Diameter of anatase TiO ₂ from XRD (nm)	Diameter of PdO from XRD (nm)	% Anatase	% Rutile
TiO ₂ FSP	26.0	n/a	91.3	8.7
0.5FSP ^a	20.9	n/a	88.4	11.6
1FSP ^a	23.7	n/a	89.2	10.8
2FSP ^a	24.0	n/a	88.3	11.7
5FSP ^a	20.6	5.9	90.1	9.9
10FSP ^a	14.6	6.3	85.1	14.9
1Im-FSP ^b	24.6	n/a	92.0	8.0
2Im-FSP ^b	24.8	n/a	91.6	8.4
5Im-FSP ^b	25.6	n/a	90.5	9.5

^a as-prepared

^b the catalysts were reduced in H₂ at 30°C for 2 h

Figure 5.2 shows the XRD patterns of Pd/TiO₂-Im-FSP catalysts with Pd loading from 1 to 5 wt% after reduction in H₂ at 30°C for 2 h. Impregnated catalysts for all Pd loadings exhibited XRD characteristic peaks of anatase titania at 25°(major), 37°, 48°, 55°, 56°, 62°, 71°, and 75° 2θ. XRD peaks for rutile titania appeared at 28°(major), 36°, 42°, 57° 2θ. The peak of Pd⁰ metal were not detect for Pd/TiO₂-Im-FSP with Pd loading 1, 2, and 5 wt%, suggesting that Pd was probably highly dispersed or its average particle size was smaller than XRD detectable limit.

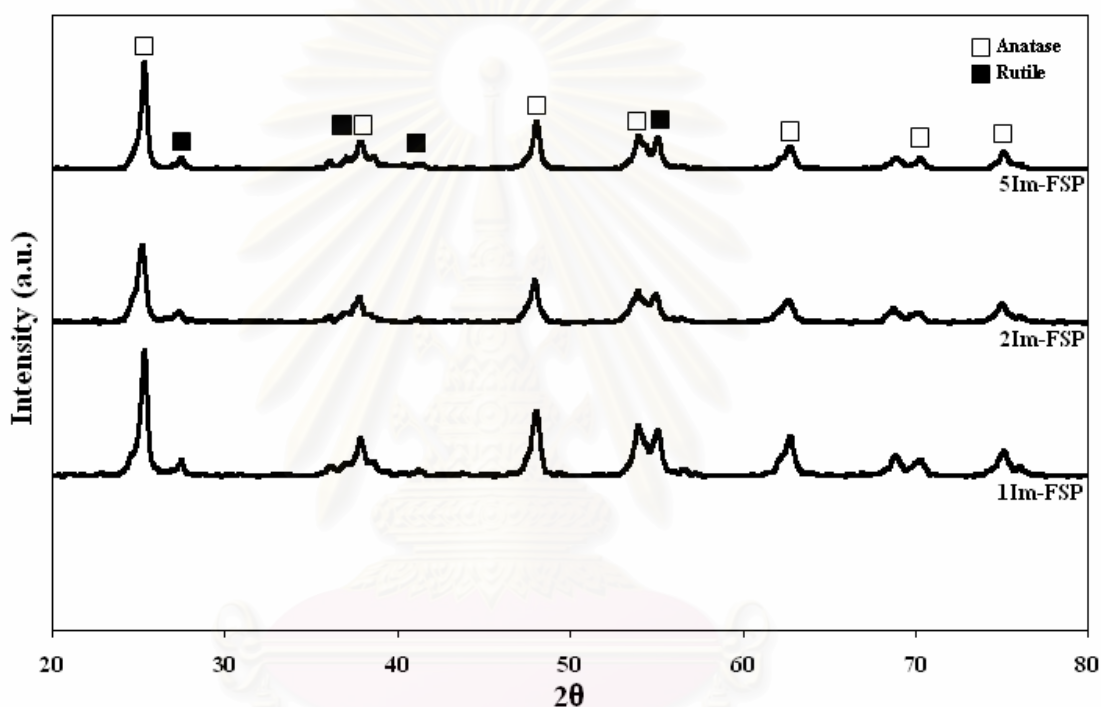


Figure 5.2 XRD patterns of all impregnated Pd/TiO₂ catalysts with Pd loading 1-5 wt% after reduction in H₂ at 30°C for 2 h

5.1.1.2 Transmission Electron Microscopy (TEM)

TEM is a useful tool determining particle size and size distribution of supported metal. It allows determination of the micro-texture and microstructure of electron transparent samples by transmission of a focused parallel electron beam to a fluorescent screen with a resolution presently better than 0.2 nm.

TEM micrographs were taken for the flame-made the Pd/TiO₂ catalysts with different Pd contents and are shown in Figure 5.3 to Figure 5.7. In general, higher palladium loading achieved by increasing Pd content leads to larger metal

particles and lower Pd dispersions. The TEM images of the other flame-made catalysts such as Pd/Al₂O₃, Pt/Al₂O₃, and Pt/TiO₂ can be found in Ref. [2, 4, 13], respectively. In most cases, small Pd clusters of 2-3 nm were observed. However, for Pt/SiO₂ prepared by FSP under similar conditions using platinum acetylacetonate as Pt precursor, some very large Pt particles (> 100 nm) were obtained due to incomplete evaporation [7]. The primary particle sizes of TiO₂ based on TEM analysis were consistent with those calculated from XRD. The 0.5, 1, 2, and 5 FSP show TiO₂ particle size of around 20-25 nm while that of 10FSP was around 15 nm. The presence of PdO or Pd⁰ metal was not clearly seen for the low loading catalysts (0.5-2 wt%). For 5FSP, only the small Pd particles were observed. The average clusters size of Pd around 3 nm was seen for 10FSP catalysts. The particles were confined to the TiO₂ surface.

Figure 5.8 to Figure 5.10 show the TEM micrographs of impregnated Pd on flame-made titania with Pd loading 1-5 wt%. The Pd clusters were found in spherical shape with 2.5 – 3.7 nm. The Pd clusters were smaller than 5 nm so it is possible that they could not be observed by XRD technique.

For TEM micrographs, the particle size of Pd or PdO of the flame-made catalysts was smaller than the impregnated catalysts. It may be due to well-dispersed Pd/PdO particles/clusters of the flame-made catalysts and/or the small Pd/PdO particles/clusters were covered by the formation of Ti-O groups during flame synthesis.

The TiO₂ and Pd/PdO particle size measured from TEM micrographs on the various Pd loadings of flame-made and impregnated catalysts are summarized in Table 5.2.

Table 5.2 Primary particle size of TiO₂ and Pd/PdO from TEM micrographs of flame-made and impregnated catalysts with various Pd loading

Catalyst	Primary particle size of TiO ₂ from TEM (nm)	Pd/PdO particle size from TEM micrographs (nm)
0.5FSP	22	n.d.
1FSP	23	n.d.
2FSP	24	n.d.
5FSP	20.5	2.5
10FSP	14.8	3.0
1Im-FSP	26.8	2.5
2Im-FSP	27.0	3.0
5Im-FSP	27.0	3.7

n.d. = not determined.

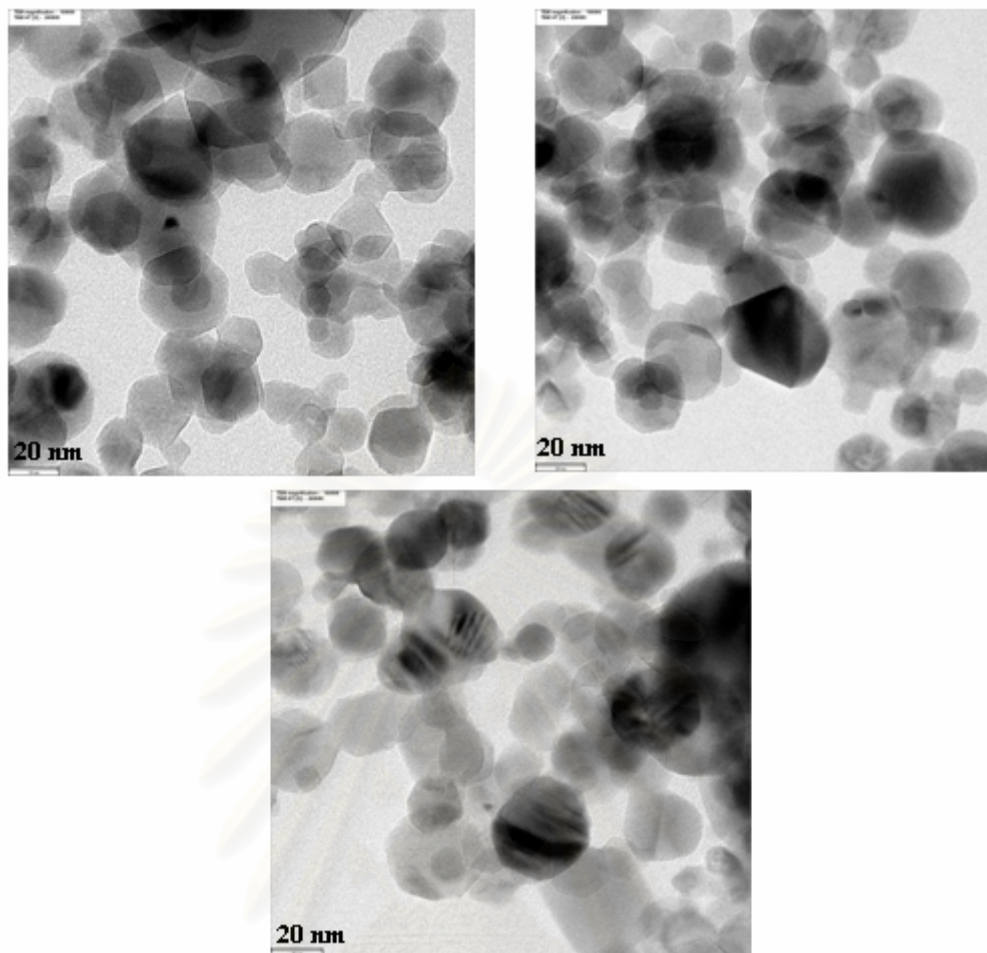


Figure 5.3 TEM micrographs of 0.5 wt% Pd/TiO₂ catalysts prepared by single-step flame synthesis (0.5FSP)

สถาบันวิทยบริการ
จุฬาลงกรณ์มหาวิทยาลัย

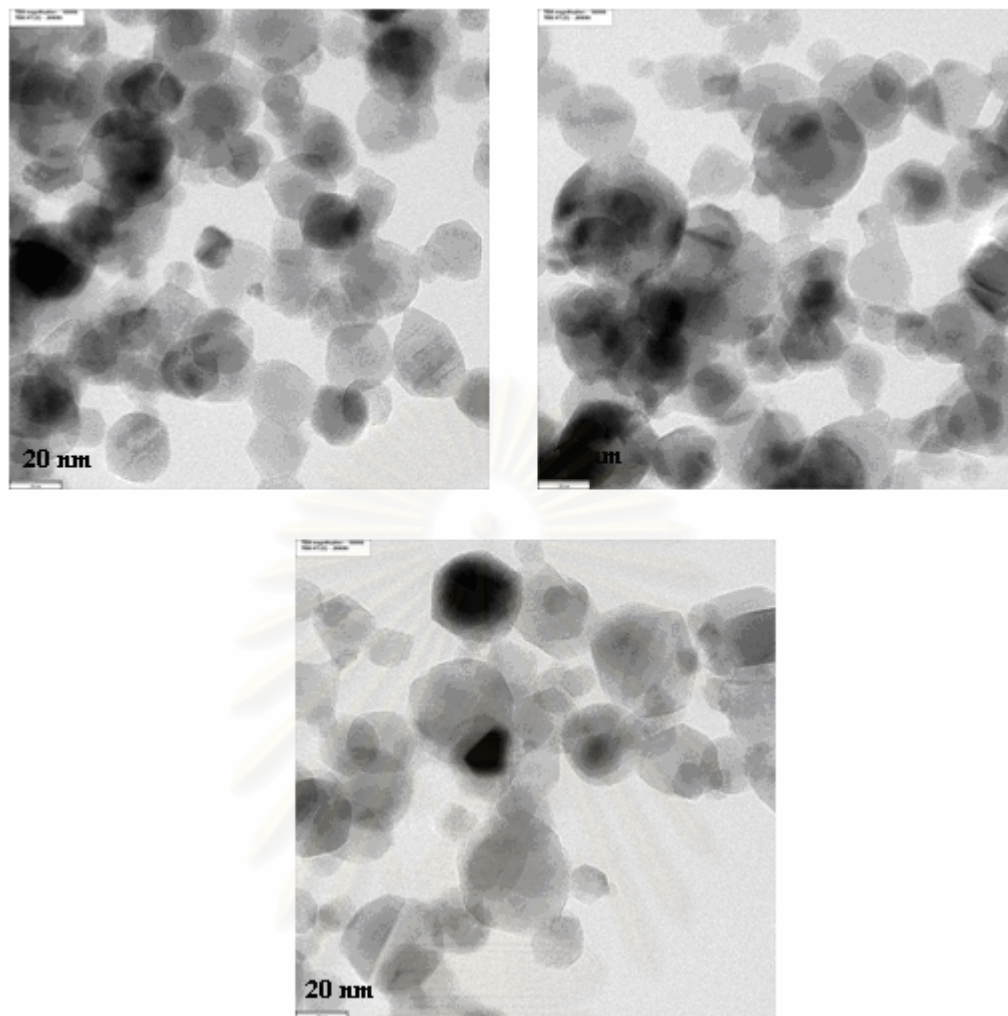


Figure 5.4 TEM micrographs of 1 wt% Pd/TiO₂ catalysts prepared by single-step flame synthesis (1FSP)

สถาบันวิทยบริการ
จุฬาลงกรณ์มหาวิทยาลัย

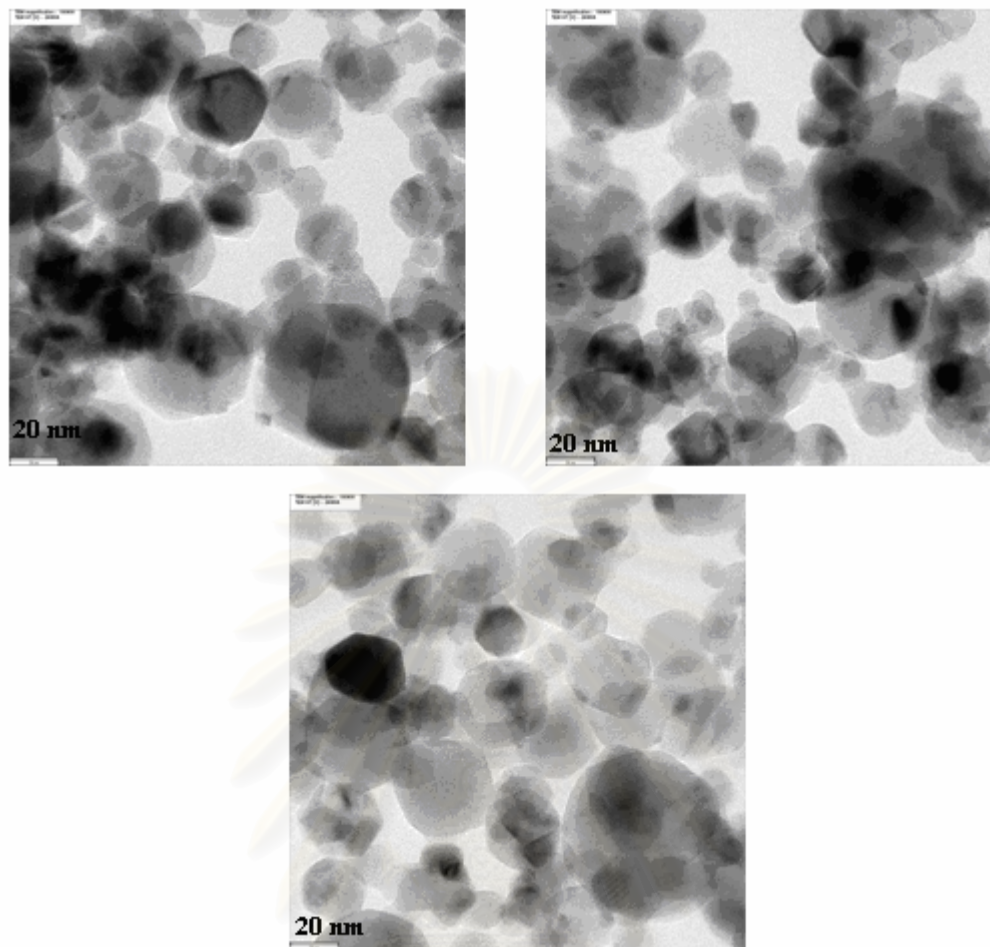


Figure 5.5 TEM micrographs of 2 wt% Pd/TiO₂ catalysts prepared by single-step flame synthesis (2FSP)

สถาบันวิทยบริการ
จุฬาลงกรณ์มหาวิทยาลัย

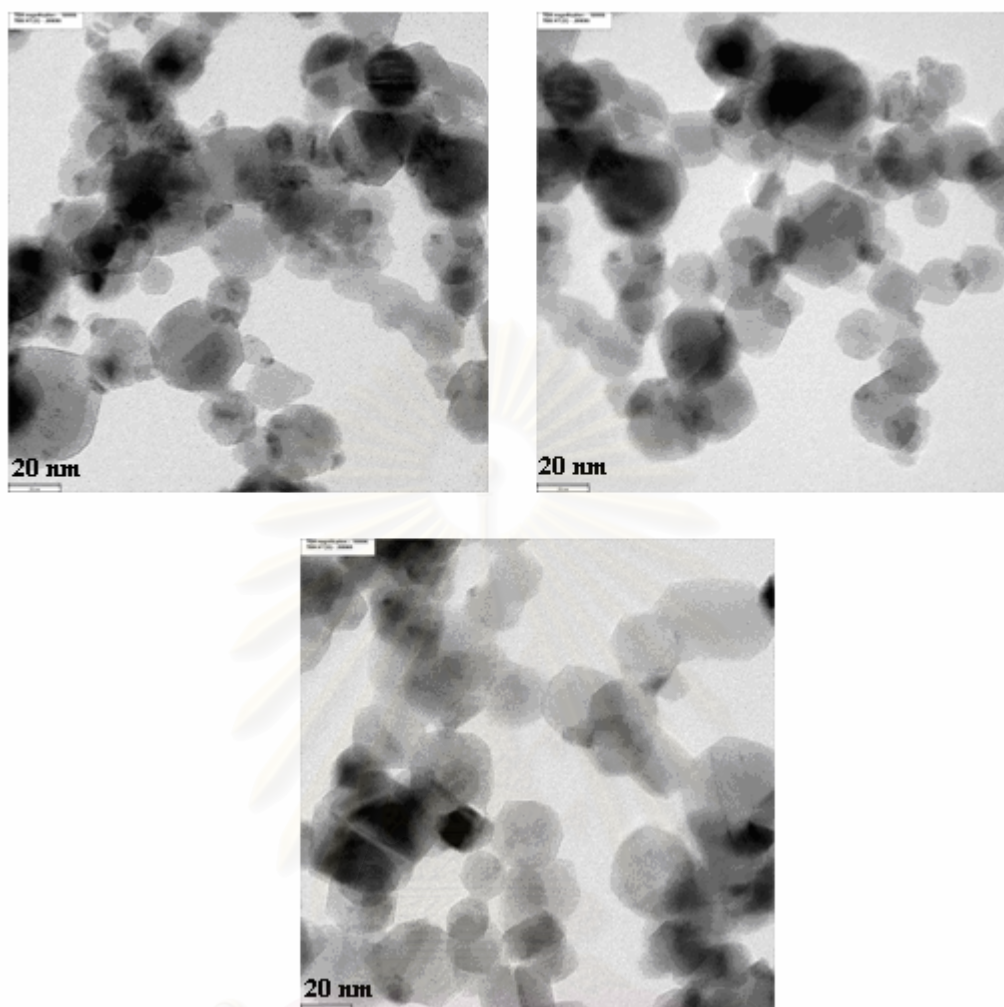


Figure 5.6 TEM micrographs of 5 wt% Pd/TiO₂ catalysts prepared by single-step flame synthesis (5FSP)

สถาบันวิทยบริการ
จุฬาลงกรณ์มหาวิทยาลัย

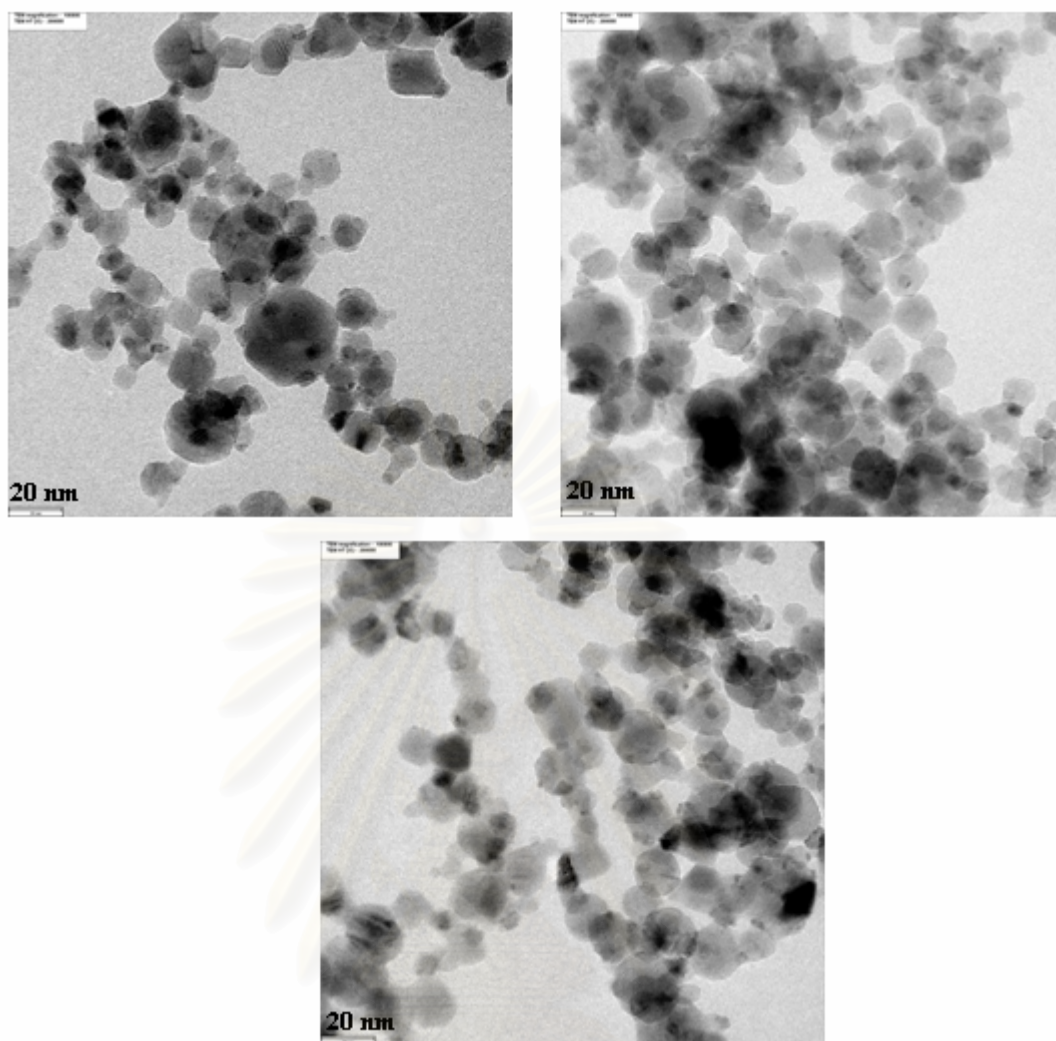


Figure 5.7 TEM micrographs of 10 wt% Pd/TiO₂ catalysts prepared by single-step flame synthesis (10FSP)

สถาบันวิทยบริการ
จุฬาลงกรณ์มหาวิทยาลัย

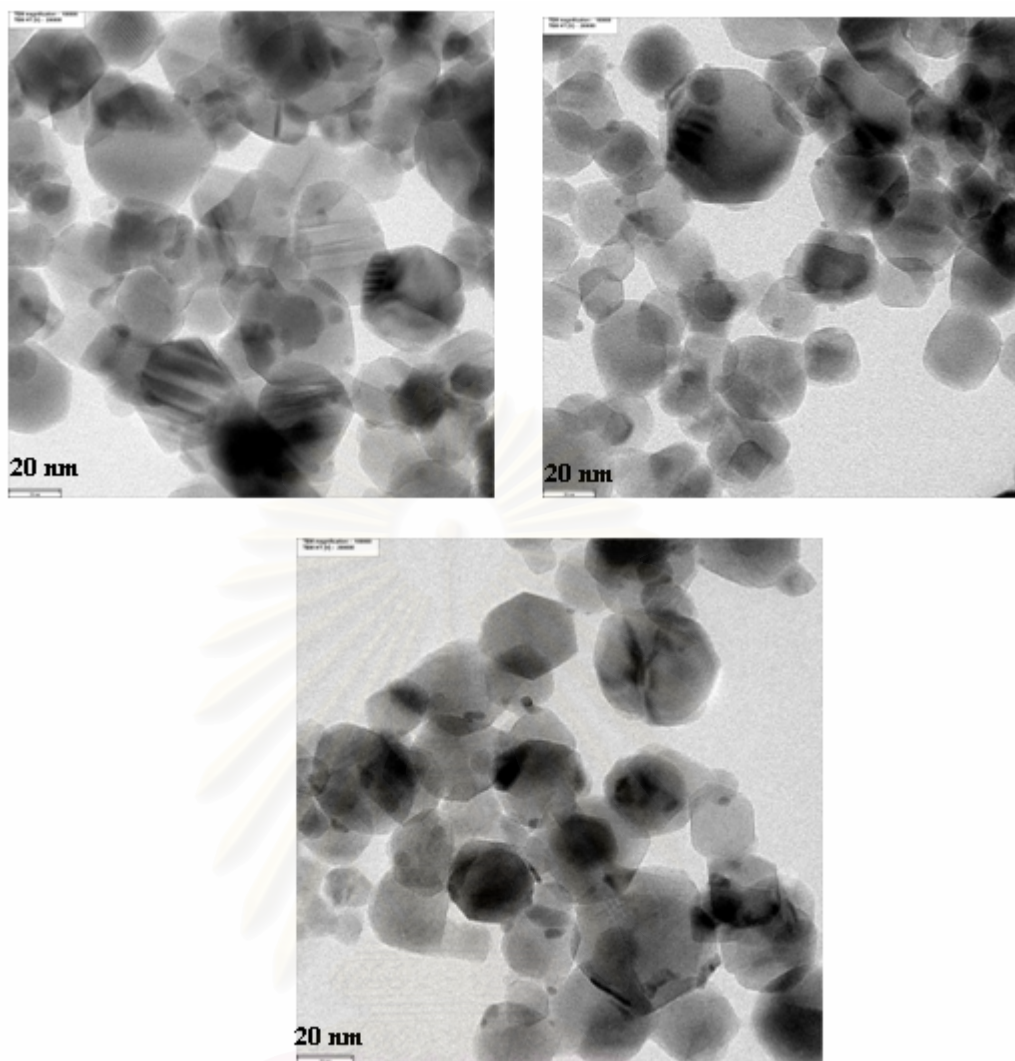


Figure 5.8 TEM micrographs of 1 wt% Pd/TiO₂ prepared by incipient wetness impregnation with flame-made TiO₂ supports (1Im-FSP)

สถาบันวิทยบริการ
จุฬาลงกรณ์มหาวิทยาลัย

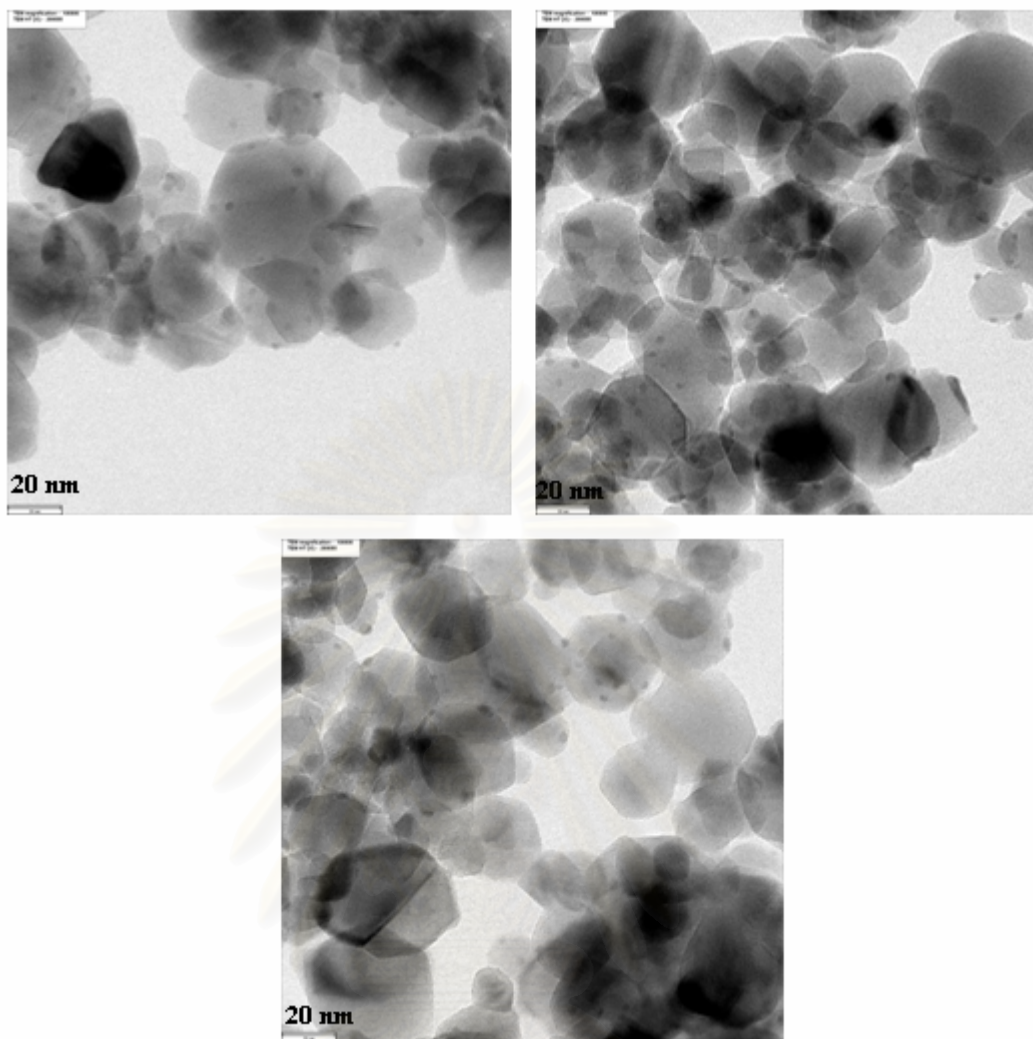


Figure 5.9 TEM micrographs of 2 wt% Pd/TiO₂ prepared by incipient wetness impregnation with flame-made TiO₂ supports (2Im-FSP)

สถาบันวิทยบริการ
จุฬาลงกรณ์มหาวิทยาลัย

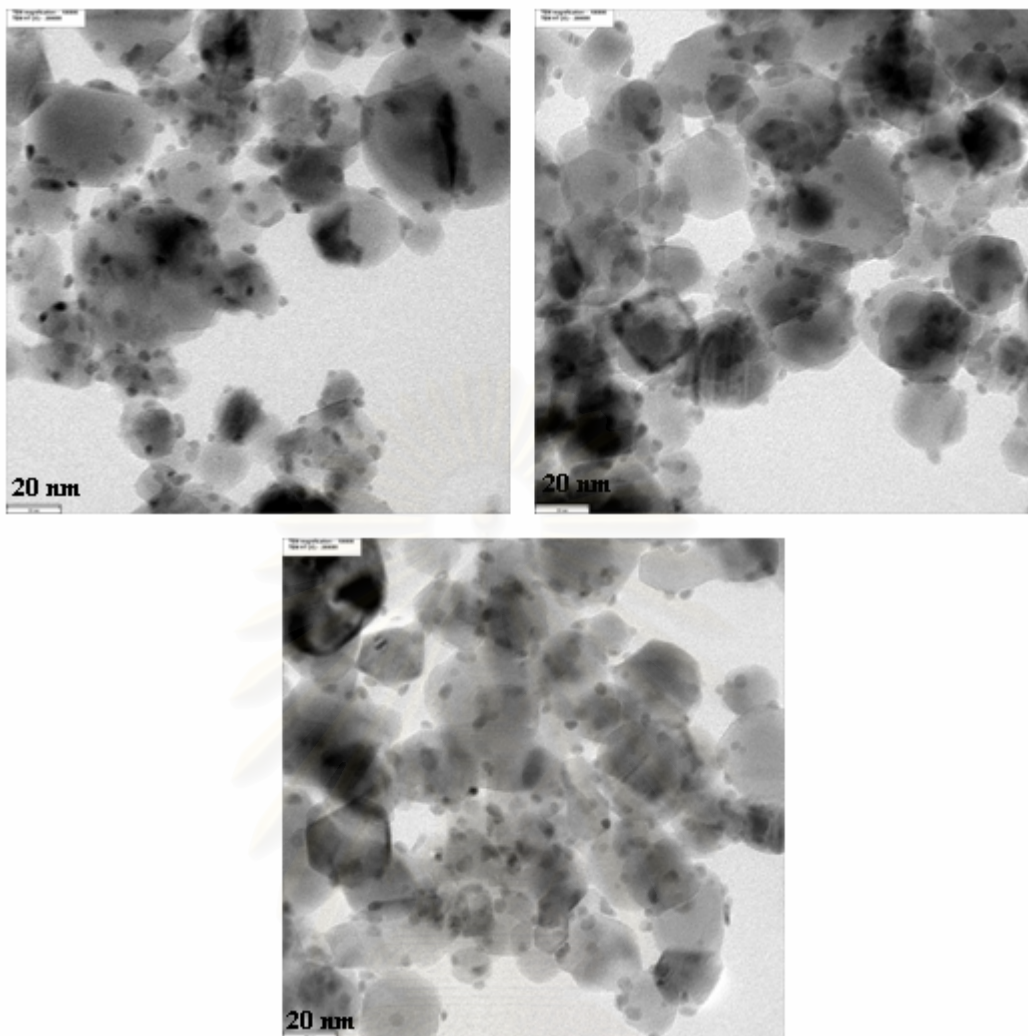


Figure 5.10 TEM micrographs of 5 wt% Pd/TiO₂ prepared by incipient wetness impregnation with flame-made TiO₂ supports (5Im-FSP)

สถาบันวิทยบริการ
จุฬาลงกรณ์มหาวิทยาลัย

5.1.1.3 N₂ Physisorption

BET surface areas, pore volume, and pore diameter of the flame-made catalysts determined from N₂ physisorption technique are shown in Table 5.3. The particle formation process of titania-supported Pd catalysts is illustrated in Figure 2.1 (Chapter 2). The vapor pressure of titania was much lower than that of Pd/PdO in the hot flame environments, and consequently titania particle formation started earlier. Further the downstream flame, at lower temperatures, Pd/PdO started to form small particles and/or deposited directly on the TiO₂ support. This particle formation mechanism was also suggested for Pd/Al₂O₃ and Pt/Al₂O₃ [2, 4]. The BET surface area of flame-made Pd/TiO₂ catalysts increased from 42.5 to 93.0 m²/g as the amount of Pd increased from 0 to 10 wt%. It is suggested that the growth of the TiO₂ particles were inhibited by Pd dopant. This result is in good agreement with the works reported by Hannemann et al. [8]. Besides, W. Y. Teoh et al. [13] found that the increase in Pt loading was found to suppress the sintering and crystallite growth of both anatase and rutile. Average pore volume of the flame-made catalysts was determined to be 0.08 – 0.18 cm³/g. It was rather constant with increasing Pd loading from 0 to 2 wt% and then increased with increasing Pd loading to 5 and 10 wt%.

The N₂ adsorption – desorption isotherms of the flame-made catalyst with Pd loading 0 – 10 wt% are shown in Figure 5.11 to Figure 5.16, respectively. According to the BET classification, isotherms of this kind belong to the isotherm of type IV describing the mesoporous material which has pore diameter between 2 and 50 nm.

The results from N₂ physisorption technique such as the BET surface area, the pore volume, and the pore size of the impregnated catalysts are shown in Table 5.3. The BET surface area of flame-made titania was 42.5 m²/g. When Pd loading increased from 1 to 5 wt%, the BET surface areas were not much different. The average pore size diameters were also nearly constant for the flame-made Pd/TiO₂ catalysts with 0.5-5 wt% Pd loading. Such results suggest that most of the Pd particles were not inside the pore of TiO₂. Moreover, it could possible be that the flame spray derived TiO₂ contained only very large pore (macropore) as seen from their isotherms so the pore volume did not change much with Pd loading. The significant increase in the BET surface area of 10FSP corresponds to the smaller crystallite size of TiO₂ obtained.

Figure 5.17 to Figure 5.19 show the N₂ adsorption – desorption isotherms of the Im-FSP catalyst. According to the BET classification, isotherms of this kind belong to the isotherm of type IV describing the mesoporous material which has pore diameter between 2 and 50 nm. The pore size distribution calculated according to the BJH equation of the impregnated catalysts show the average pore diameter in Table 5.3. The average pore sizes of impregnated catalysts increased significant from 14.9 to 23.9 nm with increased Pd loading from 1 to 5 wt%.

Table 5.3 N₂ physisorption properties of flame-made and impregnated catalysts with various Pd loading

Catalyst	N ₂ Physisorption		
	BET surface area (m ² /g)	Pore Volume (cm ³ /g)	Average Pore Diameter (nm)
TiO ₂ FSP (26 nm)	42.5	0.08	7.1
0.5FSP	51.7	0.11	7.8
1FSP	53.9	0.09	5.8
2FSP	45.6	0.08	6.6
5FSP	57.4	0.12	7.2
10FSP	93.0	0.18	6.6
1Im-FSP	48.8	0.14	14.9
2Im-FSP	44.3	0.13	18.7
5Im-FSP	42.1	0.14	23.9

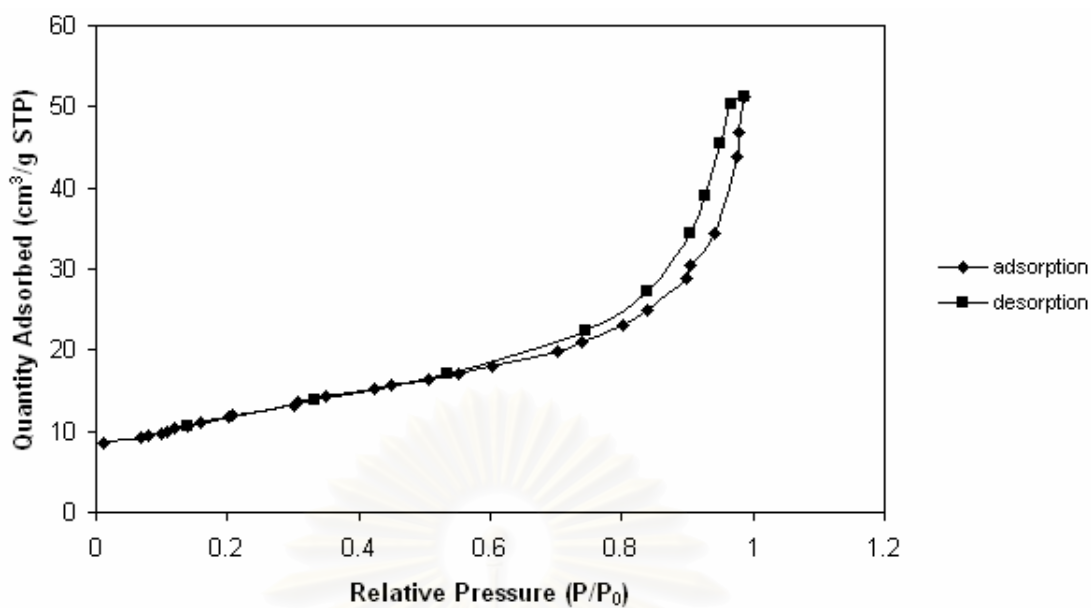


Figure 5.11 N₂ adsorption – desorption isotherms of TiO₂FSP (26 nm)

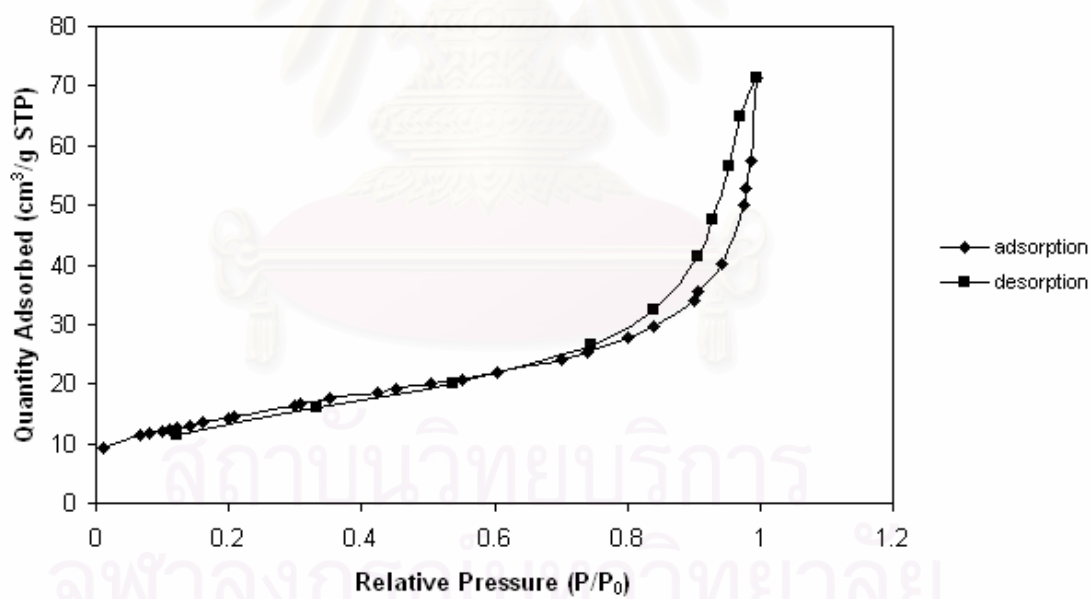


Figure 5.12 N₂ adsorption – desorption isotherms of 0.5 wt% Pd/TiO₂ catalysts prepared by single-step flame synthesis (0.5FSP)

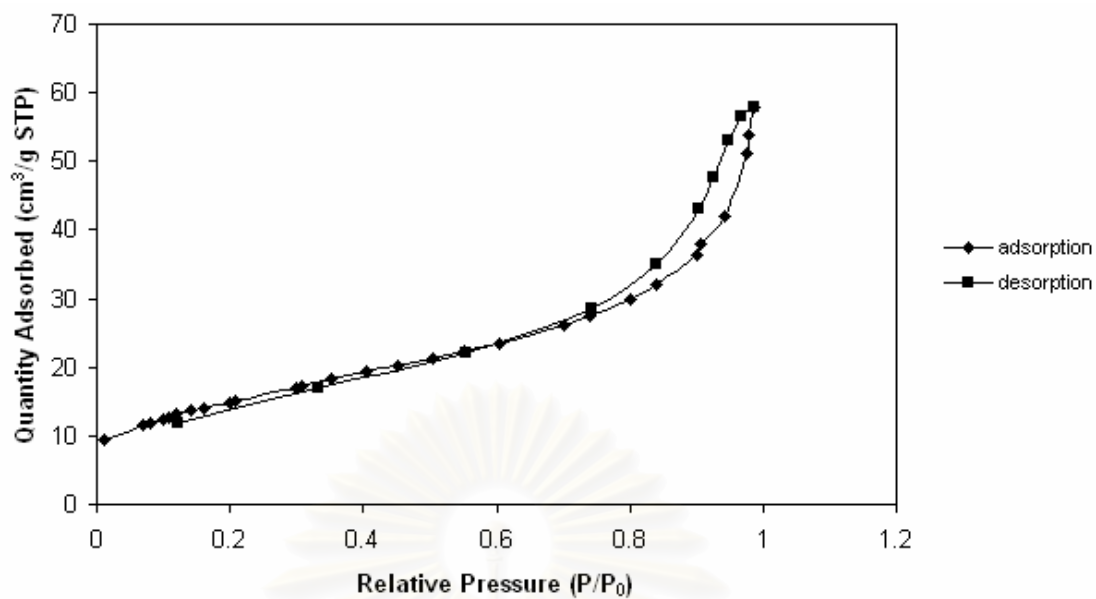


Figure 5.13 N₂ adsorption – desorption isotherms of 1 wt% Pd/TiO₂ catalysts prepared by single-step flame synthesis (1FSP)

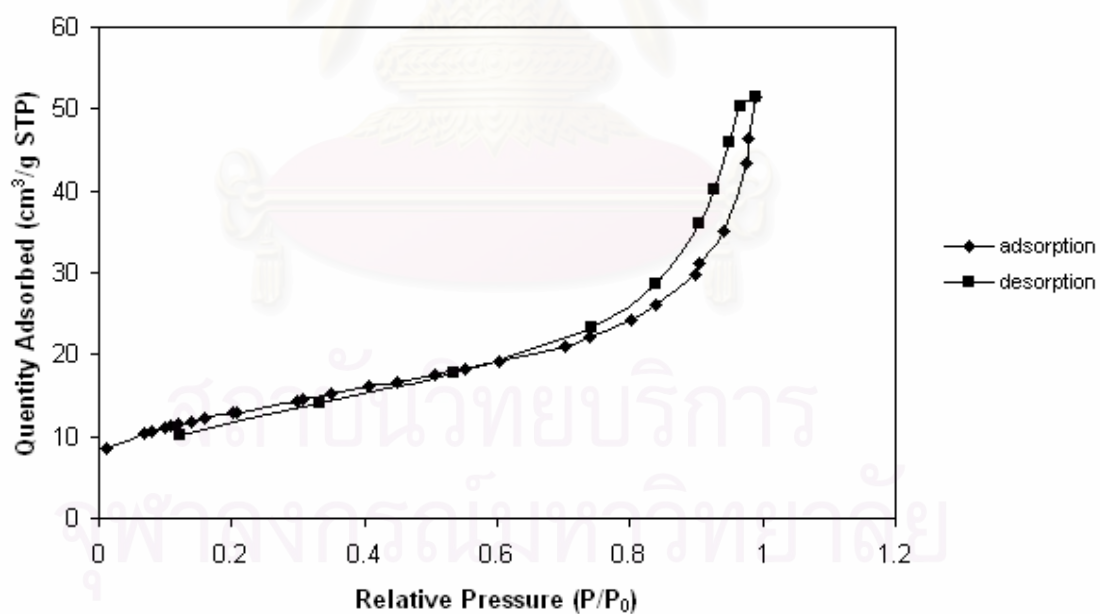


Figure 5.14 N₂ adsorption – desorption isotherms of 2 wt% Pd/TiO₂ catalysts prepared by single-step flame synthesis (2FSP)

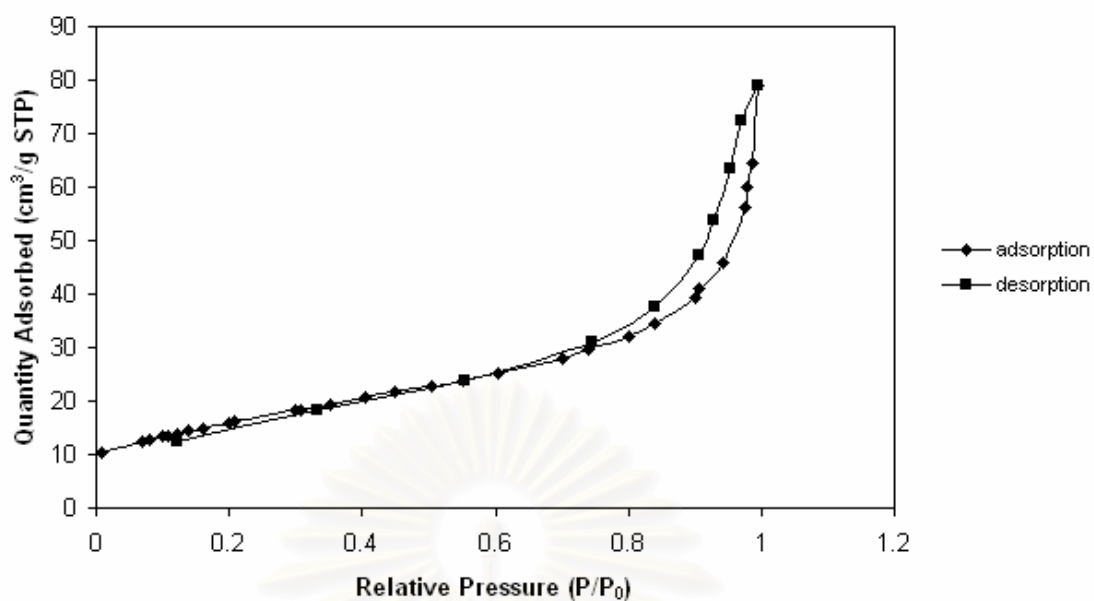


Figure 5.15 N₂ adsorption – desorption isotherms of 5 wt% Pd/TiO₂ catalysts prepared by single-step flame synthesis (5FSP)

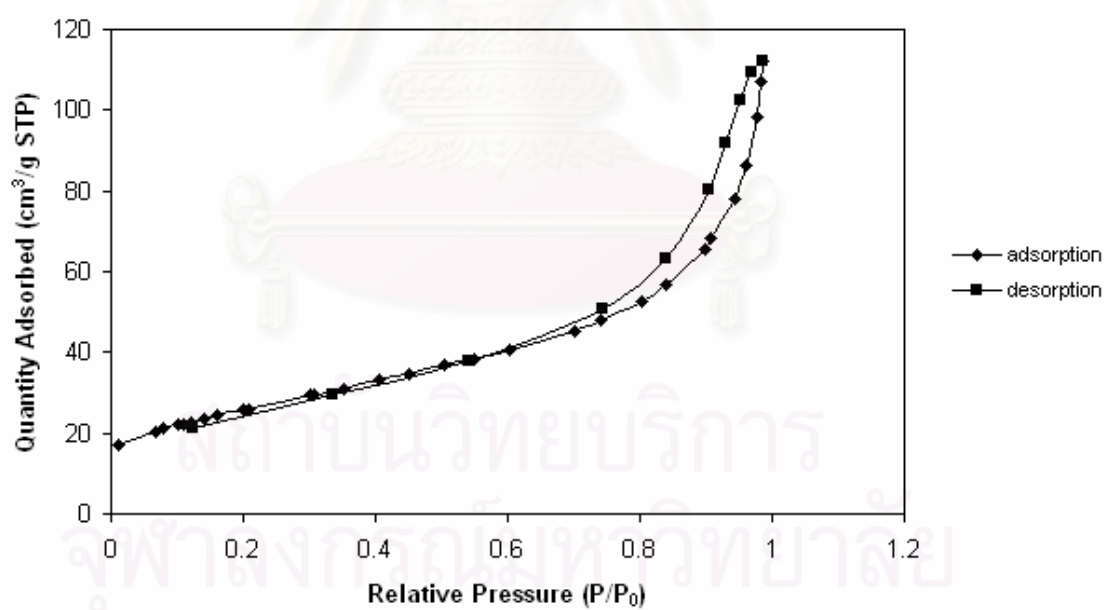


Figure 5.16 N₂ adsorption – desorption isotherms of 10 wt% Pd/TiO₂ catalysts prepared by single-step flame synthesis (10FSP)

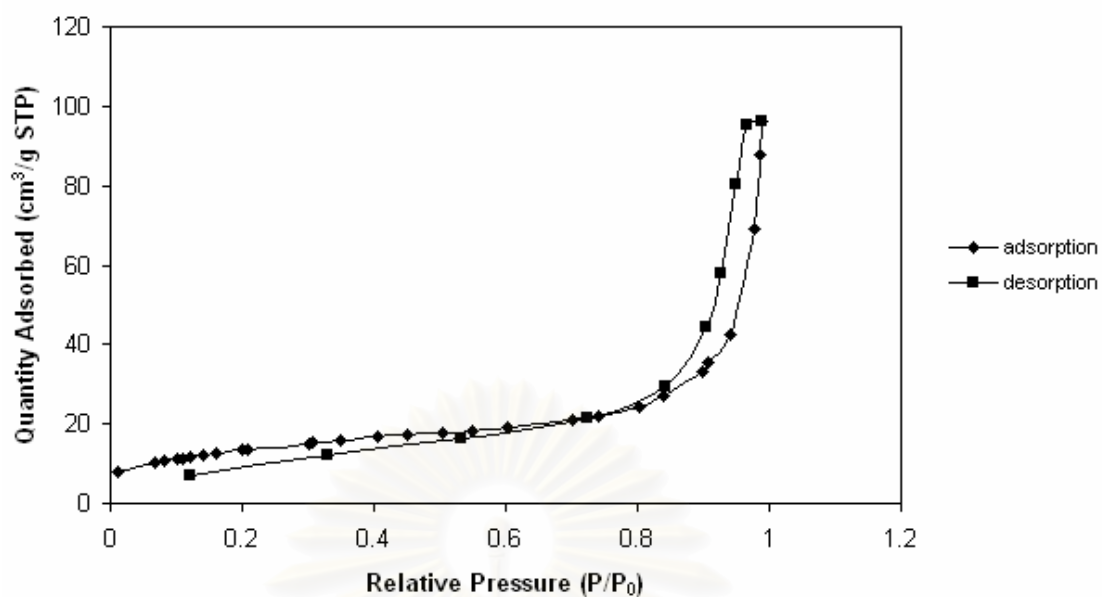


Figure 5.17 N_2 adsorption – desorption isotherms of 1 wt% Pd/TiO₂ prepared by incipient wetness impregnation with flame-made TiO₂ supports (1Im-FSP)

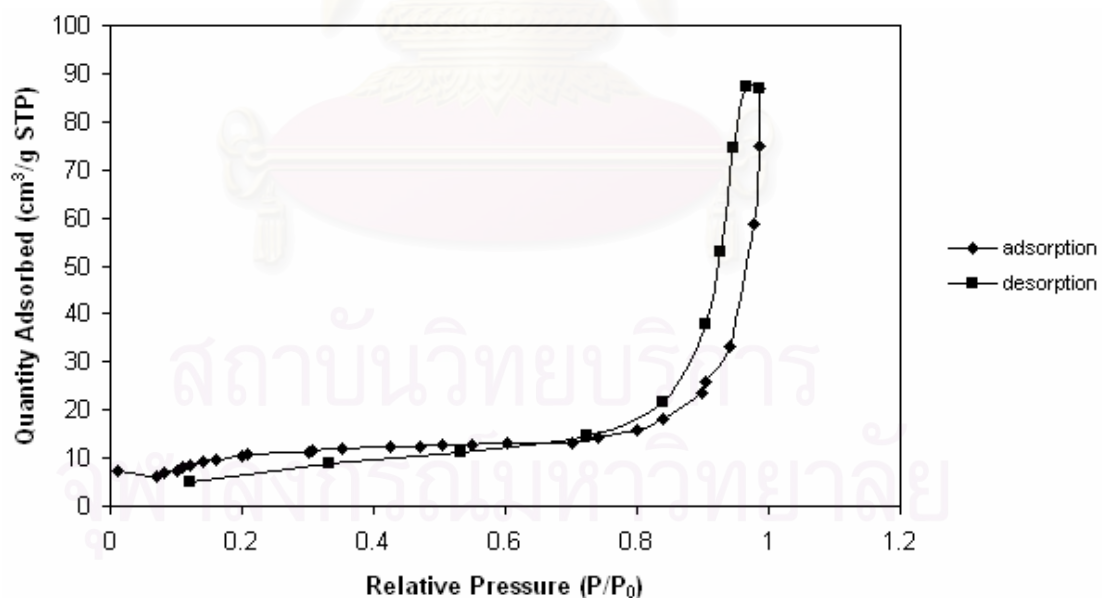


Figure 5.18 N_2 adsorption – desorption isotherms of 2 wt% Pd/TiO₂ prepared by incipient wetness impregnation with flame-made TiO₂ supports (2Im-FSP)

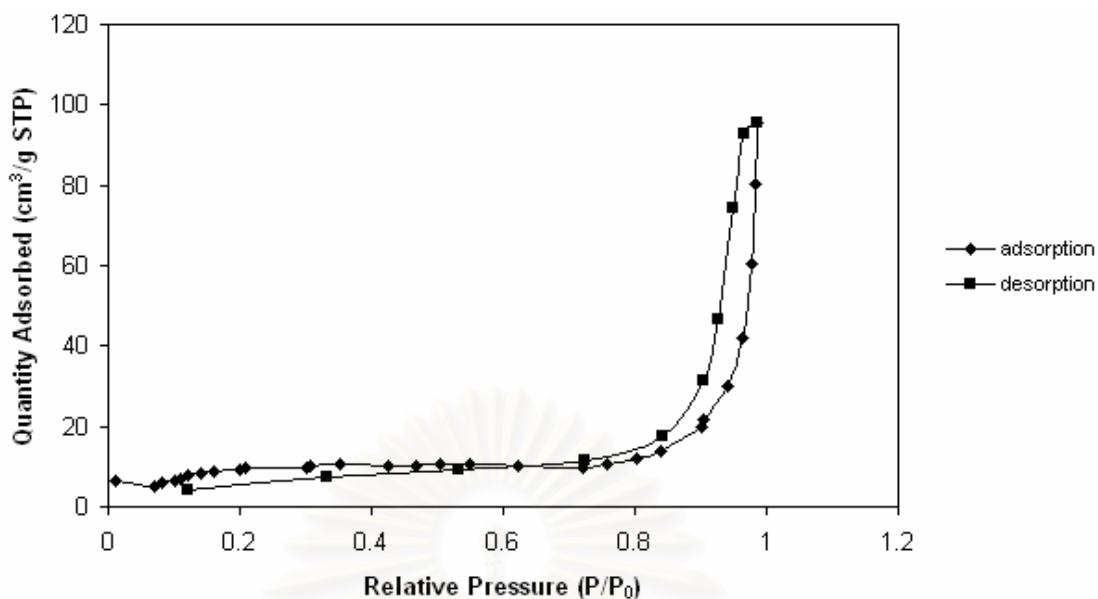


Figure 5.19 N_2 adsorption – desorption isotherms of 5 wt% Pd/TiO₂ prepared by incipient wetness impregnation with flame-made TiO₂ supports (5Im-FSP)

The BET surface areas of the flame-made catalysts increased from 0.5 to 10 wt% whereas those of the impregnated catalysts slightly decreased. Decreasing of the BET surface areas with increasing metal loading is typical for supported metal catalysts prepared by conventional impregnation method due to pore blockage of Pd/PdO clusters. For the flame-made catalysts, it is suggested that the Pd dopants inhibited the growth of TiO₂ particle resulting in an increase in BET surface area with increasing Pd loading.

5.1.1.4 CO-Pulse Chemisorptions

The relative amounts of active surface Pd metal on the catalyst samples were calculated from CO chemisorption experiments at room temperature. The calculation of Pd active sites was based on the assumption that one carbon monoxide molecule adsorbs on one palladium site [4, 28]. Table 5.4 shows the amounts of CO chemisorption on the flame-made catalysts. The active sites of the flame-made catalysts increased from 0.9×10^{18} to 9.9×10^{18} site/g-catalyst while %Pd metal dispersion decreased from 43.2 to 3.2 % as the Pd contents increased from 0.5 to 10

wt%. For TEM micrographs of 0.5FSP to 2FSP, Pd/PdO particles were not observed so it is in good agreement with the high values of %Pd metal dispersion from CO chemisorption. The average Pd⁰ metal particle sizes calculated from CO chemisorption were found to be 3 – 35 nm.

The amounts of CO chemisorption on the impregnated catalysts are given in Table 5.4. The active sites increased from 1.7×10^{18} to 13.9×10^{18} site/g catalyst corresponding to the increasing Pd contents from 1 to 5 wt% as Pd metal dispersion decreased from 6.2% to 3.8%. The Pd⁰ metal particle sizes calculated from CO chemisorption were found to be increased from 18 to 29 nm as Pd loading 1-5 wt%. The particle sizes were much larger than those based on TEM analyses. The low metal dispersion and overestimation of metal particle sizes in supported Pd catalysts based on CO chemisorptions may be due to the formation of Ti-O groups covering the small palladium particles. This was inhibited the adsorption of CO molecules, so the CO chemisorptions uptake decreased. Otherwise, CO chemisorptions suppression may be due to strong interactions between Ti and Pd in an alloy form [29].

The results from AAS indicated that the actual Pd loadings on TiO₂ from single-step flame spray synthesis were less than that expected by 54% for 0.5FSP and 38% for 10FSP. The actual Pd loadings for the impregnated catalysts, however, were not much different from those expected. The reason for low amount of Pd being loaded to the FSP catalysts may be because of the high liquid flow rate and low oxygen dispersion used. Some of the liquid may not be in good contact with flame.

Table 5.4 The amounts of CO chemisorption of flame-made and impregnated catalysts with various Pd loading

Catalyst	CO uptake ($\times 10^{-18}$ molecule CO/g-catalyst)	%Pd from AAS	%Pd dispersion	$d_p Pd^0$ (nm)
0.5FSP	0.9	0.23	43.2	3
1FSP	1.8	0.49	34.6	3
2FSP	1.9	0.95	27.3	4
5FSP	2.8	2.10	6.6	17
10FSP	9.9	6.20	3.2	35
1Im-FSP	1.7	0.76	6.2	18
2Im-FSP	2.4	1.50	4.6	24
5Im-FSP	13.9	4.20	3.8	29

5.1.1.5 X-ray Photoelectron Spectroscopy (XPS)

XPS is a useful technique to determine the composition of element on surface and electronic state. XPS results such as binding energies and surface composition of flame-made and impregnated catalysts are shown in Figure 5.20, Figure 5.21, and summarized in Table 5.5. For the FSP catalysts, XPS peaks for Pd 3d_{5/2} were not clearly seen except that of 10 FSP where the binding energy of Pd 3d_{5/2} was observed at 336.4 eV with FWHM 1.583 eV. The binding energy of Pd 3d_{5/2} in 10FSP was close to binding energy of PdO, which would be expected between 335.4-337.5 eV. It is speculated that oxygen atoms from TiO₂ were adsorbed on Pd. There was also probably a change of electronic state of Pd in 10FSP catalyst. On the other hand,

Pd $3d_{5/2}$ binding energy recorded for 5Im-FSP was typical for metallic Pd (335.0-335.4 eV) [31]. However, FWHM > 2 suggests that more than one species of Pd could be presented on the catalyst.

Atomic ratio of Pd and Ti for all the flame-made catalysts were very small indicating that low amounts of Pd were presented on the TiO_2 surface corresponding to the low amount of CO uptakes. This result is consistent with BET surface area results which were found that Pd were deposited outside the pores of flame-made TiO_2 . Therefore, Pd particles may be probably covered by Ti-O groups during one-step flame spray pyrolysis.

For the impregnated catalysts, atomic ratios of Pd/Ti were more than those of the flame-made catalysts, this results corresponded to the results from CO chemisorption. It is likely that during the preparation of catalysts by impregnation method, Pd metals may be deposited on TiO_2 whereas those from flame spray synthesis, Pd may be covered by Ti-O groups.

When considered atomic ratios of Ti/O for high Pd loadings (5-10 wt%), the Pd/ TiO_2 catalysts that prepared by one-step flame spray pyrolysis showed much lower values than those of the impregnated catalysts. It is indicated that larger oxygen atoms were on the FSP catalyst surface than the impregnated catalysts especially for high Pd loaded catalysts. The model of Pd/ TiO_2 catalysts from one-step flame spray pyrolysis and impregnation method is suggested in Figure 5.22.

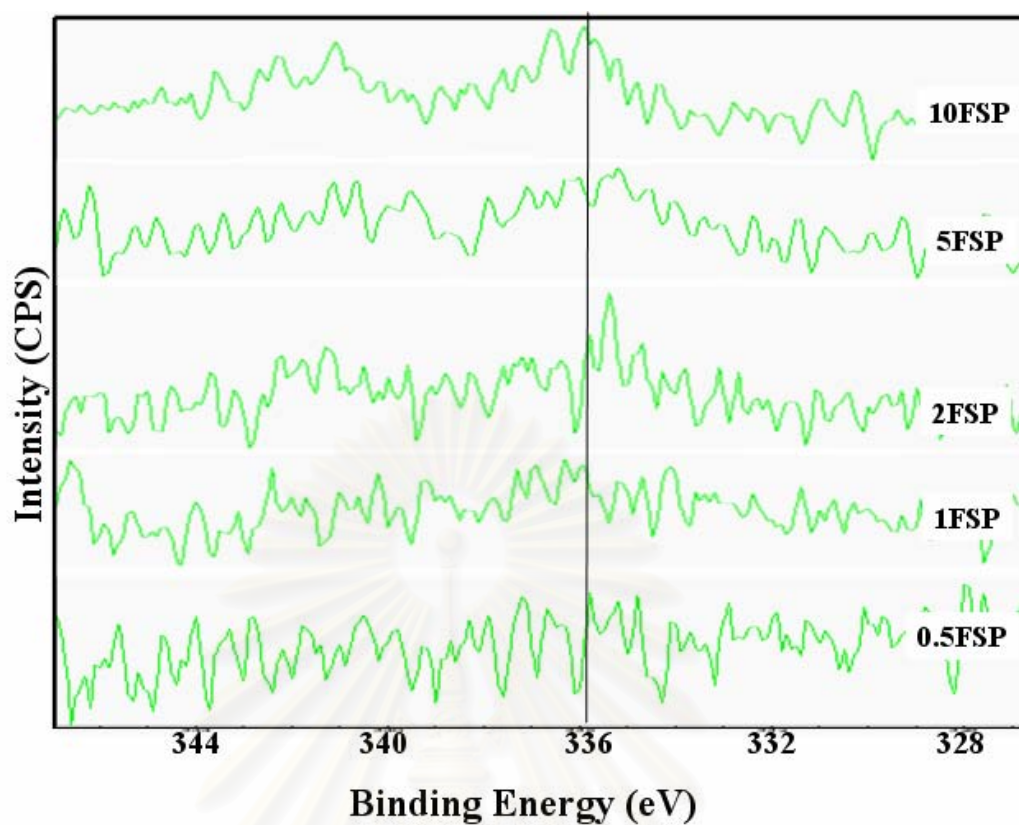


Figure 5.20 Binding energies of various Pd loading flame-made catalysts

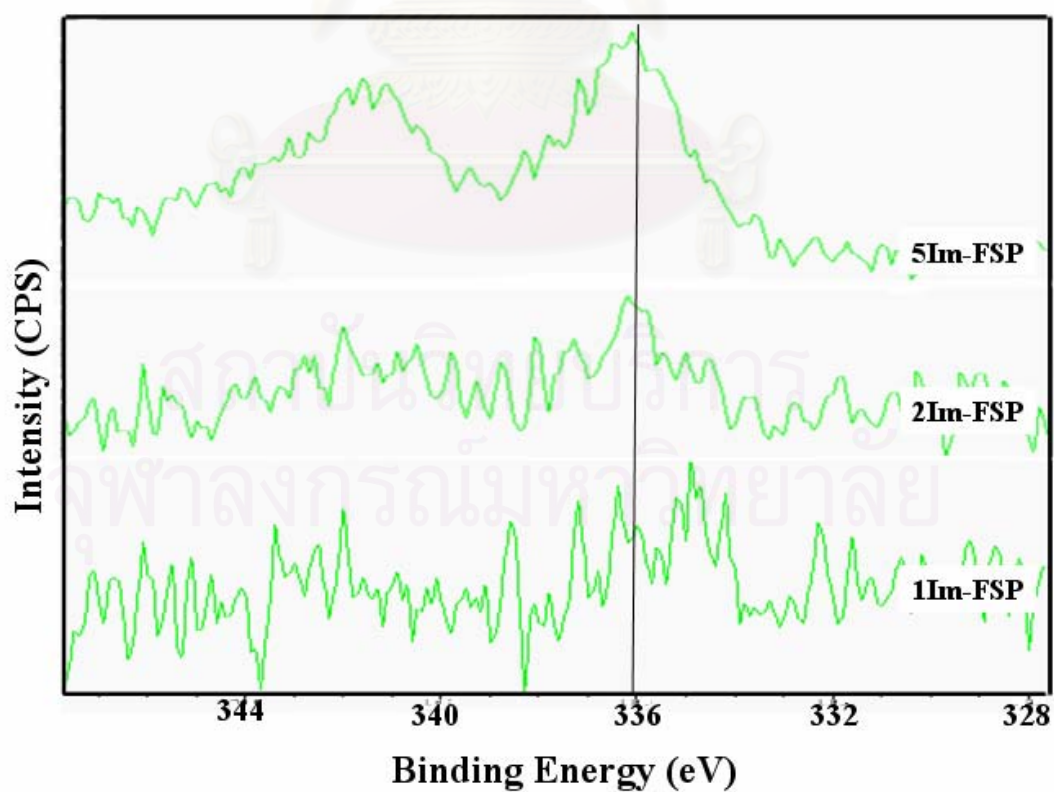


Figure 5.21 Binding energies of various Pd loading impregnated catalysts

Table 5.5 Binding energies and surface composition from XPS of flame-made and impregnated catalysts with various Pd loading

Catalyst	Pd 3d _{5/2}		Atomic ratio	
	B.E. (eV)	FWHM	Pd/Ti	Ti/O
0.5FSP	n.d.	n.d.	n.d.	n.d.
1FSP	n.d.	n.d.	n.d.	n.d.
2FSP	n.d.	n.d.	0.0073	0.0788
5FSP	n.d.	n.d.	0.0116	0.0556
10FSP	336.4	1.583	0.0635	0.0405
1Im-FSP	n.d.	n.d.	0.0038	0.0728
2Im-FSP	n.d.	n.d.	0.0178	0.0979
5Im-FSP	335.6	2.152	0.1016	0.1779

n.d. = not determined

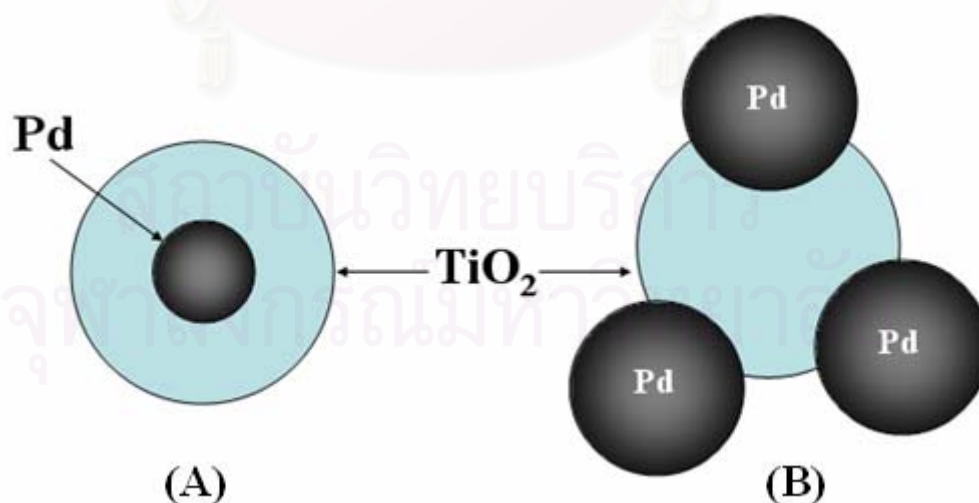


Figure 5.22 Suggested model for Pd/TiO₂: prepared by (A) one-step flame spray pyrolysis (B) two-step Impregnation (Pd were loaded on flame-made TiO₂ support)

5.1.2 Selective 1-Heptyne Hydrogenation Study

The catalytic behavior of the flame-made catalysts was investigated in liquid-phase selective hydrogenation in a batch system in a 50 ml autoclave reactor. The reaction was operated with high stirring rate (1000 rpm) in order to eliminate the external mass transfer of hydrogen problem. The reaction was carried out using 2% v/v heptyne in toluene at 30°C and 1 bar H₂ pressure for 5-40 minute. The products were analyzed by gas chromatography with flame ionization detector (FID) using GS-alumina column.

The concentrations of 1-heptyne versus time-on-stream with various Pd loadings of flame-made catalysts are shown in Figure 5.23. The hydrogenation rate of 1-heptyne on the flame-made catalysts clearly increased when increased Pd loading to 2 wt% but increasing Pd loading up to 10 wt% has no more effect to hydrogenation rate of 1-heptyne. Figure 5.24 and Figure 5.25 show the concentration of 1-heptene and concentration of 1-heptane versus time-on-stream of all the flame-made catalysts. The selectivities of 1-heptene increased with increasing Pd loading from 0.5 wt% to 2 wt% and remained relatively constant when Pd loading was increased to 10 wt%.

The specific activity (TOF) of various Pd loading catalyst is given in Table 5.6. Turnover frequencies (TOF) is defined as mole of product per mole of metal per time. TOFs of the flame-made catalysts decreased from 66.3 to 15.4 s⁻¹ with increased 0.5-10 wt% Pd loading probably due to increasing of Pd particle size and/or stronger interaction of Pd and TiO₂. The Pd particles may also be covered by Ti-O groups during one-step flame spray pyrolysis resulting in low CO chemisorption measurements. The other supported Pd catalysts such as flame-made Pd/SiO₂ [30] also give TOF value decrease when increasing Pd particle size but flame-made Pd/Al₂O₃ [2] is difference, increasing Pd particle size resulted in increasing TOF value.

The concentrations of 1-heptyne versus time on stream of the impregnated catalysts are shown in Figure 5.26. The hydrogenation rate of 1-heptyne significantly increased when increased Pd loading. Figure 5.27 and Figure 5.28 show the concentration of 1-heptene and concentration of 1-heptane versus time on stream of all the impregnated catalysts. The selectivities of 1-heptene was slightly increased when increased Pd loading. TOFs of the impregnated catalysts also decreased with

increasing Pd loading suggesting that TOF decrease with increasing of Pd particle size.

For better comparison, the concentrations of 1-heptyne versus time on stream of all the catalysts are shown in Figure 5.29. The hydrogenation rate of 1-heptyne of the flame-made catalysts was higher than the impregnated catalysts. Figure 5.30 and Figure 5.31 show the concentration of 1-heptene and concentration of 1-heptane versus time on stream of all the catalysts. The selectivities of 1-heptene of flame-made catalysts were higher than the impregnated catalysts. TOFs of the flame-made catalysts are higher than the impregnated catalysts at equal amount of Pd loading probably due to support interaction during one-step flame spray pyrolysis.

The flame-made catalyst with low Pd loading (2 wt%) showed the hydrogenation rate of 1-heptyne similar to high Pd loading (5 wt%) from impregnation method. Moreover it should be noted that 2FSP had lower active site but it exhibited higher TOF value than 5Im-FSP.

When considered hydrogenation rate of 1-heptyne, all the one-step synthesized FSP catalysts showed higher activity than the impregnated ones except 0.5FSP that exhibited relatively low hydrogenation activity due to low amount of Pd present and very small Pd particle size. It is considered that single-step flame spray synthesis is more suitable than impregnation synthesis for selective 1-heptyne hydrogenation. Liquid-phase selective hydrogenation of alkyne on supported Pd catalysts may be depend on many factors such as Pd particle size, SMSI between metal and support, etc.

Table 5.6 Specific activity (TOFs, s^{-1}) on the various Pd loading flame-made and impregnated catalysts

Catalyst	TOF (s^{-1})
0.5FSP	66.3
1FSP	68.9
2FSP	75.7
5FSP	54.1
10FSP	15.4
1Im-FSP	45.9
2Im-FSP	43.4
5Im-FSP	10.2

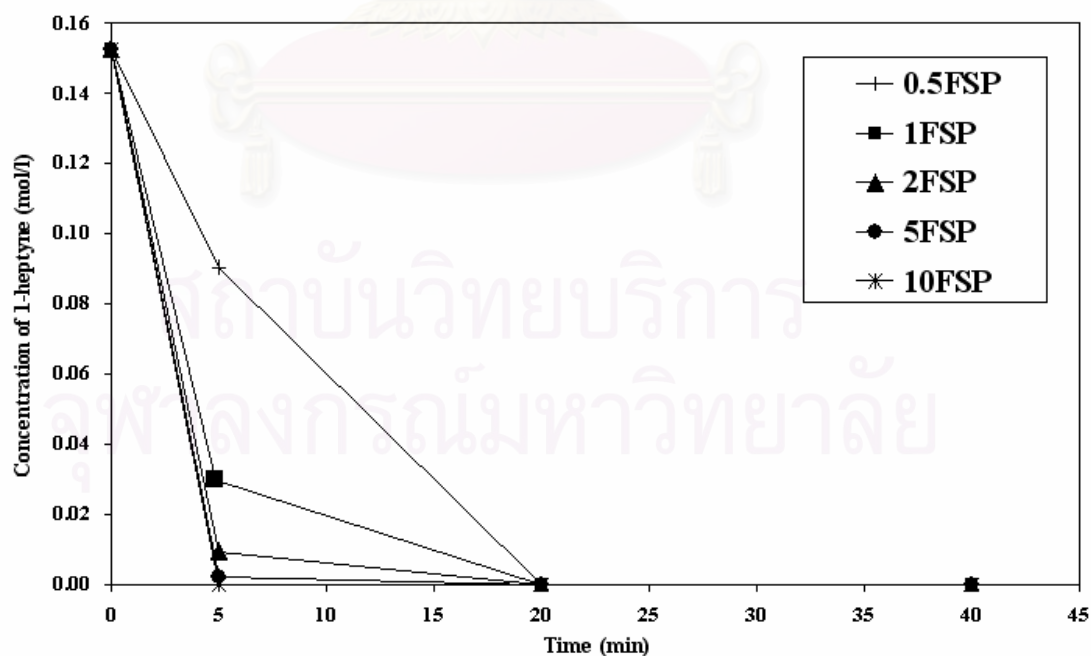


Figure 5.23 Time on stream with concentration of 1-heptyne on flame-made Pd/TiO₂ catalysts prepared in single-step with Pd loading 0.5, 1, 2, 5, and 10 wt%

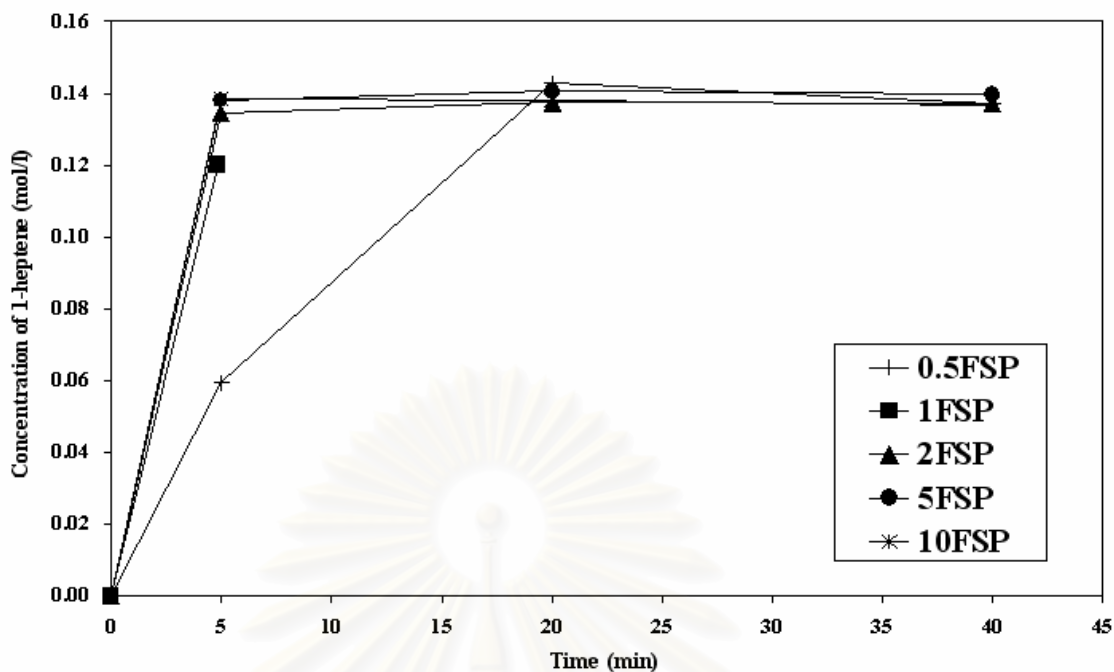


Figure 5.24 Time on stream with concentration of 1-heptene on flame-made Pd/TiO₂ catalysts prepared in single-step with Pd loading 0.5, 1, 2, 5, and 10 wt%

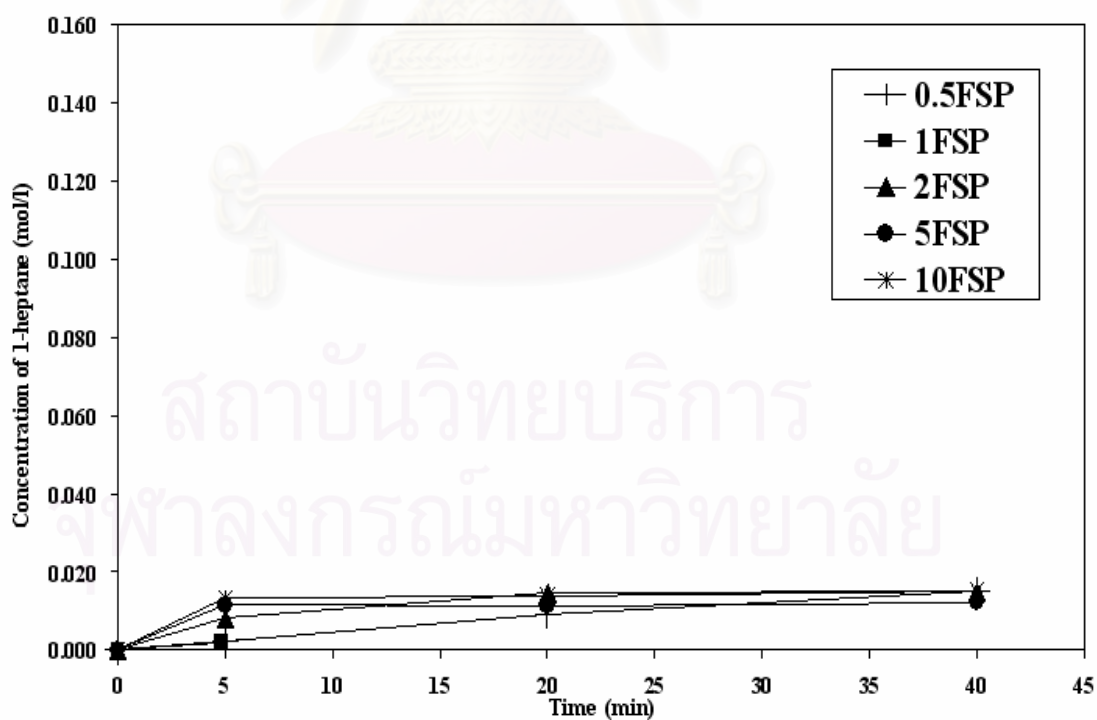


Figure 5.25 Time on stream with concentration of 1-heptane on flame-made Pd/TiO₂ catalysts prepared in single-step with Pd loading 0.5, 1, 2, 5, and 10 wt%

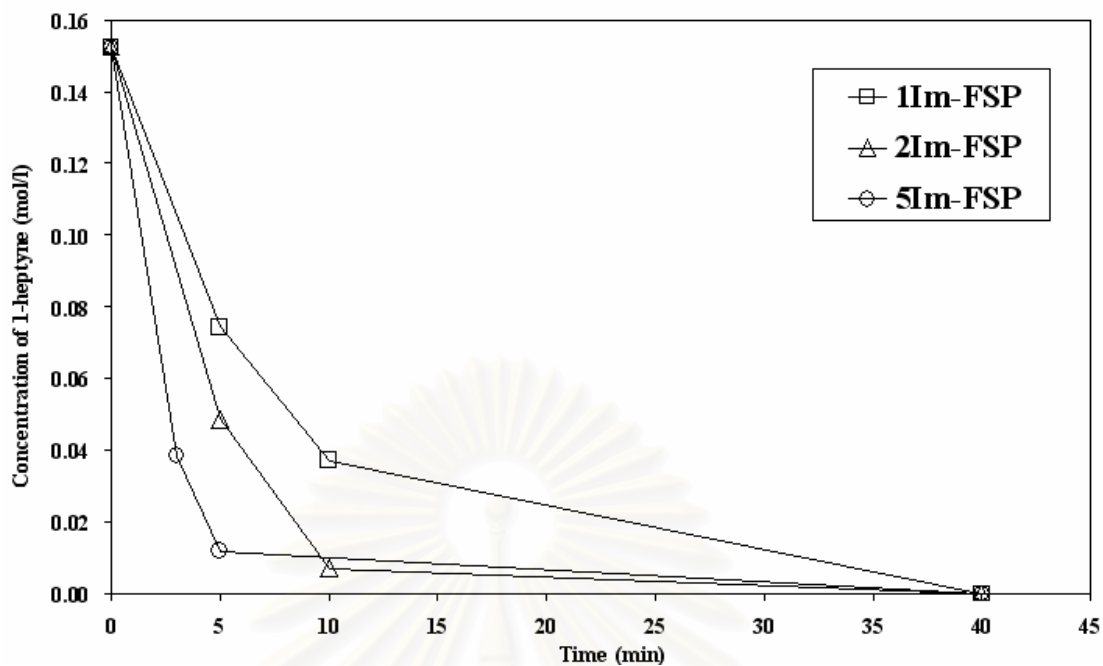


Figure 5.26 Time on stream with concentration of 1-heptyne on Pd catalysts prepared on flame-made TiO_2 supports by incipient wetness impregnation with Pd loading 1, 2, and 5 wt%

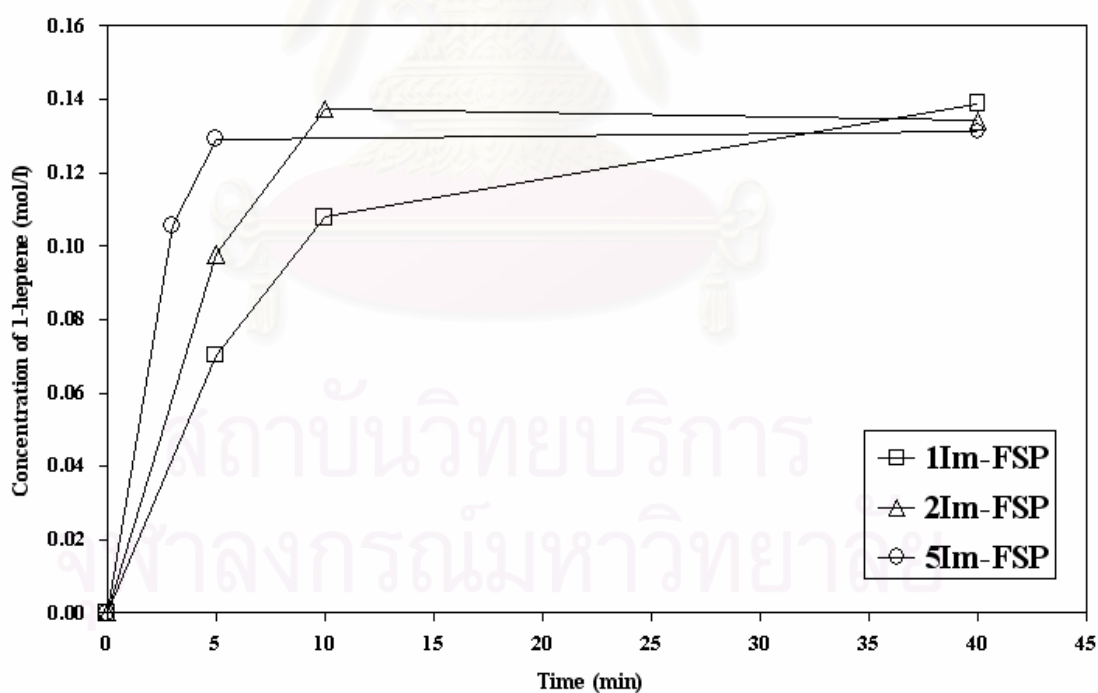


Figure 5.27 Time on stream with concentration of 1-heptene on Pd catalysts prepared on flame-made TiO_2 supports by incipient wetness impregnation with Pd loading 1, 2, and 5 wt%

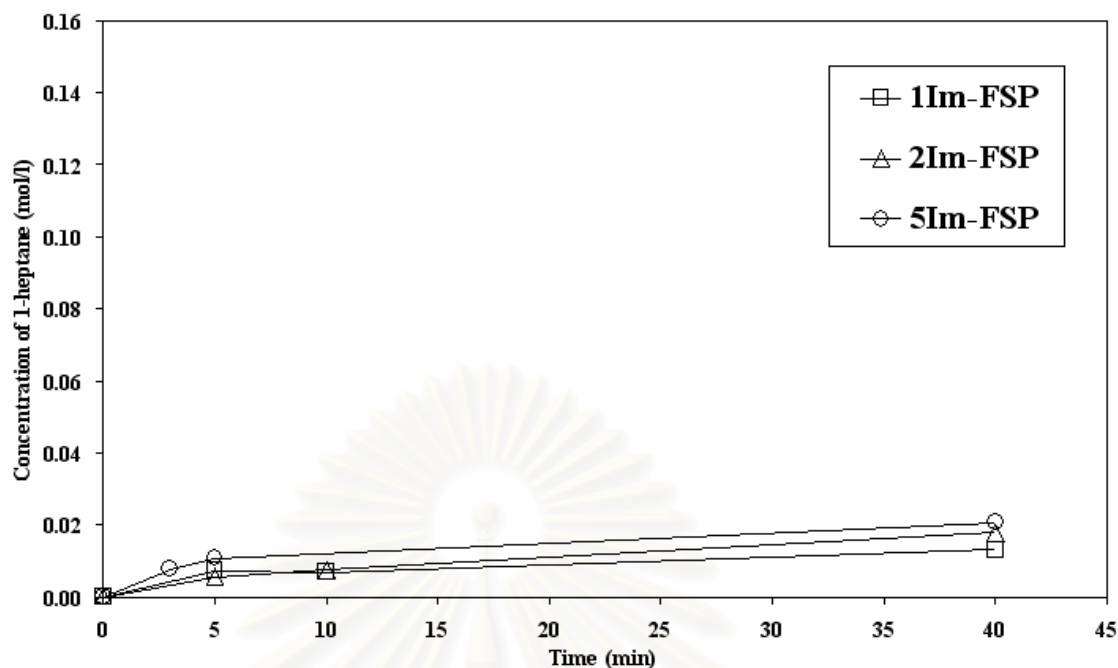


Figure 5.28 Time on stream with concentration of 1-heptane on Pd catalysts prepared on flame-made TiO_2 supports by incipient wetness impregnation with Pd loading 1, 2, and 5 wt%

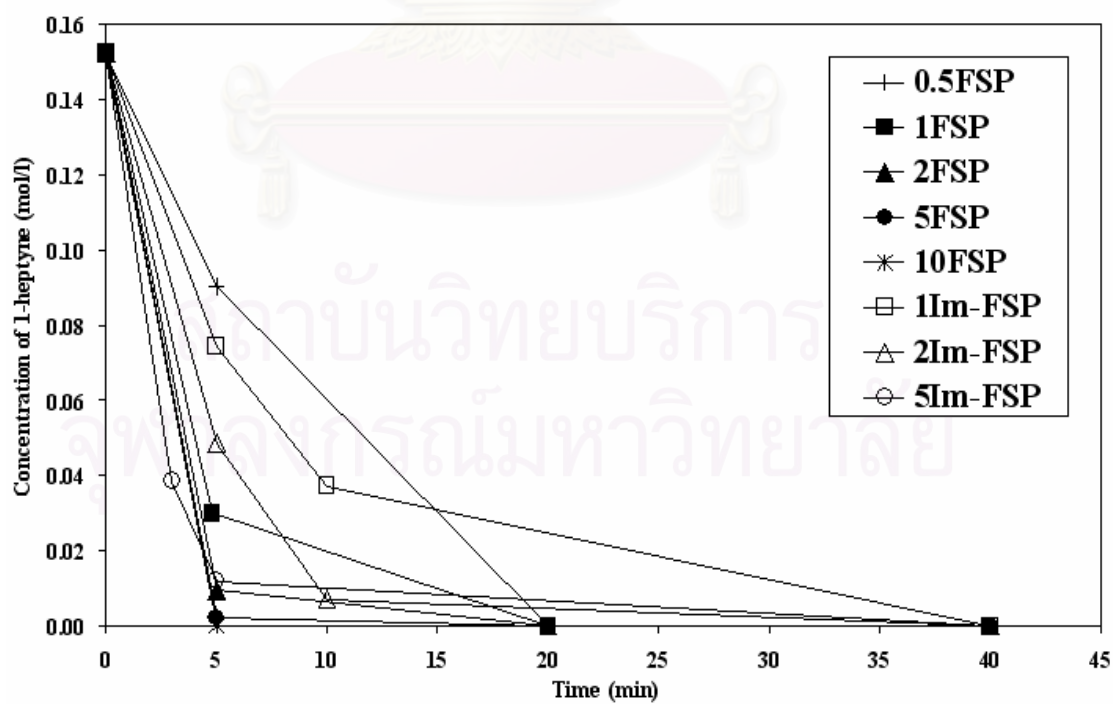


Figure 5.29 Time on stream with concentration of 1-heptyne on various Pd loading of flame-made and impregnated catalysts

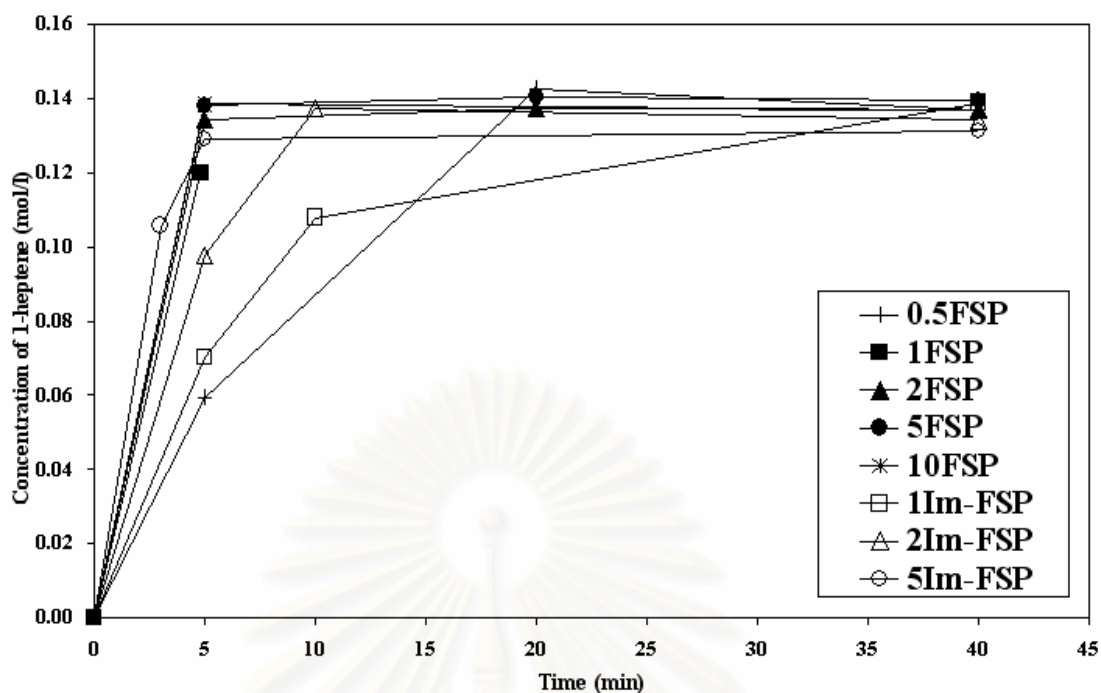


Figure 5.30 Time on stream with concentration of 1-heptene on various Pd loading of flame-made and impregnated catalysts

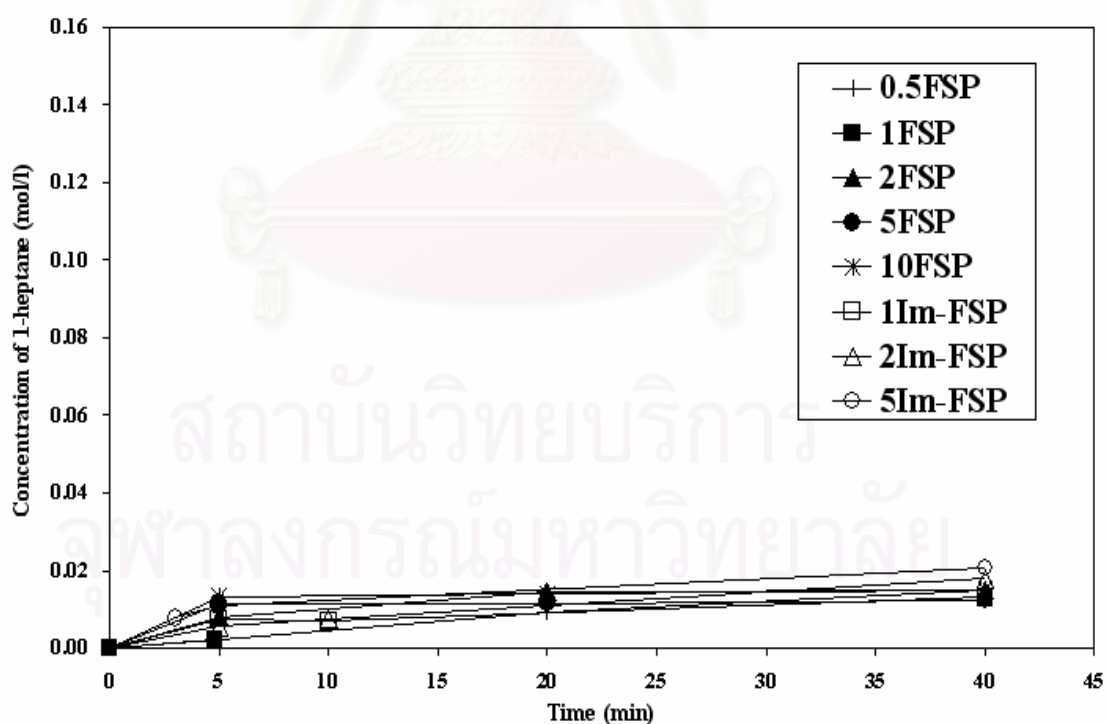


Figure 5.31 Time on stream with concentration of 1-heptane on various Pd loading of flame-made and impregnated catalysts

5.2 The Effect of TiO₂ Crystallite Size on the Properties of Pd/TiO₂ Catalysts

5.2.1 Characterization of the Catalysts

5.2.1.1 X-ray Diffraction (XRD)

The XRD patterns of flame-made 5 wt% Pd/TiO₂ catalysts with various crystallite sized are shown in Figure 5.32. All the samples exhibited XRD characteristic peak of anatase titania at 25°(major), 37°, 48°, 55°, 56°, 62°, 71°, and 75° , while the XRD peaks of rutile phase were observed at 28°(major), 36°, 42°, 57°. The XRD peaks for PdO were also observed at 33° for the 5FSP15.7 and 5FSP-24.6 catalysts samples.

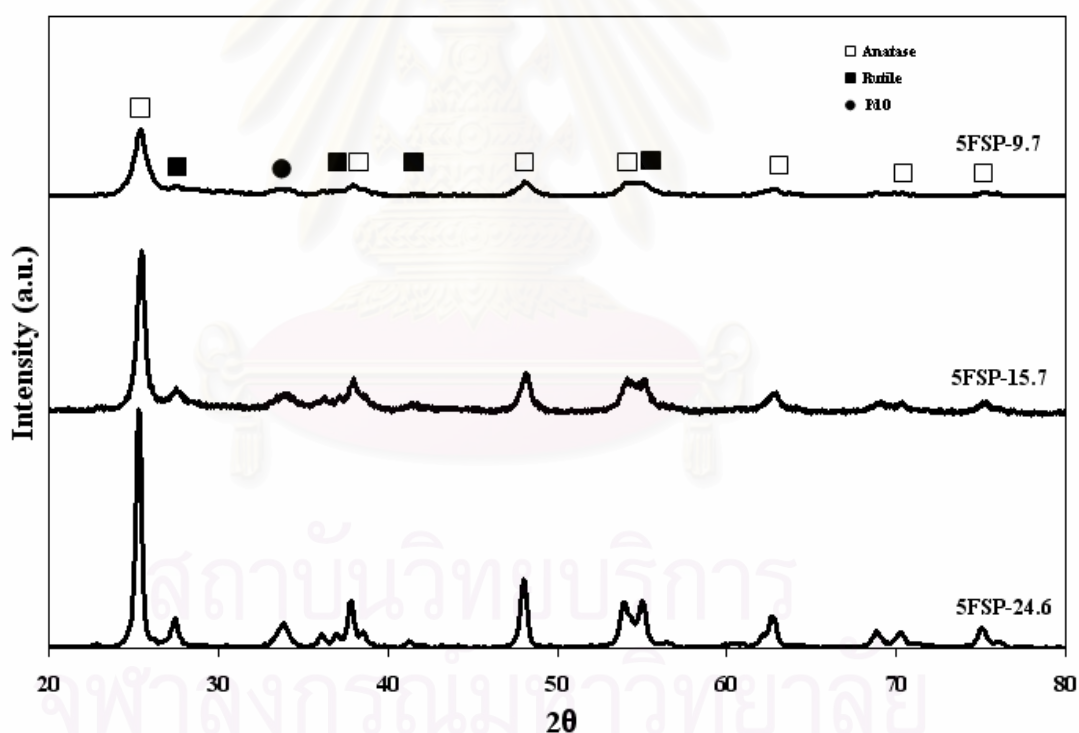


Figure 5.32 XRD patterns of 5 wt% Pd/TiO₂ catalysts prepared by single-step flame synthesis with average crystallite sizes of 9.7, 15.7, and 24.6 nm

The results of XRD analysis such as the crystallite size of anatase TiO₂ from flame and impregnated-made catalysts, PdO and composition of anatase and rutile phase are shown in Table 5.7. The crystallite size of the flame-made catalysts

increased from 9.7 to 24.6 nm. It was also found that %rutile increased from 2.3 % to 13.2% with the increasing of TiO₂ crystallite size from 9.7 nm to 24.6 nm. It is considered that rutile phase composition was affected by crystallite size of flame-made titania. This result is in good agreement with H. Chang et al. [27], who reported that the transformation of anatase to rutile was enhanced with increasing precursor concentration. The increasing of precursor concentration resulted in the increasing of average particle diameter of TiO₂ during synthesis of titania nanoparticles in flame spray pyrolysis. This would be due to the increasing of atomic concentration of atom in gas-phase, which led to the increasing of metal atoms collisions and sintering.

Preparation of Pd/TiO₂ by one-step flame spray pyrolysis with TiO₂ crystallite size of 24.6 nm resulted in the formation of PdO as seen from XRD results in Figure 5.32. The PdO crystallite size of Pd/TiO₂-15.7 nm and Pd/TiO₂-24.6 nm were 4.9 and 6.0 nm, respectively, while the XRD peaks for PdO or Pd⁰ metal were not observed for other flame-made Pd/TiO₂ catalyst with smaller size (9.7 nm). This was probably due to the low amount of Pd content, and/or their crystallite size was smaller than XRD detectable limit.

Table 5.7 XRD analysis results and phase composition of flame-made and impregnated catalysts with various TiO₂ crystallite sizes

Catalyst	Diameter of anatase TiO ₂ from XRD (nm)	Diameter of PdO from XRD (nm)	% Anatase	% Rutile
5FSP-9.7 ^a	9.7	n/a	97.7	2.3
5FSP-15.7 ^a	15.7	4.9	90.4	9.6
5FSP-24.6 ^a	24.6	6.0	86.8	13.2
5Im-FSP-9.8 ^b	9.8	n/a	95.9	4.1
5Im-FSP-15 ^b	15.0	n/a	91.3	8.7
5Im-FSP-26 ^b	25.8	n/a	90.5	9.5
5Im-nano ^b	9.0	n/a	98.5	1.5
5Im-P25 ^b	25.0	n/a	79.0	21.0
5Im-micron ^b	100.0	n/a	97.0	3.0

^a as-prepared

^b the catalysts were reduced in H₂ at 30°C for 2 h

The XRD patterns of all Pd/TiO₂-Im-FSP catalysts with various crystallite sizes after reduction in H₂ at 30°C for 2 h are shown in Figure 5.33. Impregnated catalysts exhibited XRD characteristic peaks of anatase phase of titania at 25°(major), 37°, 48°, 55°, 56°, 62°, 71°, and 75° 2θ. XRD peaks for rutile phase appeared at 28°(major), 36°, 42°, 57° 2θ. The peak of Pd⁰ was not observed for all impregnated-made Pd supported on flame made supports after reduction at 30°C. The result suggests that the Pd is probably highly dispersed or its average particle size is smaller than XRD detectable limit.

For the impregnation-made Pd/TiO₂ catalysts, the crystallite size of TiO₂ and %rutile was in a good agreement with the value measured from flame-made catalysts. This result indicates that the present of Pd with Ti atom in flame does not affected the crystallization of TiO₂.

Physical properties of Pd supported on commercial TiO₂ are also given in Table 5.7. The %rutile TiO₂ increased in the order of 5Im-P25 > 5Im-micron > 5Im-nano, while the crystallite size of TiO₂ increased in the order of 5Im-nano > 5Im-P25 > 5Im-micron.

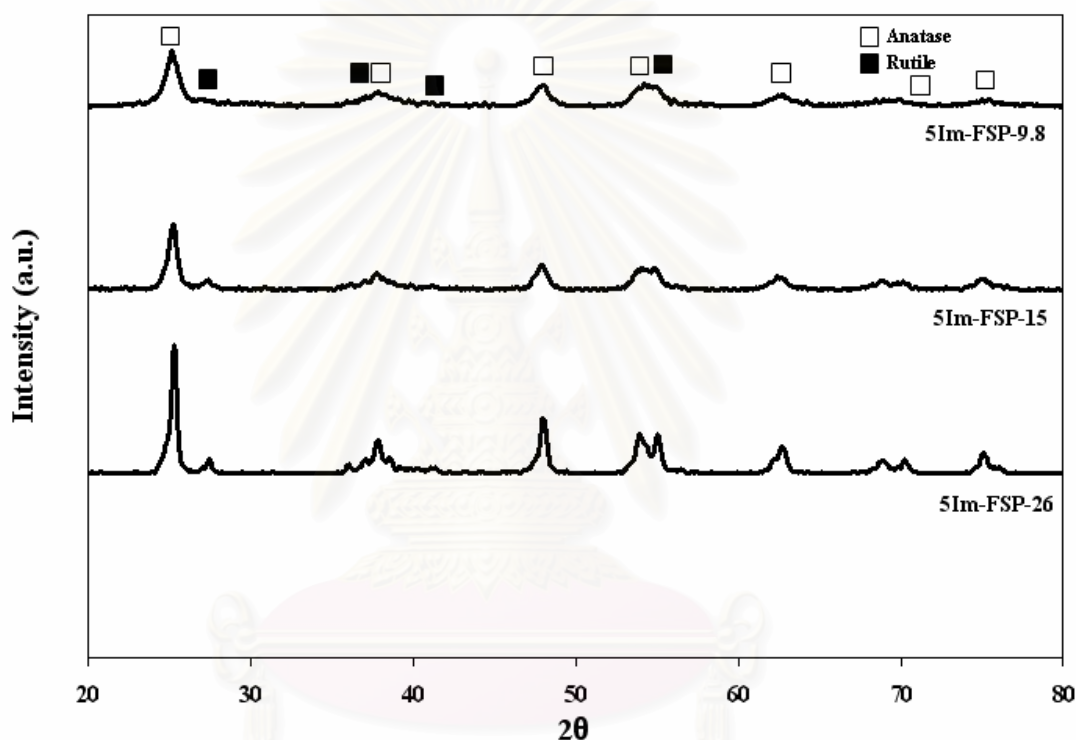


Figure 5.33 XRD patterns of 5 wt% Pd/TiO₂ catalysts prepared by incipient wetness impregnation with flame-made TiO₂ supports average crystallite sizes of 9.8, 15, and 26 nm after reduction in H₂ at 30°C for 2 h

5.2.1.2 Transmission Electron Microscopy (TEM)

TEM micrographs of the flame-made 5 wt% Pd/TiO₂ catalysts with different TiO₂ crystallite size are shown in Figure 5.34 to 5.36. The primary particles with spherical and polyhedral shapes with average size around 9.5 to 24.6 nm were observed for flame-made Pd/TiO₂ catalysts. These values were consistent with those calculated from XRD, indicates that the obtained TiO₂ crystals are single crystal. The spherical PdO/Pd⁰ clusters with approximately size around 1.0-3.5 nm were confined on surface of TiO₂ supports. The crystallite size of PdO/Pd⁰ clusters increased from 1 to 3.5 nm with increasing of the crystallite size of titania.

Figure 5.37 to 5.39 show the TEM micrographs of 5 wt% Pd/TiO₂ catalysts prepared by incipient wetness impregnation of palladium nitrate on the flame-made TiO₂ supports with average crystallite sizes of 9.8, 15, and 26 nm, respectively. The Pd clusters were found in spherical shape with sizes around 3.2 – 3.7 nm. The Pd clusters were smaller than 5 nm so it is possible that they could not be observed by XRD technique. The TEM micrographs of reference catalysts (5Im-nano, 5Im-P25 and 5Im-micron) are also shown in Figure 5.40 to Figure 5.42. The Pd deposits are approximately 3.9-8.3 nm. It is considered that Pd/PdO particle size increased with increasing crystallite size of titania.

The particle size of TiO₂ and Pd/PdO measured from TEM micrographs on the flame-made and impregnated catalysts are summarized in Table 5.8. The particle size of Pd or PdO of the flame-made catalysts was smaller than the impregnated catalysts according to TEM micrographs. It may be due to well-dispersed Pd/PdO particles/clusters of the flame-made catalysts.

Table 5.8 Primary particle size of TiO₂ and Pd/PdO from TEM micrographs of flame-made and impregnated catalysts with various TiO₂ crystallite sizes

Catalyst	Primary particle size of TiO ₂ from TEM micrographs (nm)	Pd/PdO particle size from TEM micrographs (nm)
5FSP-9.7	9.5	1.0
5FSP-15.7	15.0	2.0
5FSP-24.6	24.0	3.5
5Im-FSP-9.8	10.0	3.2
5Im-FSP-15	16.0	3.5
5Im-FSP-26	27.0	3.7
5Im-nano	9.5	3.9
5Im-P25	25.8	4.5
5Im-micron	105.7	8.3

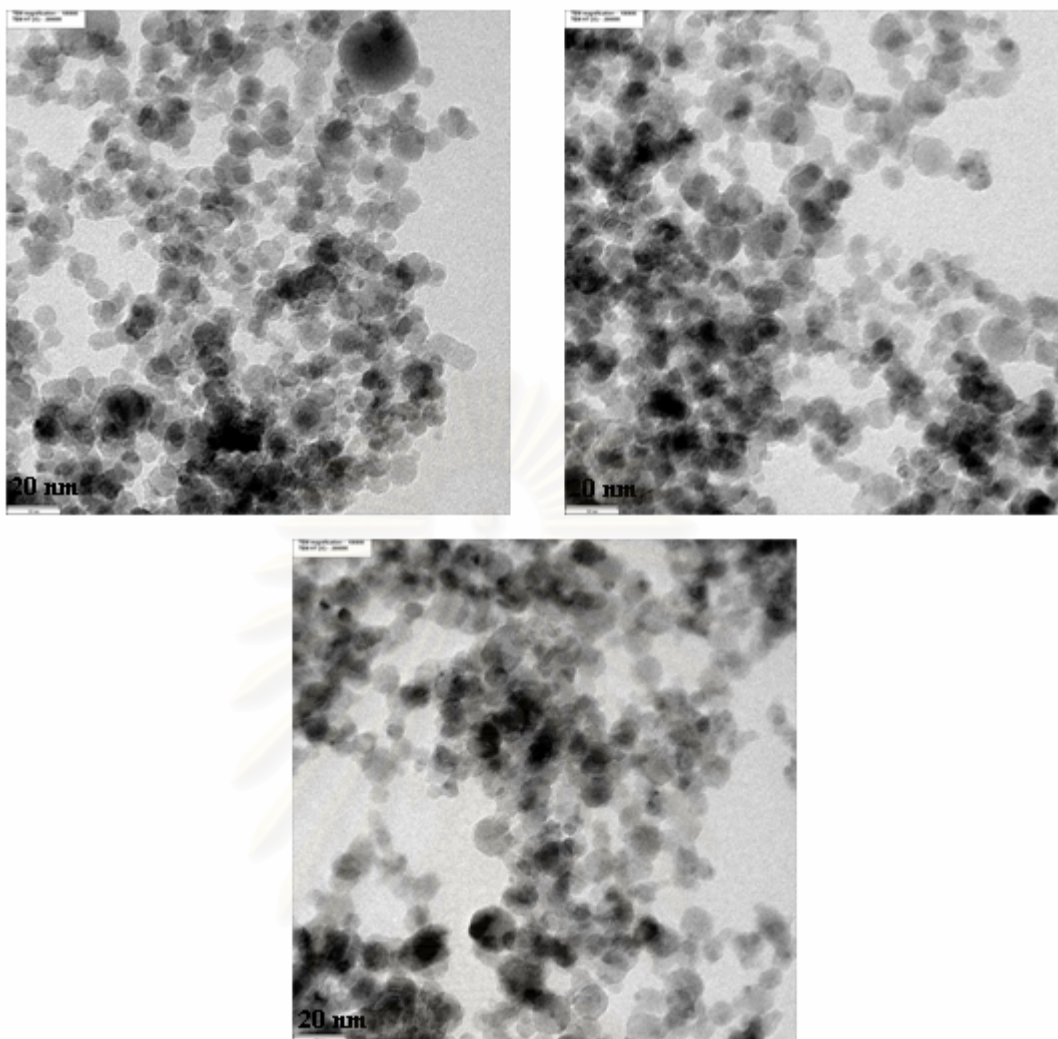


Figure 5.34 TEM micrographs of 5 wt% Pd/TiO₂ catalysts prepared by single-step flame synthesis with average crystallite sizes of 9.7 nm (5FSP-9.7)

สถาบันวิทยบริการ
จุฬาลงกรณ์มหาวิทยาลัย

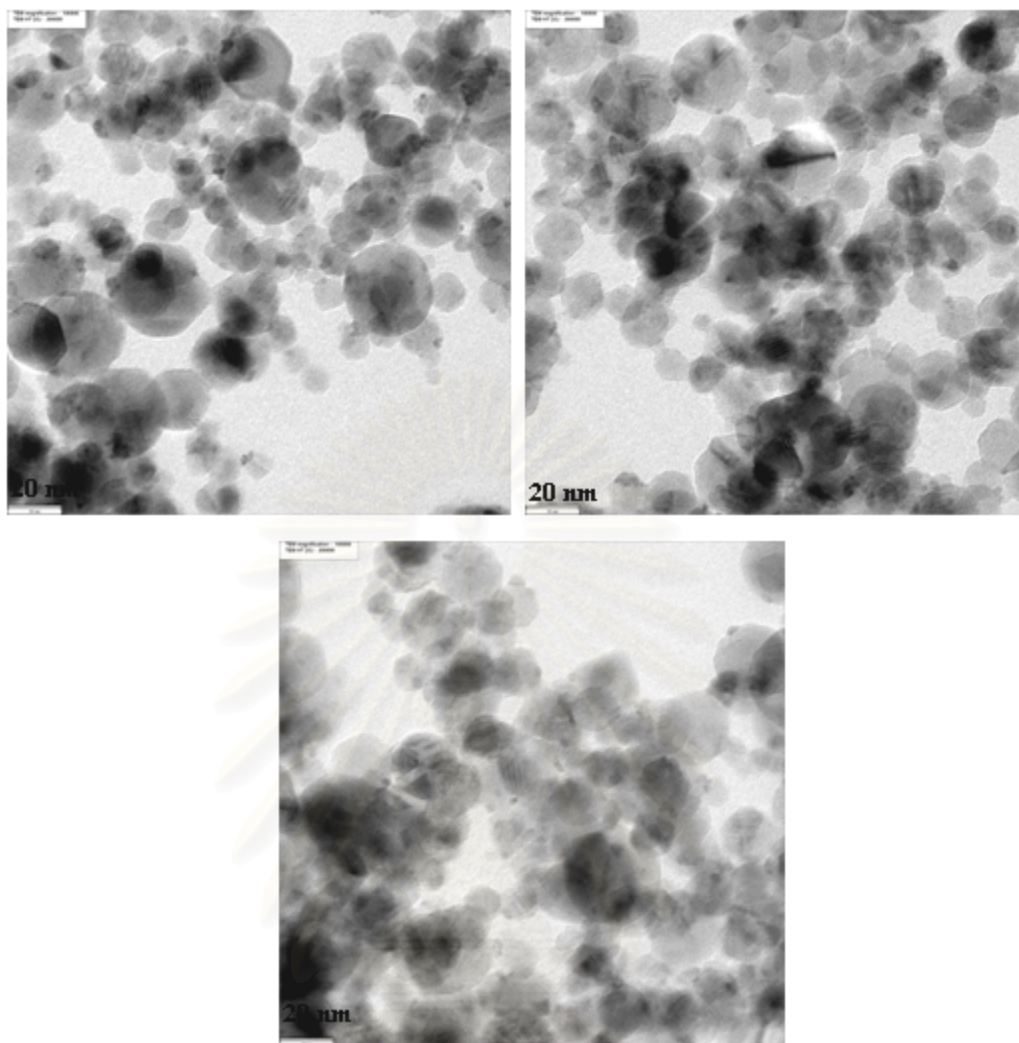


Figure 5.25 TEM micrographs of 5 wt% Pd/TiO₂ catalysts prepared by single-step flame synthesis with average crystallite sizes of 15.7 nm (5FSP-15.7)

สถาบันวิทยบริการ
จุฬาลงกรณ์มหาวิทยาลัย

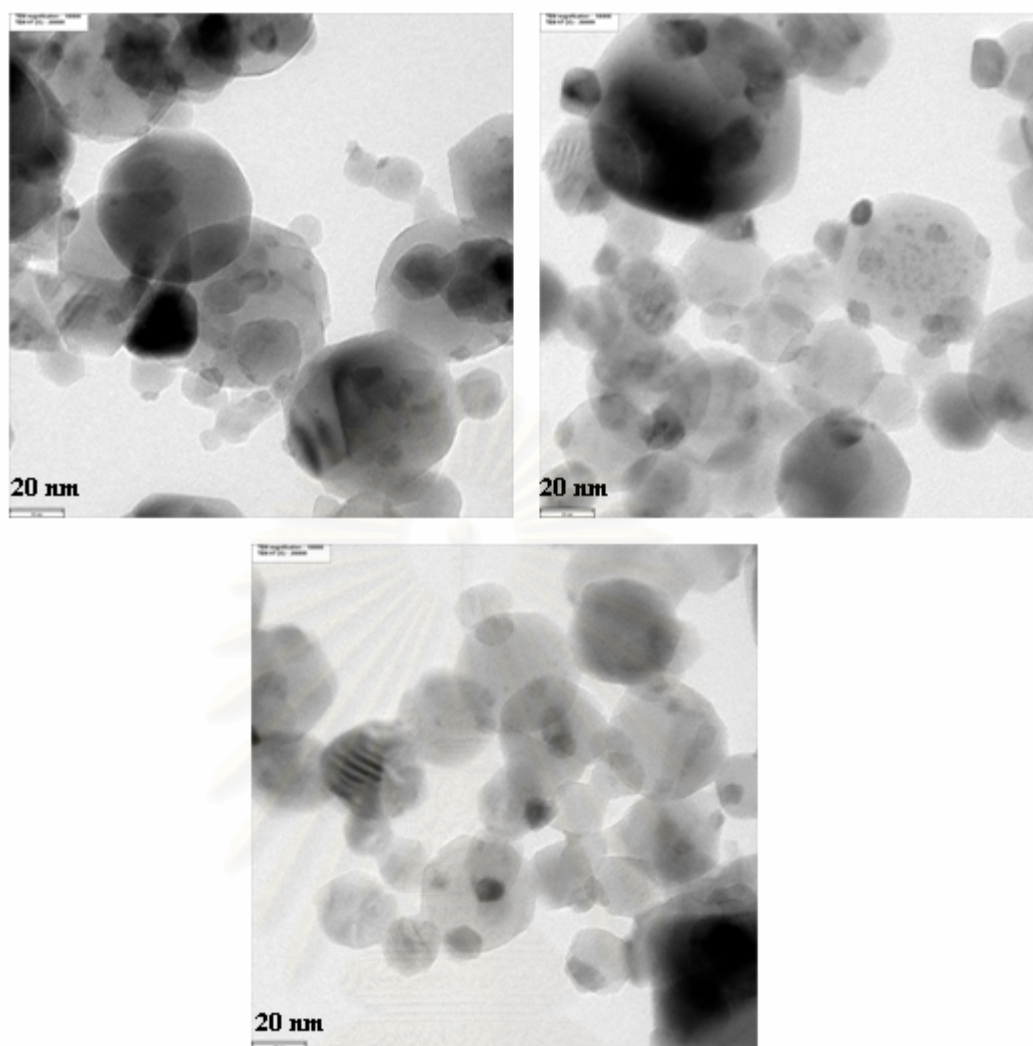


Figure 5.36 TEM micrographs of 5 wt% Pd/TiO₂ catalysts prepared by single-step flame synthesis with average crystallite sizes of 24.6 nm (5FSP-24.6)

สถาบันวิทยบริการ
จุฬาลงกรณ์มหาวิทยาลัย

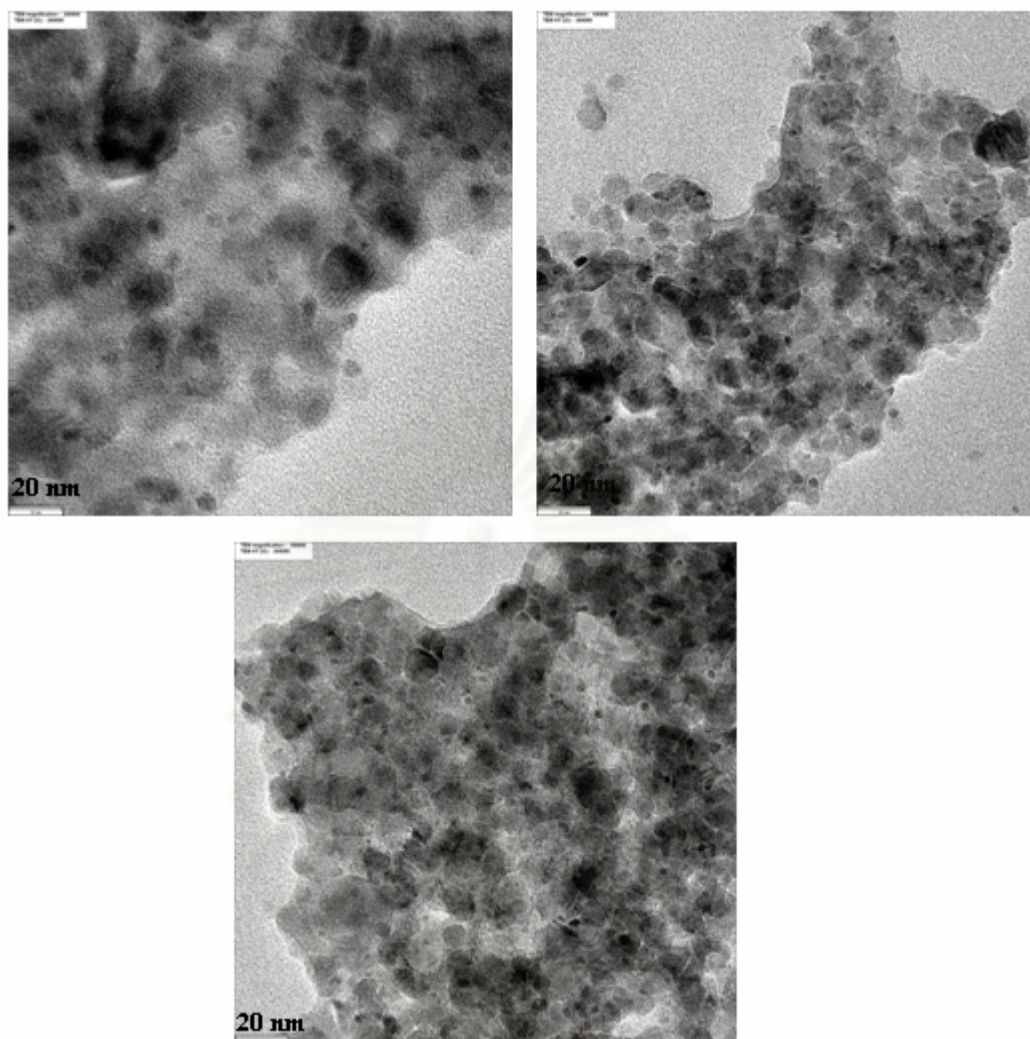


Figure 5.37 TEM micrographs of 5 wt% Pd/TiO₂ catalysts prepared by incipient wetness impregnation with flame-made TiO₂ supports average crystallite sizes of 9.8 nm (5Im-FSP-9.8)

สถาบันวิทยบริการ
จุฬาลงกรณ์มหาวิทยาลัย

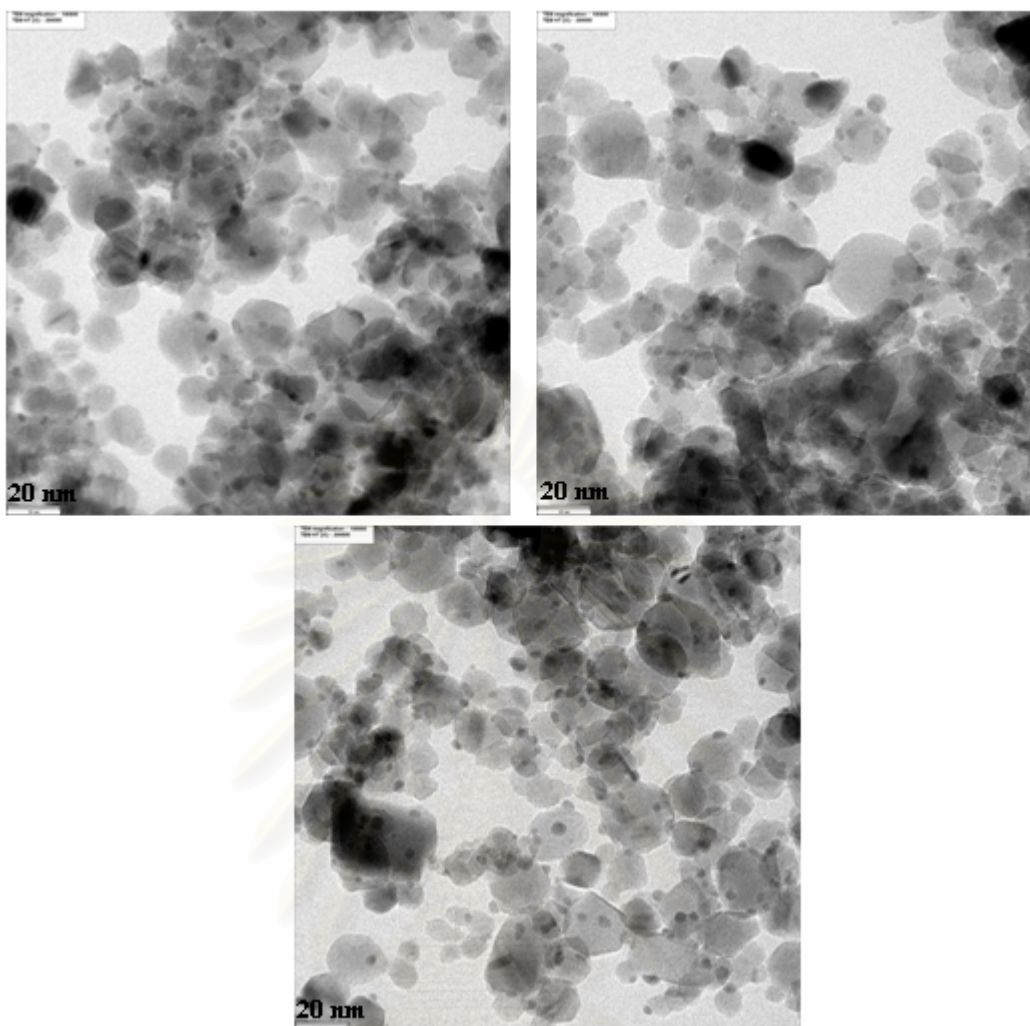


Figure 5.38 TEM micrographs of 5 wt% Pd/TiO₂ catalysts prepared by incipient wetness impregnation with flame-made TiO₂ supports average crystallite sizes of 15 nm (5Im-FSP-15)

สถาบันวิทยบริการ
จุฬาลงกรณ์มหาวิทยาลัย

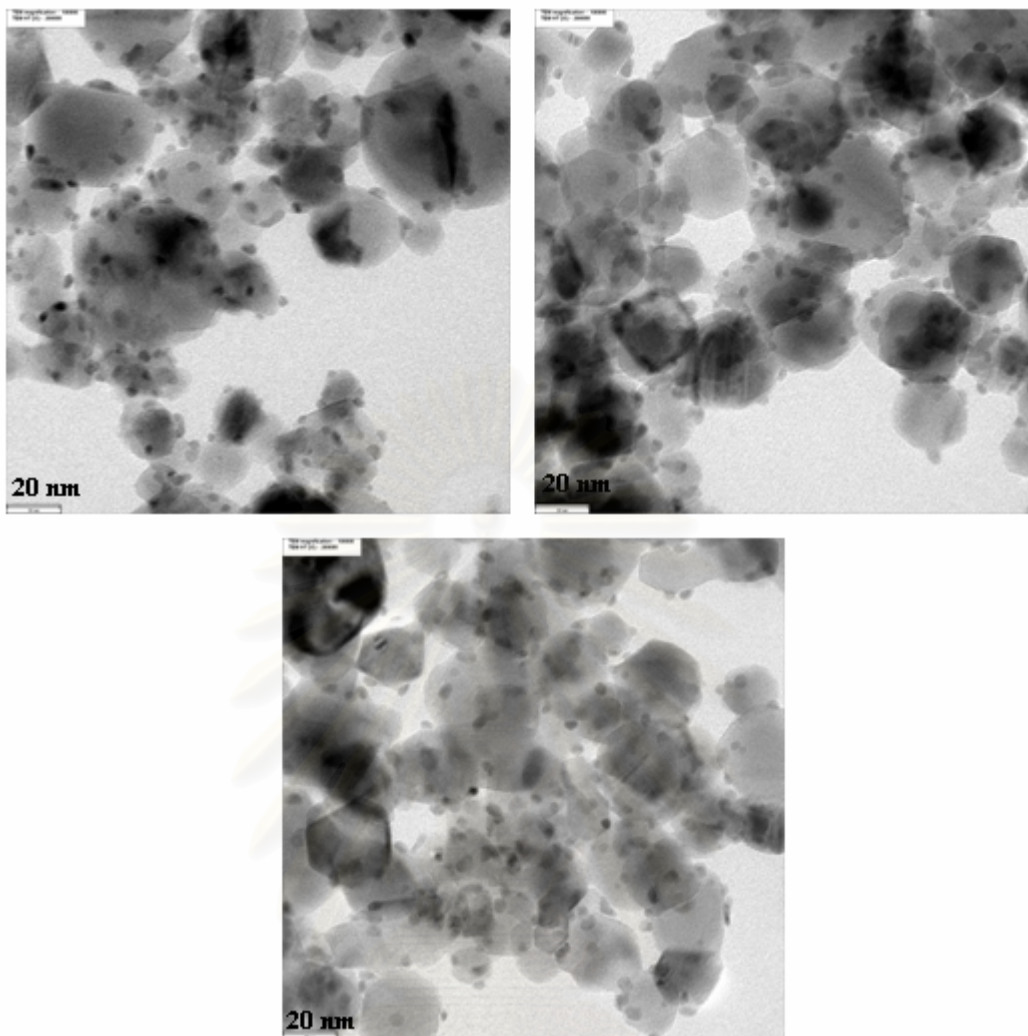


Figure 5.39 TEM micrographs of 5 wt% Pd/TiO₂ catalysts prepared by incipient wetness impregnation with flame-made TiO₂ supports average crystallite sizes of 26 nm (5Im-FSP-26)

สถาบันวิทยบริการ
จุฬาลงกรณ์มหาวิทยาลัย

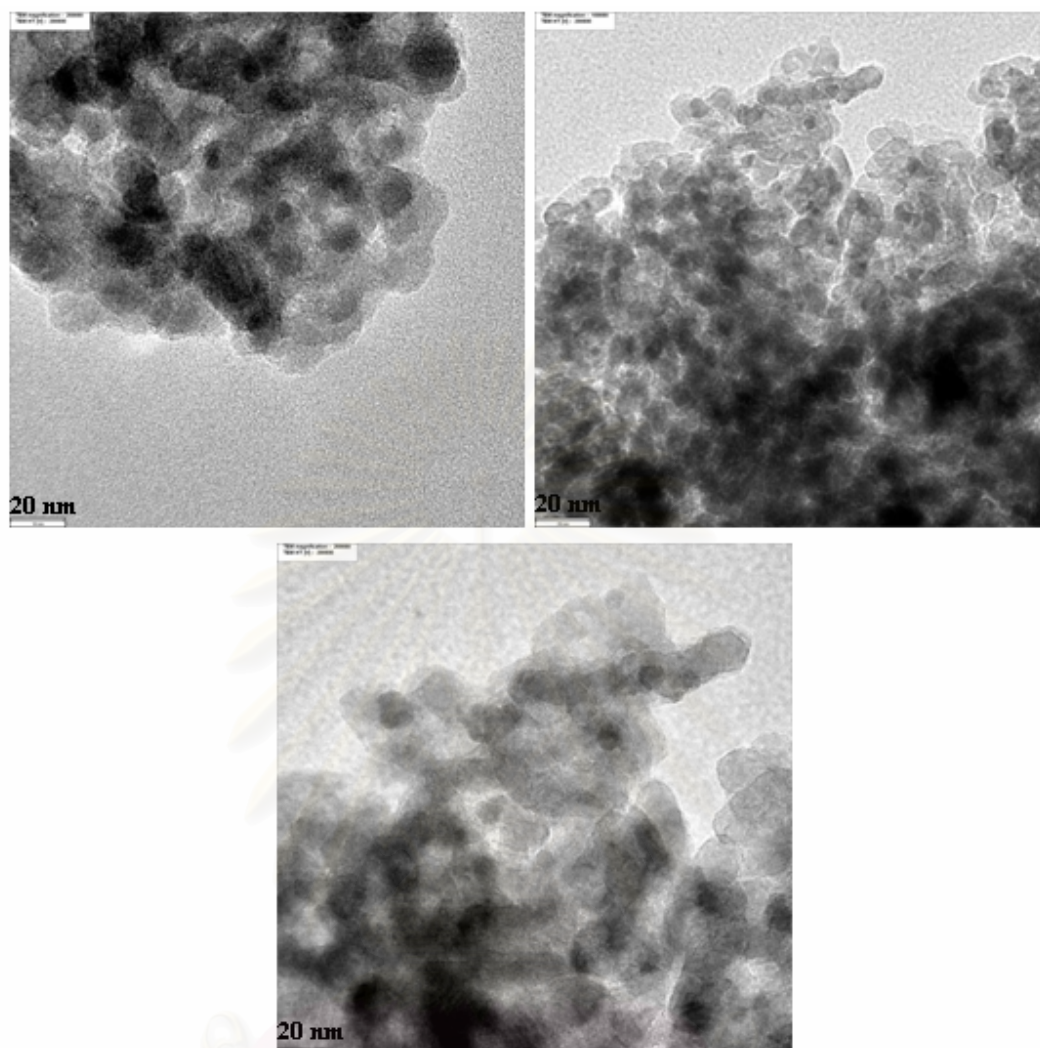


Figure 5.40 TEM micrographs of references catalysts (5Im-nano)

สถาบันวิทยบริการ
จุฬาลงกรณ์มหาวิทยาลัย

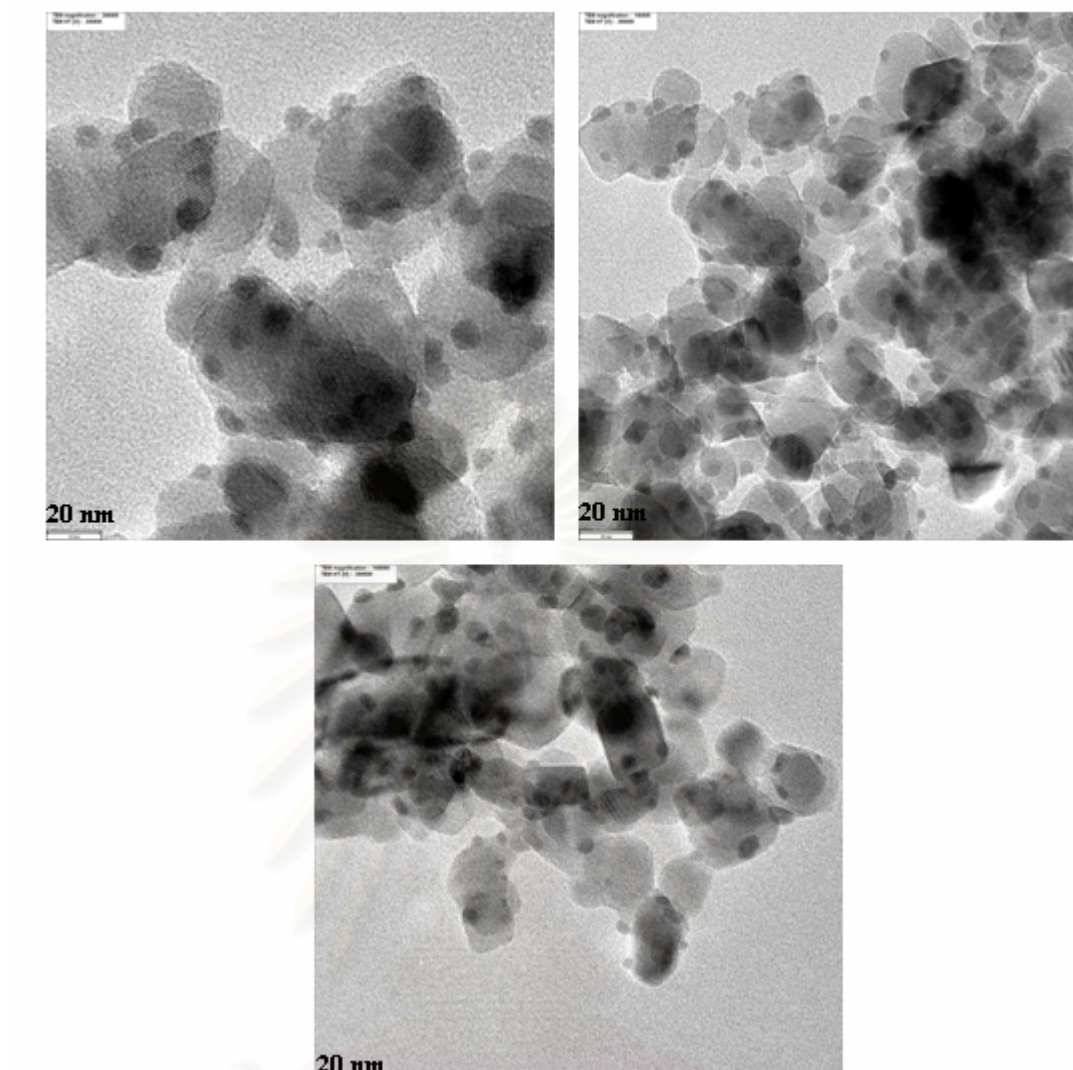


Figure 5.41 TEM micrographs of references catalysts (5Im-P25)

สถาบันวิทยบริการ
จุฬาลงกรณ์มหาวิทยาลัย

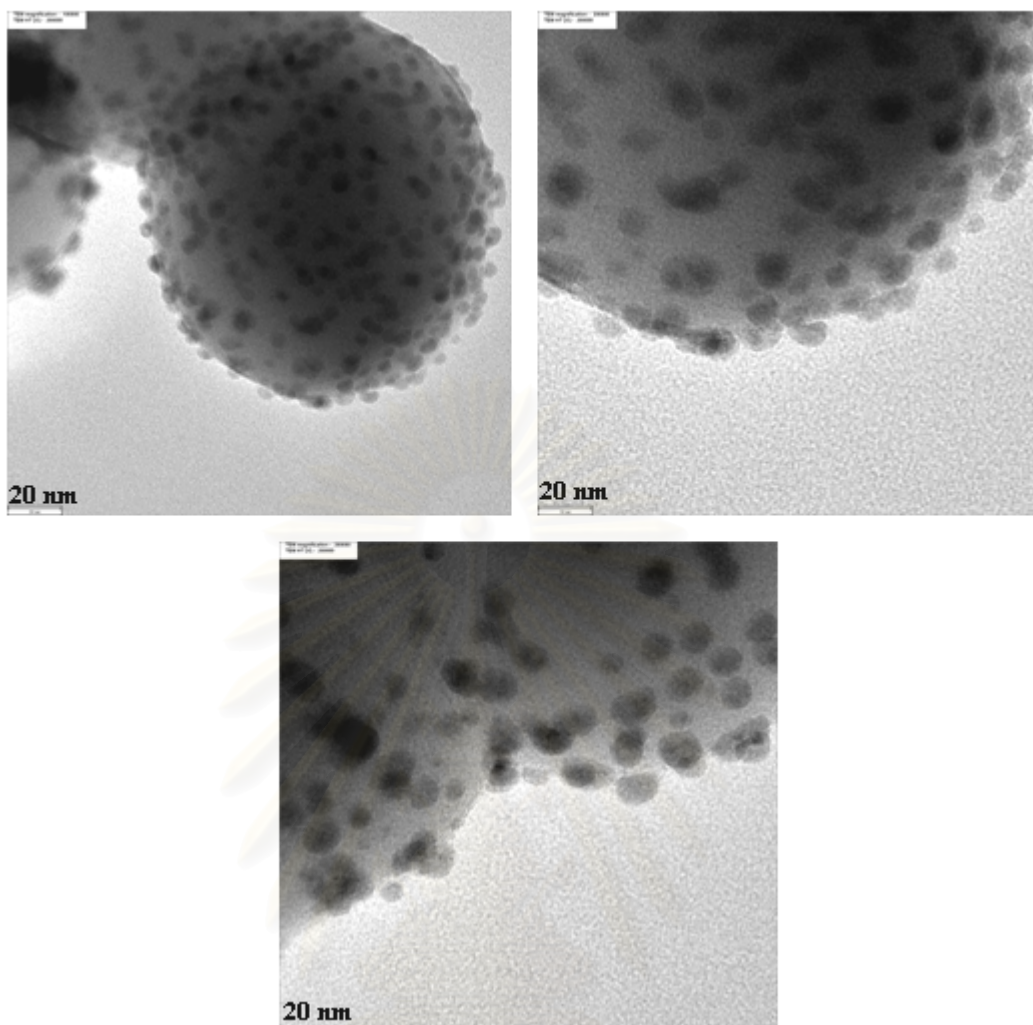


Figure 5.42 TEM micrographs of references catalysts (5Im-micron)

สถาบันวิทยบริการ
จุฬาลงกรณ์มหาวิทยาลัย

5.2.1.3 N₂ Physisorption

5 wt% Pd/TiO₂ catalysts with various TiO₂ crystallite sizes were prepared by single-step flame spray method and impregnation method. The BET surface area, the pore volume, and the average pore diameter of all flame-made catalysts are summarized in Table 5.9. The BET surface area of flame-made 5 wt% Pd/TiO₂ catalysts decreased from 147.7 to 37.6 m²/g as the TiO₂ crystallite sizes increased from 9.7 to 24.6 nm. Compared to the flame-made TiO₂ support, the BET surface areas were not much difference, the pore volume and average pore size diameter were nearly constant for all catalysts. This result suggests that most of the Pd particles were not inside the pore of TiO₂. The pore volume of flame-made catalysts also decreased from 0.35 to 0.06 cm³/g with increasing TiO₂ crystallite size. This would be explaining by the increasing of sintering.

The N₂ adsorption – desorption isotherms of the flame-made catalyst with various crystallite sizes are shown in Figure 5.43 to 5.45, respectively. According to the BET classification, isotherms of this kind belong to the isotherm of type IV describing the mesoporous material which has pore diameter between 2 and 50 nm. The pore size distribution calculated according to the BJH equation of the flame-made catalysts show the average pore diameter in Table 5.9. The average pore diameter of 5 wt% Pd/TiO₂ decreased from 8.3 to 5.9 nm with increasing crystallite size of TiO₂.

The results of N₂ physisorption of the 5 wt% Pd/TiO₂ impregnation-made catalysts were also summarized in Table 5.9. The BET surface areas of impregnated catalysts are decreased with increasing crystallite size from 9.8 to 26 nm. The BET surface areas of the impregnated catalysts were not much difference from flame-made titania support.

The N₂ adsorption – desorption isotherm of impregnated-made 5 wt% Pd/TiO₂ catalysts are shown in Figure 5.46 to 5.48, respectively. According to the BET classification, isotherms of this kind belong to the isotherm of type IV describing the mesoporous material which has pore diameter between 2 and 50 nm. The pore size distribution and average pore diameter calculated from the BJH equation of the impregnated-made catalysts are also summarized in Table 5.9. The average pore diameter increased slightly with increasing crystallite size to 26 nm.

Table 5.9 N₂ physisorption properties of the flame and impregnated-made 5 wt% Pd/TiO₂ catalysts with various TiO₂ crystallite sizes

Catalyst	N ₂ Physisorption		
	BET surface area (m ² /g)	Pore Volume (cm ³ /g)	Average Pore Diameter (nm)
TiO ₂ FSP(9.8 nm)	147.9	0.34	8.2
TiO ₂ FSP(15 nm)	92.2	0.18	6.7
TiO ₂ FSP(26 nm)	42.5	0.08	7.1
5FSP-9.7	147.7	0.35	8.3
5FSP-15.7	72.5	0.14	7.9
5FSP-24.6	37.6	0.06	5.9
5Im-FSP-9.8	137.1	0.49	10.7
5Im-FSP-15	85.9	0.35	14.2
5Im-FSP-26	42.1	0.14	23.9

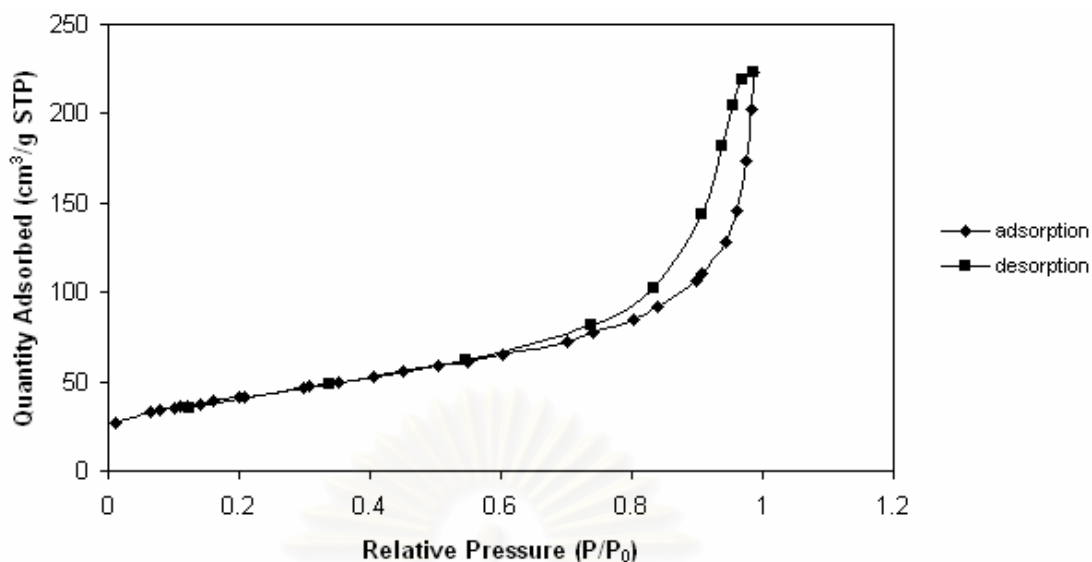


Figure 5.43 N₂ adsorption – desorption isotherms of 5 wt% Pd/TiO₂ catalysts prepared by single-step flame synthesis with average crystallite sizes of 9.7 nm (5FSP-9.7)

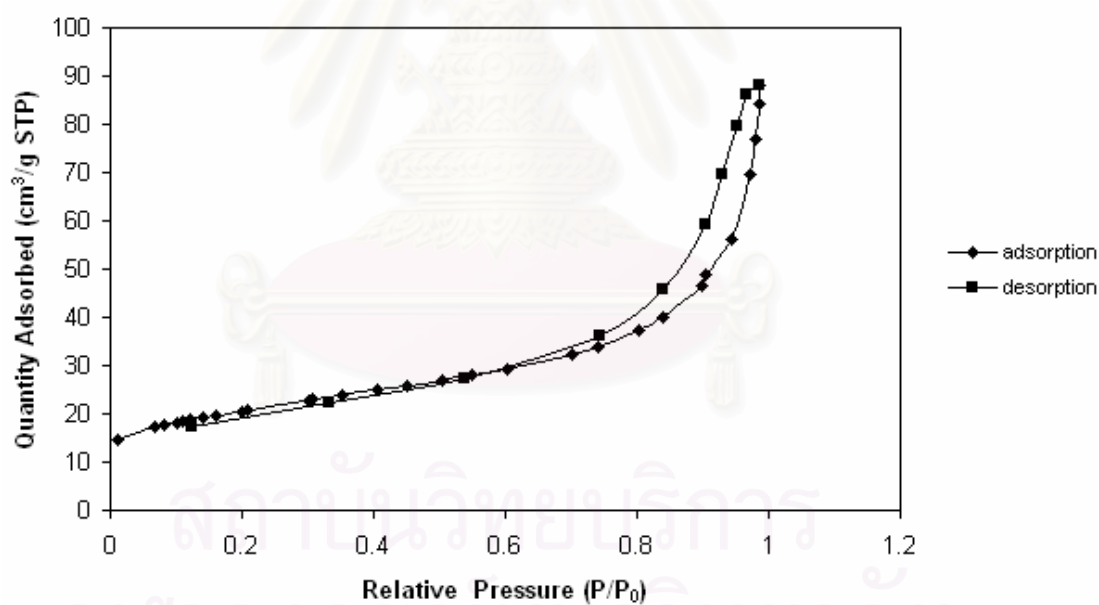


Figure 5.44 N₂ adsorption – desorption isotherms of 5 wt% Pd/TiO₂ catalysts prepared by single-step flame synthesis with average crystallite sizes of 15.7 nm (5FSP-15.7)

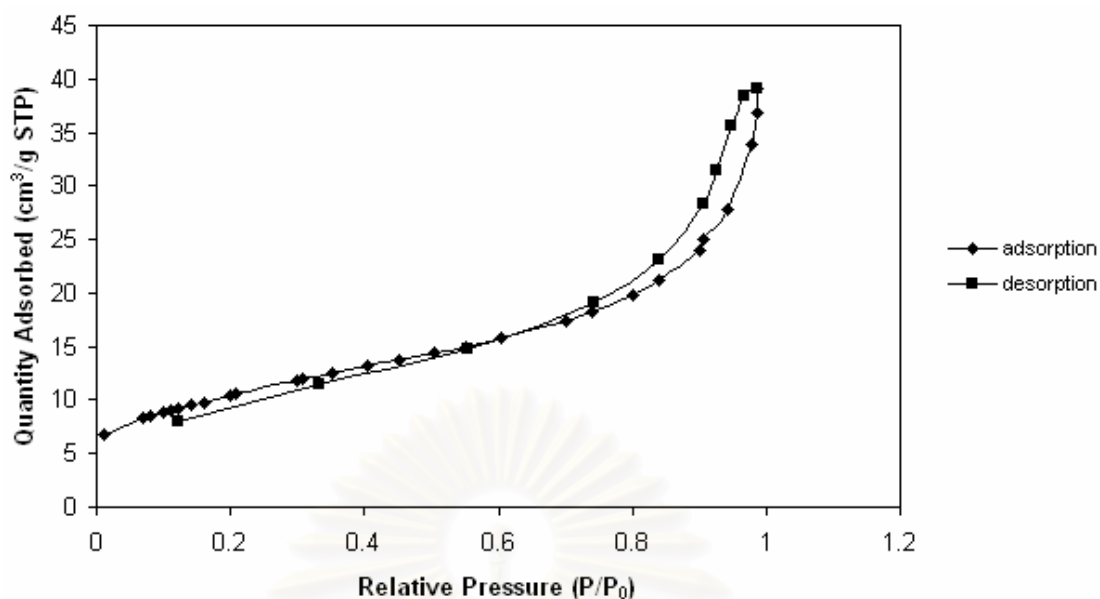


Figure 5.45 N₂ adsorption – desorption isotherms of 5 wt% Pd/TiO₂ catalysts prepared by single-step flame synthesis with average crystallite sizes of 24.6 nm (5FSP-24.6)

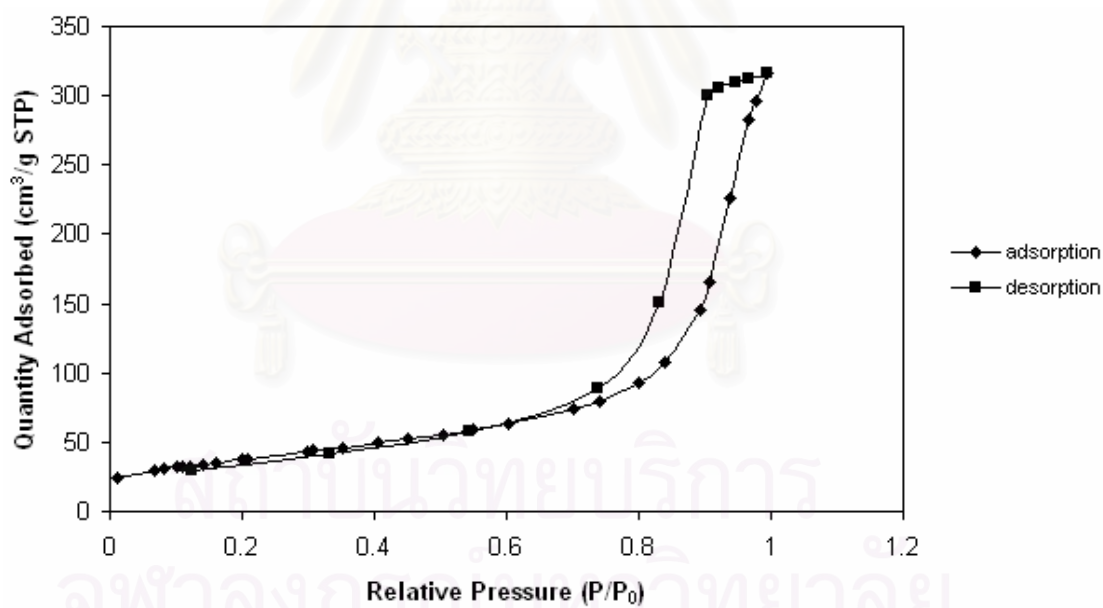


Figure 5.46 N₂ adsorption – desorption isotherms of 5 wt% Pd/TiO₂ catalysts prepared by incipient wetness impregnation with flame-made TiO₂ supports average crystallite sizes of 9.8 nm (5Im-FSP-9.8)

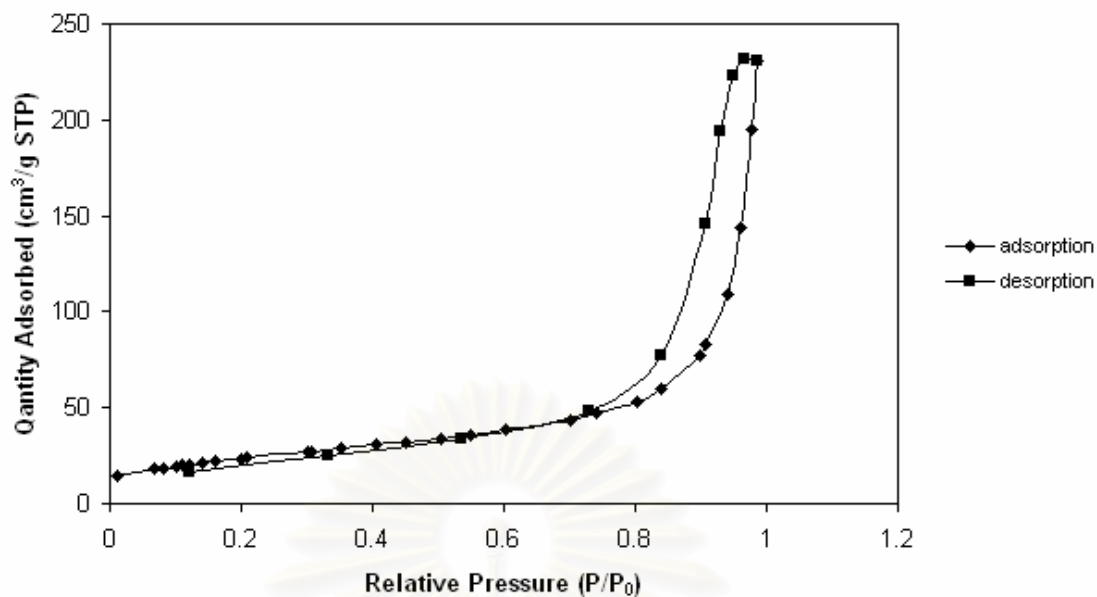


Figure 5.47 N₂ adsorption – desorption isotherms of 5 wt% Pd/TiO₂ catalysts prepared by incipient wetness impregnation with flame-made TiO₂ supports average crystallite sizes of 15 nm (5Im-FSP-15)

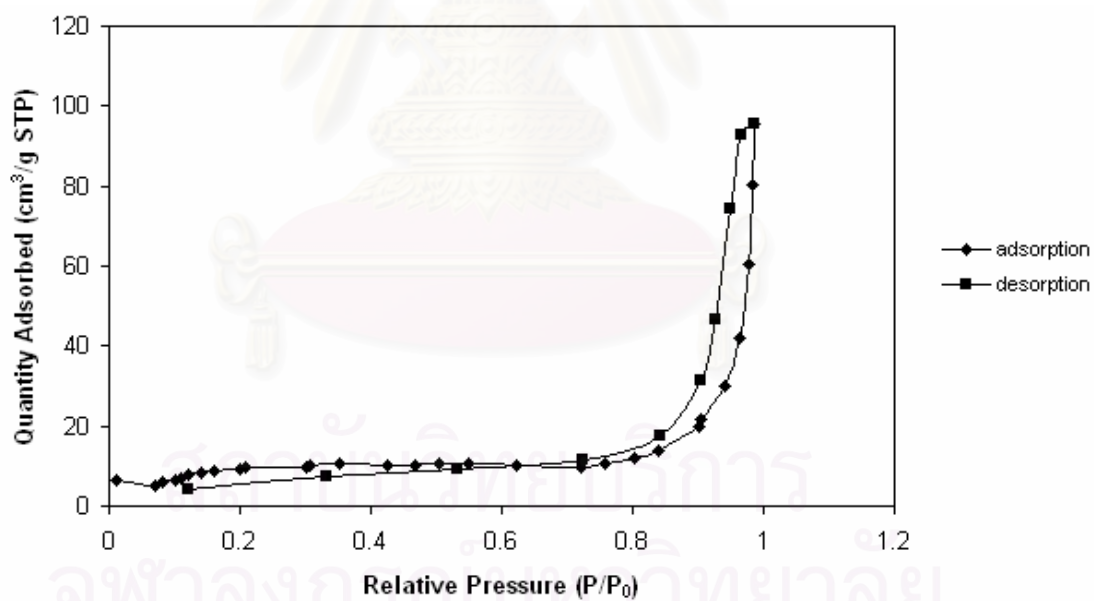


Figure 5.48 N₂ adsorption – desorption isotherms of 5 wt% Pd/TiO₂ catalysts prepared by incipient wetness impregnation with flame-made TiO₂ supports average crystallite sizes of 26 nm (5Im-FSP-26)

5.2.1.4 CO-pulse chemisorptions

CO chemisorption technique provides the information on the number of palladium active sites and percentages of palladium metal dispersion. The total CO uptakes, % Pd from AAS, the percentages of palladium metal dispersion and diameter of palladium metal are reported in Table 5.10. The active sites of the flame-made Pd/TiO₂ catalysts increased from 1.5×10^{18} to 6.4×10^{18} site/g-catalyst corresponding to %Pd metal dispersion decreased from 15.6 to 6.3 % as the average crystallite sizes of titania increased from 9.7 to 24.6 nm, respectively. The average Pd⁰ metal particle sizes calculated from CO chemisorption were found to be 7 – 18 nm. It can be noted that one-step flame spray pyrolysis with smaller crystallite size TiO₂ resulted in the smaller Pd particles and the Pd particle sizes were much larger than those observed from TEM analyses. The low metal dispersion and overestimation of metal particle sizes in supported Pd catalysts based on CO chemisorptions may be due to the formation of Ti-O groups covering the small palladium particles. This was inhibited the adsorption of CO molecules, so the CO chemisorptions uptake decreased. Otherwise, CO chemisorptions suppression may be due to strong interactions between Ti and Pd in an alloy form [29].

The amounts of CO chemisorption on the impregnated-made Pd catalysts supported on flame-made TiO₂ are also given in Table 5.10. The active sites decreased from 16.2×10^{18} to 13.9×10^{18} site/g catalyst corresponding to %Pd metal dispersion decreased from 13.7 to 3.8 % as the average crystallite sizes of titania increased from 9.8 to 26.0 nm, respectively.

From AAS analysis, it was found that the smaller TiO₂ crystallite size has percentage of loaded Pd more than the larger crystallite size. The actual Pd loading was less than that expected by 38% for 5FSP-9.7 and 64% for 5FSP-24.6. The actual Pd loading for the impregnated catalysts were less than that expected by 13%. The reason for low amount of Pd being loaded to the FSP catalysts may be because of the high liquid flow rate and low oxygen dispersion used. Some of the liquid may not be in contact with flame and slipped out of the reactor.

The amounts of CO chemisorption on the reference catalysts are given in Table 5.10. The amounts of CO chemisorption can be ranged in the order of 5Im-nano > 5Im-P25 > 5Im-micron.

Table 5.10 The amounts of CO chemisorption of flame-made and impregnated catalysts with various TiO₂ crystallite sizes

Catalyst	CO uptake ($\times 10^{-18}$ molecule CO/g-catalyst)	%Pd from AAS	%Pd dispersion	d _p Pd ⁰ (nm)
5FSP-9.7	1.5	3.1	15.6	7
5FSP-15.7	2.6	2.9	7.5	15
5FSP-24.6	6.4	1.8	6.3	18
5Im-FSP-9.8	16.2	4.0	13.7	8
5Im-FSP-15	17.4	4.3	12.5	9
5Im-FSP-26	13.9	4.2	3.8	29
5Im-nano	19.7	4.5	9.2	12
5Im-P25	15.2	4.7	6.6	17
5Im-micron	12.5	3.9	6.5	17

5.2.1.5 X-ray Photoelectron Spectroscopy (XPS)

XPS results such as XPS spectra, binding energies and surface composition of flame and impregnated-made catalysts are reported in Figure 5.49 to 5.50, and also summarized in Table 5.11 and the XPS spectra of the reference catalysts are also shown in Figure 5.51. XPS peaks for Pd 3d_{5/2} were clearly seen for 5FSP-9.7 and 5FSP-24.6 where the B.E. of Pd 3d_{5/2} was observed at 335.5 and 336.6 eV with FWHM 1.986 and 2.101, respectively. B.E. of Pd 3d_{5/2} in 5FSP-15.7 and 5FSP-24.6 are close to PdO signal, which would expect between 335.4-337.5 eV [31]. It is considered that oxygen atoms from TiO₂ were adsorbed on Pd. There is probably a change of electronic state of Pd in 5FSP-15.7 and 5FSP-24.6 catalysts. In the same way, B.E. of Pd 3d_{5/2} in 5ImFSP-15 and 5ImFSP-26 are also close to PdO signal. However, FWHM > 2 suggests that more than one species presented on the catalyst [31].

Pd/Ti atomic ratio of all flame-made catalysts is very small indicating low amount of Pd present on the TiO₂ surface corresponding to low amount of CO uptake. This result was consistent with BET surface areas which found that Pd deposits outside the pore of flame-made TiO₂, so the Pd particles would probably be covered by Ti-O groups during one-step flame-spray pyrolysis.

For the impregnated catalysts, Pd/Ti atomic ratio is greater than the flame-made catalysts. It is probably due to the preparation of catalysts by impregnation method. Pd metal may be deposited on TiO₂ better than those from flame spray synthesis.

Considered atomic ratio of Ti/O, the Pd loading catalysts prepared by flame spray pyrolysis showed lower value than the impregnated catalyst, suggesting that the flame-made catalysts were covered by oxygen atoms on titania surface more than the impregnated catalysts. The suggested model for Pd/TiO₂ prepared by one-step flame spray pyrolysis and two step impregnation method are reported in Figure 5.22.

B.E. of Pd 3d_{5/2} in the reference catalysts were not clearly seen except that of 5Im-micron where the B.E. of Pd 3d_{5/2} was observed at 336.7 eV with FWHM 2.43 eV. B.E. of the 5Im-cicron catalysts are close to PdO signal and FWHM value > 2 suggests that more than one species presented on the catalyst.

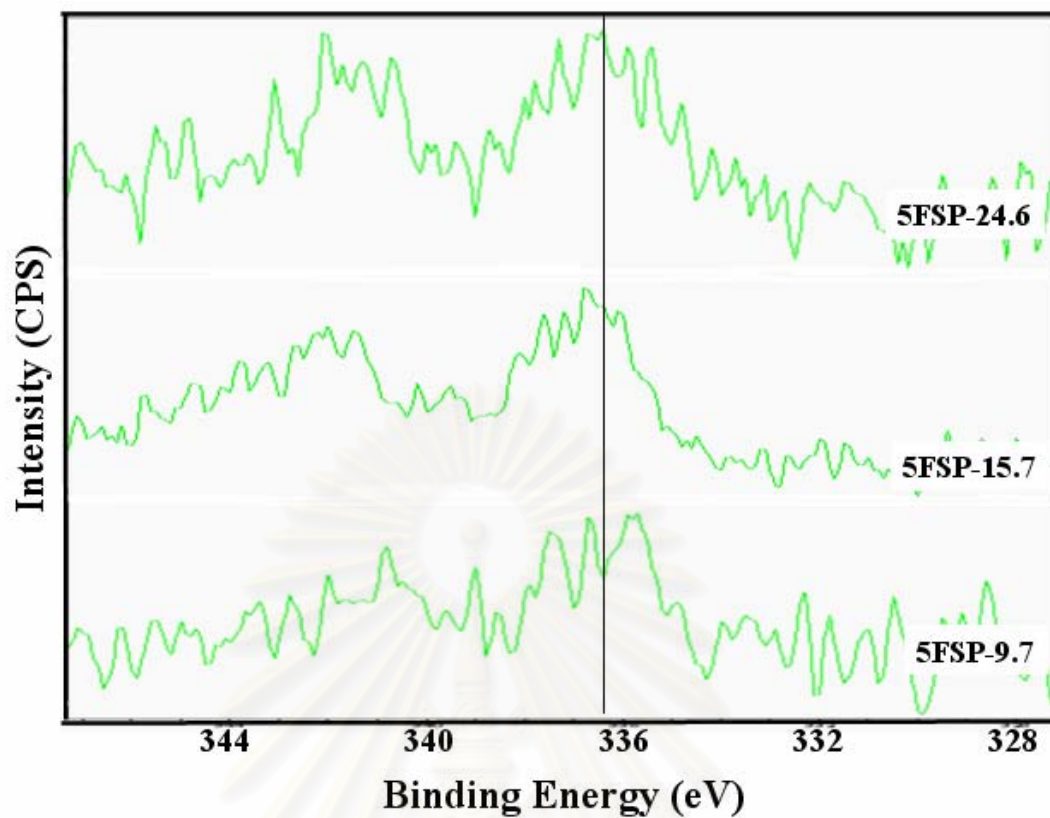


Figure 5.49 Binding energies of various crystallite size flame-made catalysts

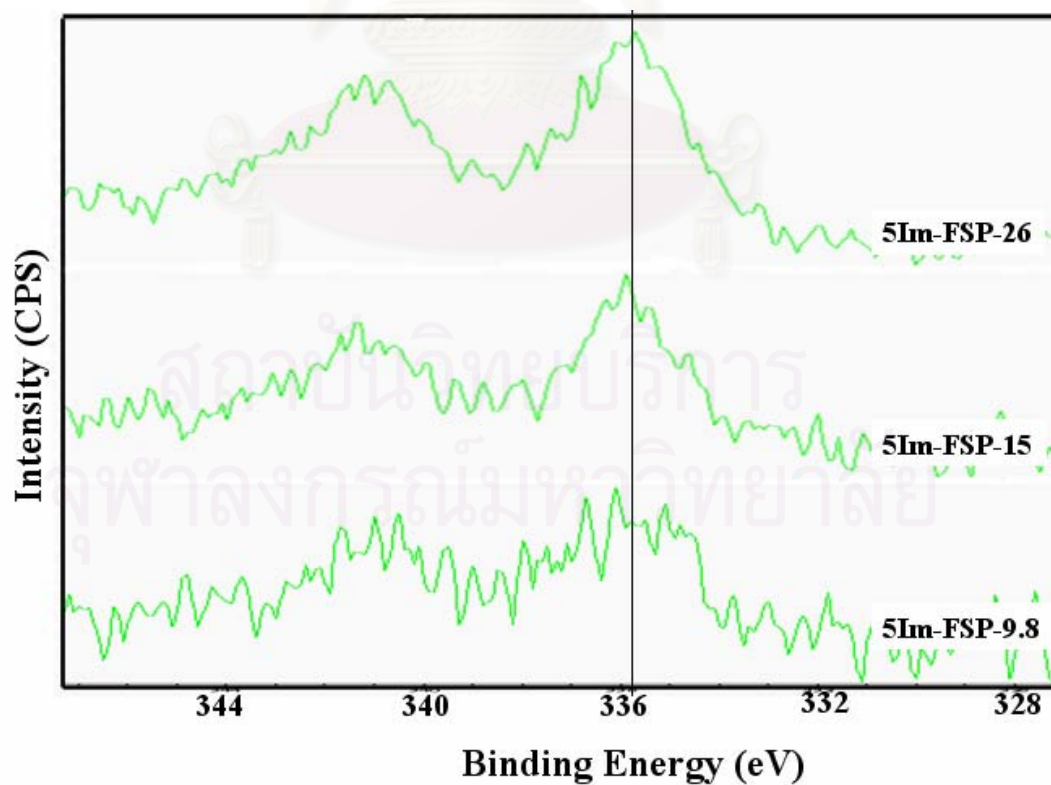


Figure 5.50 Binding energies of various crystallite size impregnated catalysts

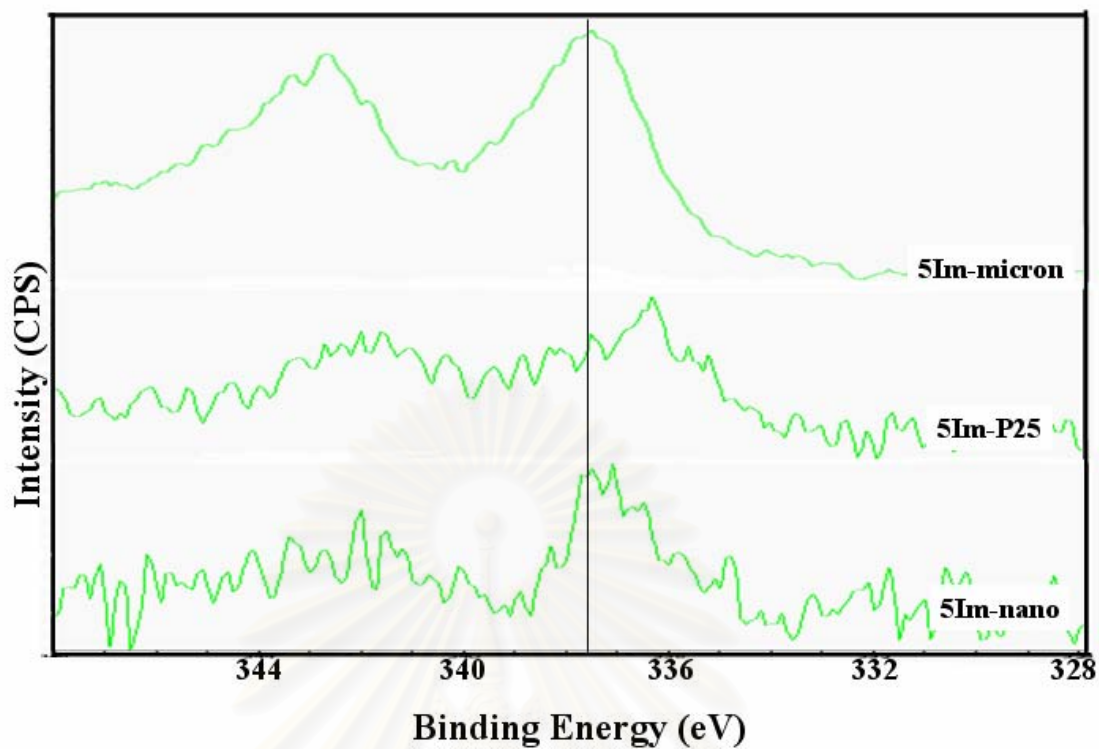


Figure 5.51 Binding energies of reference catalysts

Table 5.11 Binding energies and surface composition from XPS on various crystallite sizes of flame-made and impregnated catalysts

Catalyst	Pd 3d _{5/2}		Atomic ratio	
	B.E. (eV)	FWHM	Pd/Ti	Ti/O
5FSP-9.7	n.d.	n.d.	0.0155	0.0601
5FSP-15.7	335.5	1.986	0.0334	0.1682
5FSP-24.6	336.6	2.101	0.0329	0.0726
5ImFSP-9.8	n.d.	n.d.	0.0196	0.1149
5ImFSP-15	336.1	1.566	0.0412	0.1369
5ImFSP-26	335.6	2.152	0.1016	0.1779
5Im-nano	n.d.	n.d.	0.0114	0.1838
5Im-P25	n.d.	n.d.	0.0316	0.1000
5Im-micron	336.7	2.43	0.5400	0.1043

n.d. = not determined

5.2.2 Selective 1-Heptyne Hydrogenation Study

The performance of all Pd/TiO₂ catalysts was assessed using 2% v/v heptyne in toluene at the temperature 30°C and 1 bar of H₂ pressure for 3-40 minute in liquid-phase selective hydrogenation in a 50 ml autoclave reactor. The reaction was operated with high stirring rate (1000 rpm) in order to eliminate the external mass transfer of hydrogen problem. The products were analyzed by gas chromatography with flame ionization detector (FID) using GS-alumina column.

The concentration of 1-heptyne versus time on stream obtained by using difference crystallite size flame-made catalysts is shown in Figure 5.52. The hydrogenation rates of 1-heptyne on the all flame-made catalysts were nearly same. Figure 5.53 and 5.54 show the concentration of 1-heptene and 1-heptane versus time on stream of the flame-made catalyst. The selectivities of 1-heptene are closely same among all flame-made catalysts except 5FSP-9.7, which gave the lowest 1-heptene selectivities.

The specific activities (TOF) of Pd/TiO₂ catalysts with difference crystallite size are summarized in Table 5.12. TOFs of the flame-made catalysts decreased from 102.0 to 23.0 s⁻¹ as the crystallite size of catalysts increased from 9.7 to 24.6 nm, which resulted in larger Pd particle size from 1 to 3.5 nm.

The concentration of 1-heptyne versus time on stream of the impregnated catalysts is shown in Figure 5.55. The 1-heptyne hydrogenation rate of all impregnated is relatively constant as the TiO₂ crystallite size increased from 9.8 to 26 nm. The concentration of 1-heptene and 1-heptane versus time on stream are shown in Figure 5.56 and 5.57. The selectivities of 1-heptene of all impregnated catalysts are closely the same expect but 5Im-FSP-9.8, which showed the lowest selectivities of 1-heptene due to the smallest Pd particle that confirm by TEM micrograph. It interesting that TOFs of the impregnated catalysts were relatively constant with increasing TiO₂ crystallite size.

The concentration of 1-heptyne versus time on stream of all flame-made and impregnated catalysts is shown in Figure 5.58. The hydrogenation rate of 1-heptyne of flame-made catalysts was greater than the impregnated-made catalysts. TOFs of the flame-made catalysts were higher than the impregnated catalysts at the same TiO₂ crystallite size probably due to support interaction during

one-step flame spray pyrolysis. Figure 5.59 and 5.60 show the concentration of 1-heptene and 1-heptane versus time on stream of all flame-made and impregnated catalysts. The selectivities of 1-heptene of the flame-made catalysts are better than the impregnated catalysts. 5Im-P25 show the lowest selectivities of 1-heptene due to the highest rutile phase composition (21% rutile phase according to Table 5.7). The presence of high %rutile TiO_2 result in Pd/ TiO_2 resulted on lower selectivities [32]. TOFs of the reference catalysts were not much difference. Compared to flame-made catalysts, it found that TOF value of the flame-made catalysts is better than the reference catalysts. This would be due to the strong interaction between Pd and TiO_2 , which lowered the desorption temperature of alkene [33]. It is considered that one-step flame spray pyrolysis is more suitable than impregnation method for selective 1-heptyne hydrogenation.

Table 5.12 Specific activity (TOFs, s^{-1}) on the various TiO_2 crystallite size flame-made and impregnated catalysts

Catalyst	TOF (s^{-1})
5FSP-9.7	102.0
5FSP-15.7	58.3
5FSP-24.6	23.0
5Im-FSP-9.8	8.1
5Im-FSP-15	7.8
5Im-FSP-26	10.1
5Im-nano	6.2
5Im-P25	9.9
5Im-micron	11.9

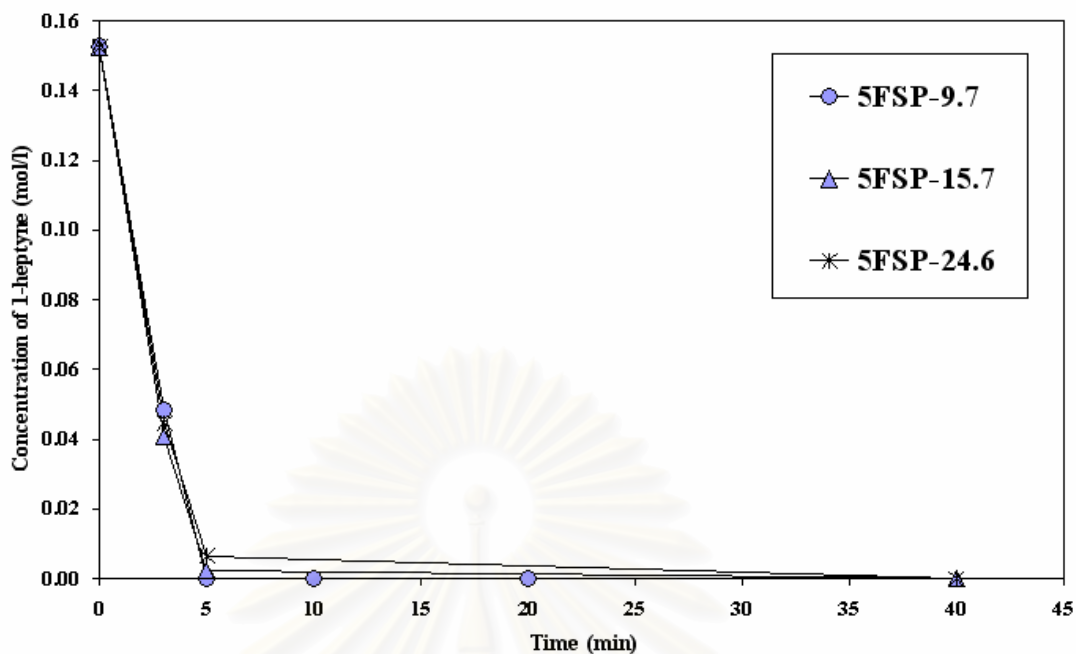


Figure 5.52 Time on stream with concentration of 1-heptyne on 5 wt% Pd/TiO₂ catalysts prepared by single-step flame synthesis with average crystallite sizes of 9.7, 15.7, and 24.6 nm

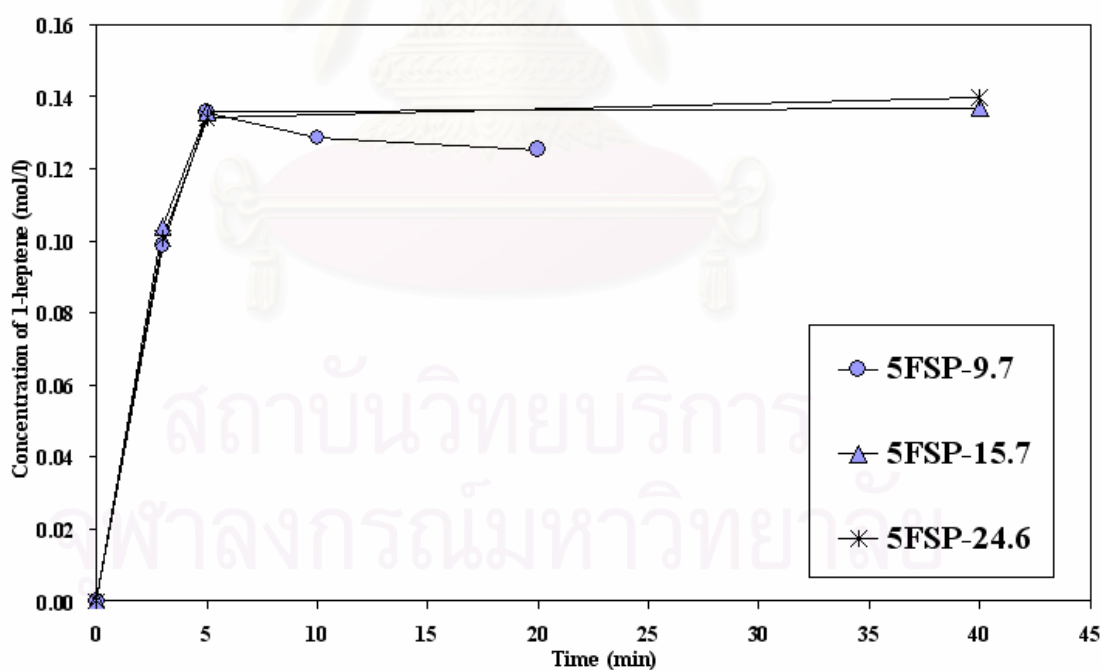


Figure 5.53 Time on stream with concentration of 1-heptene on 5 wt% Pd/TiO₂ catalysts prepared by single-step flame synthesis with average crystallite sizes of 9.7, 15.7, and 24.6 nm

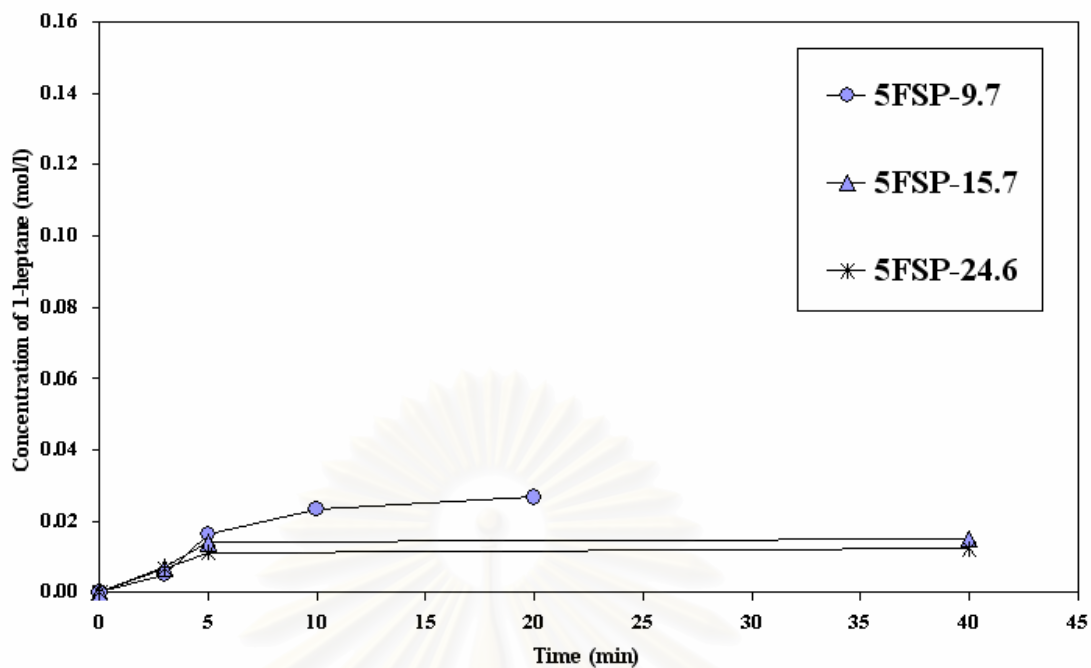


Figure 5.54 Time on stream with concentration of 1-heptane on 5 wt% Pd/TiO₂ catalysts prepared by single-step flame synthesis with average crystallite sizes of 9.7, 15.7, and 24.6 nm

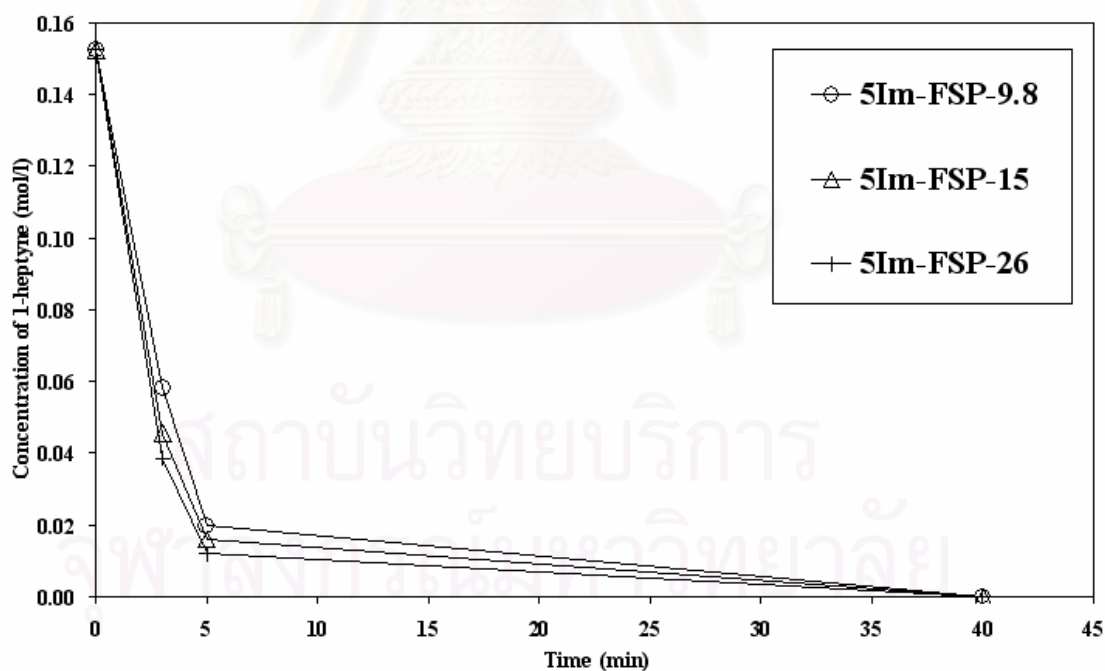


Figure 5.55 Time on stream with concentration of 1-heptyne on 5 wt% Pd/TiO₂ catalysts prepared by incipient wetness impregnation with flame-made TiO₂ supports average crystallite sizes of 9.8, 15, and 26 nm

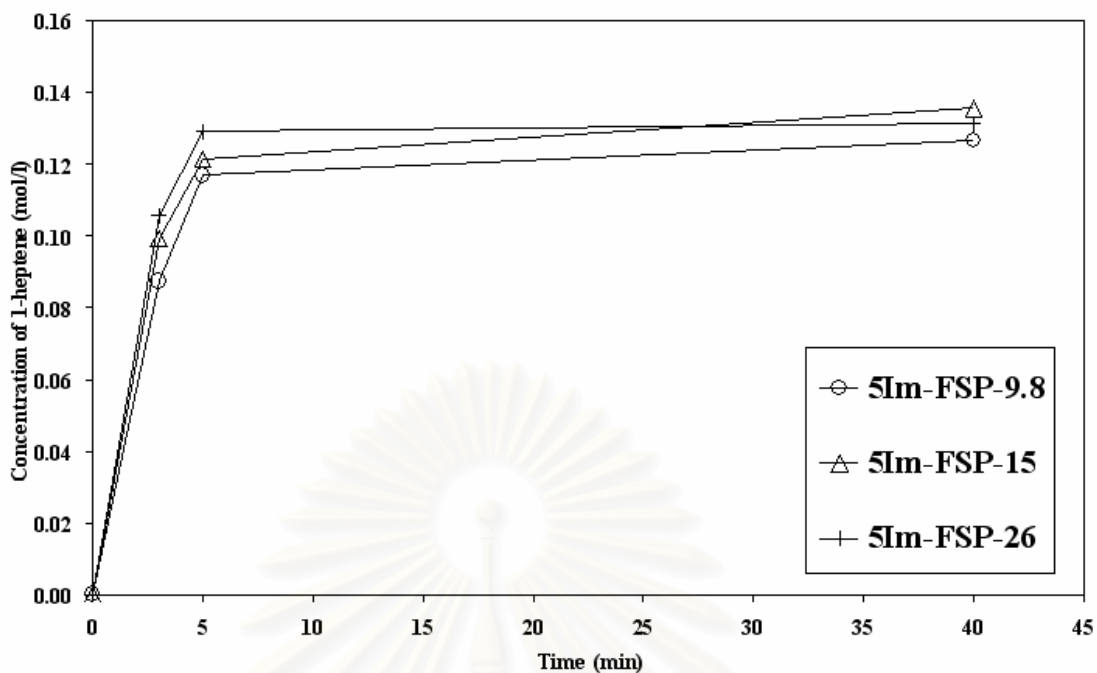


Figure 5.56 Time on stream with concentration of 1-heptene on 5 wt% Pd/TiO₂ catalysts prepared by incipient wetness impregnation with flame-made TiO₂ supports average crystallite sizes of 9.8, 15, and 26 nm

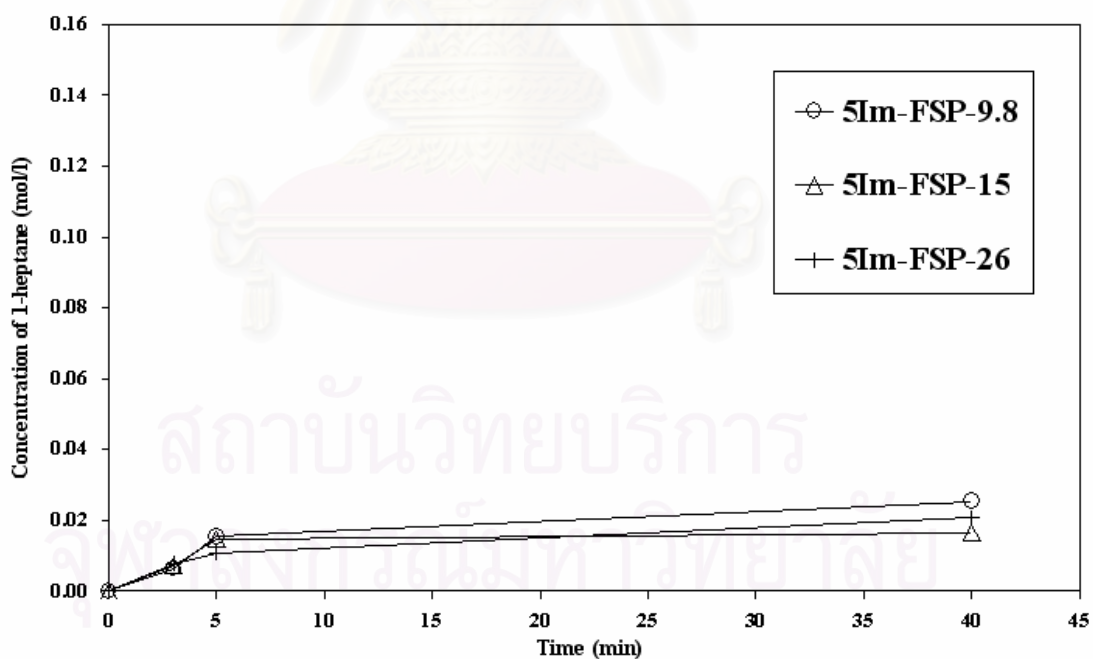


Figure 5.57 Time on stream with concentration of 1-heptane on 5 wt% Pd/TiO₂ catalysts prepared by incipient wetness impregnation with flame-made TiO₂ supports average crystallite sizes of 9.8, 15, and 26 nm

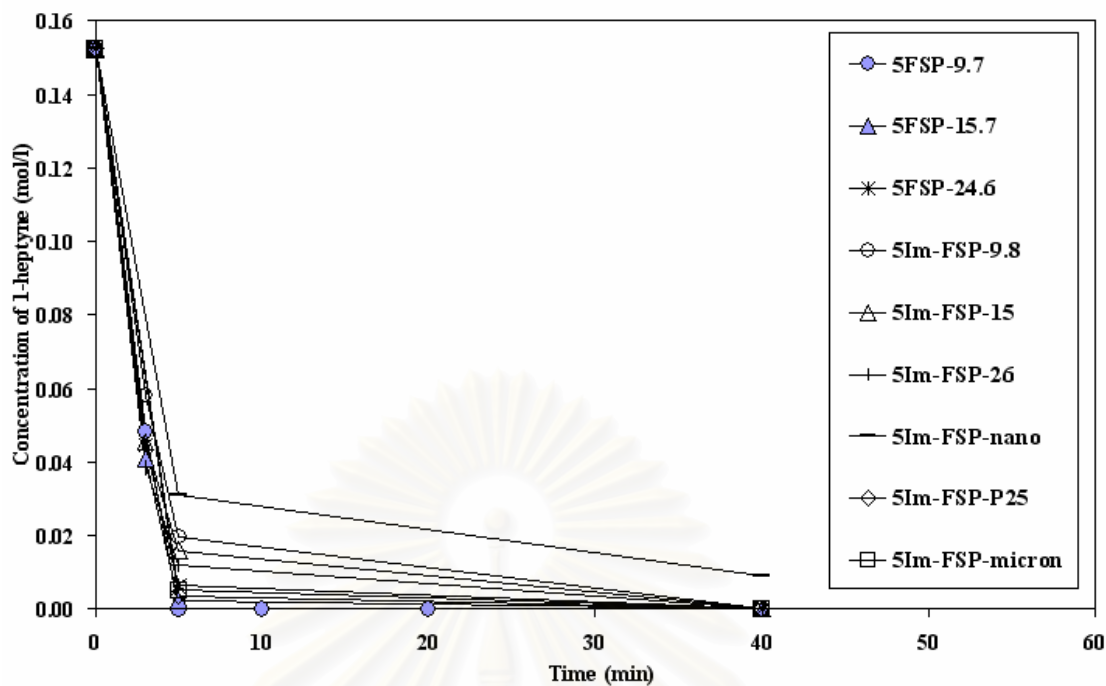


Figure 5.58 Time on stream with concentration of 1-heptyne on various crystallite size TiO_2 of flame-made and impregnated catalysts

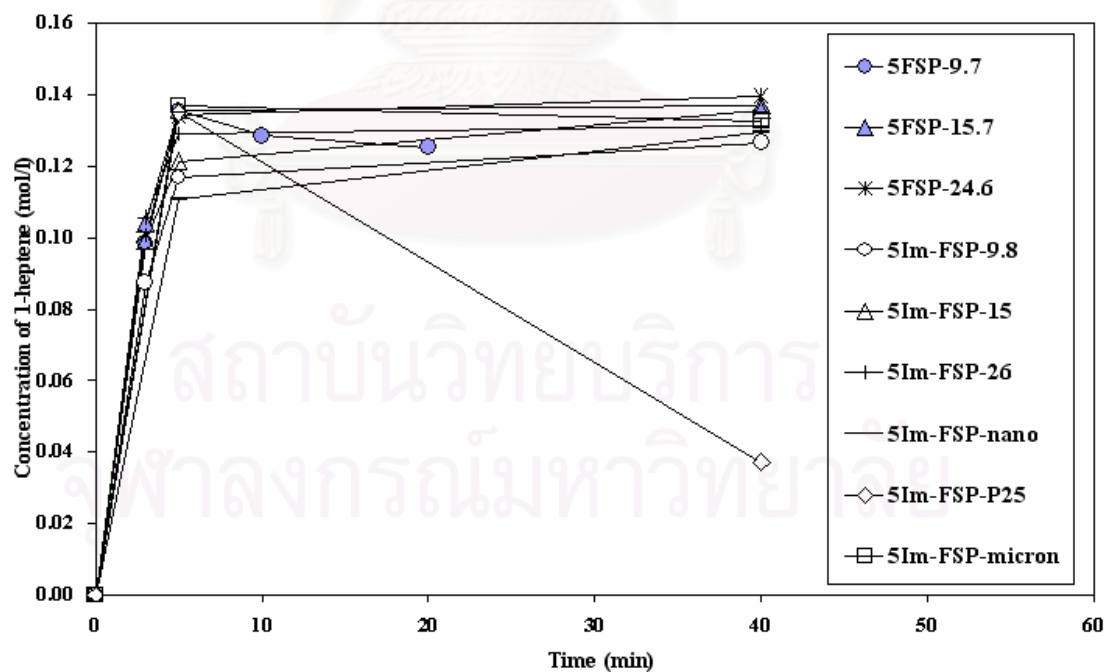


Figure 5.59 Time on stream with concentration of 1-heptene on various crystallite size TiO_2 of flame-made and impregnated catalysts

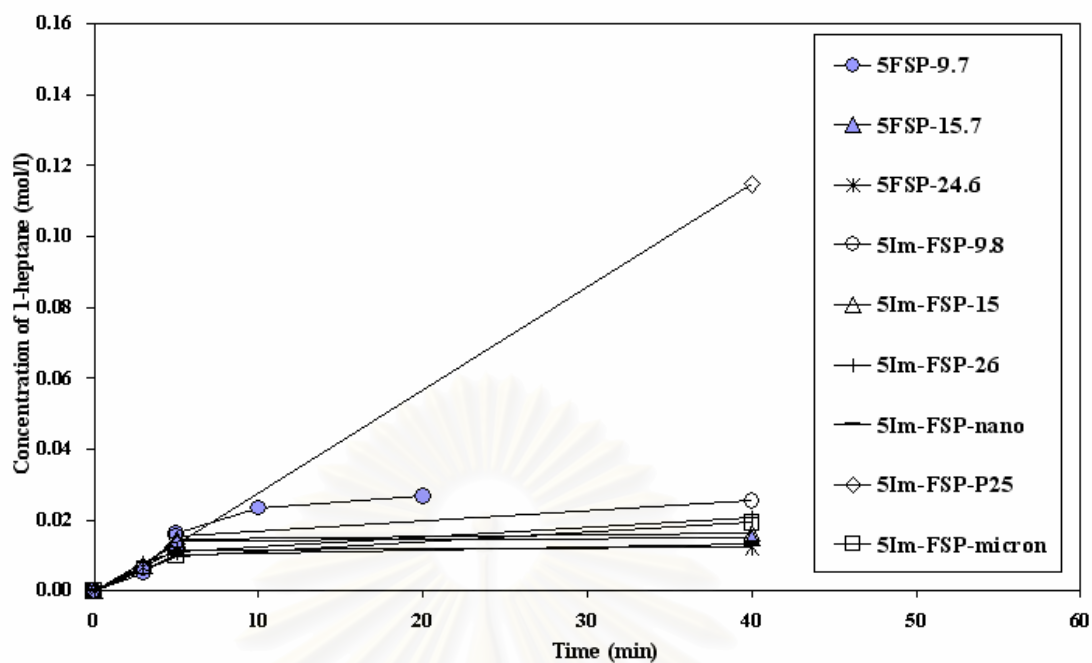


Figure 5.60 Time on stream with concentration of 1-heptane on various crystallite size TiO_2 of flame-made and impregnated catalysts

CHAPTER VI

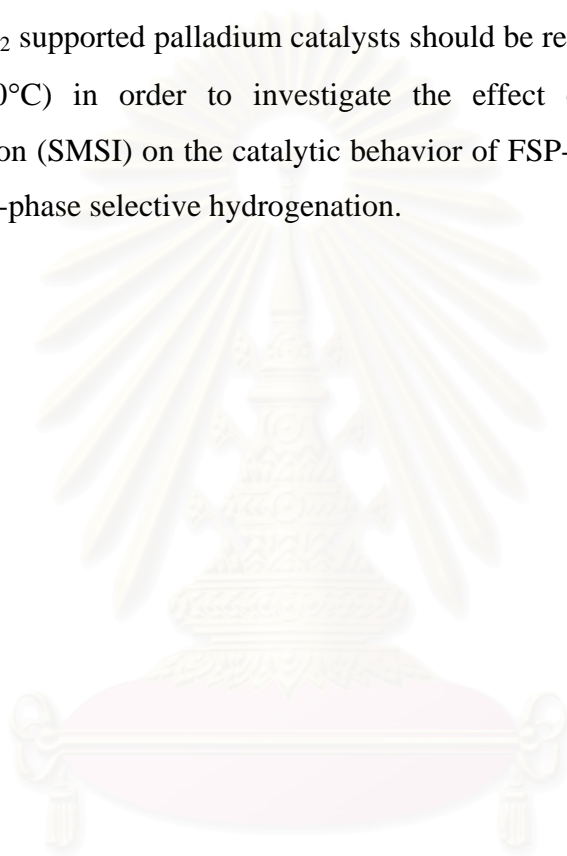
CONCLUSIONS AND RECOMMENDATIONS

6.1 Conclusions

1. The single-step flame spray pyrolysis has been successfully employed for synthesis of Pd nanoparticles with average crystallite size of 1 to 3.5 nm on TiO₂ supports. The flame spray technique has also been applied to produce Pd/TiO₂ catalysts with TiO₂ crystallite size of 9.8 to 26 nm.
2. Addition of Pd during one-step flame spray synthesis of Pd/TiO₂ catalysts results in smaller crystallite size of TiO₂ and higher amount of %rutile phase in the TiO₂ especially at 10 wt% Pd loading.
3. Based on CO chemisorption and XPS results, Pd/TiO₂ synthesized single-step FSP technique had much lower Pd dispersion (lower amount of Pd on surface) compared to those prepared by conventional impregnation method. However, for a similar Pd loading, the FSP-derived Pd/TiO₂ catalysts exhibited higher TOF than the impregnated ones for 1-heptyne hydrogenation with no difference in 1-heptene selectivity.
4. The TOFs of FSP catalysts decreased from 66 to 15 s⁻¹ when Pd loading increased from 0.5-10 wt% suggesting the dependence of specific hydrogenation activity on Pd particle size.
5. When TiO₂ crystallite size increased from 9.7 to 24.6 nm, the TOFs of FSP-Pd/TiO₂ catalysts decreased from 102-23 s⁻¹. There was no such effect for the impregnated catalysts and the catalysts prepared on commercial TiO₂; the TOFs of those catalysts were 6-12 s⁻¹.
6. It is suggested that the use of one-step flame spray pyrolysis synthesis caused modification of catalytic properties of Pd/TiO₂ catalysts in which their specific activities (TOF) were enhanced especially for the catalysts with low Pd loading and small TiO₂ crystallite size.

6.2 Recommendations

1. Additional crystallite sizes of TiO_2 synthesized by flame-spray method should be prepared in order to confirm the effect of TiO_2 crystallite size on the properties of Pd/TiO_2 catalysts.
2. The TiO_2 supported palladium catalysts should be reduced at high temperature (300-500°C) in order to investigate the effect of strong metal support interaction (SMSI) on the catalytic behavior of FSP-derived Pd/TiO_2 catalysts in liquid-phase selective hydrogenation.



สถาบันวิทยบริการ
จุฬาลงกรณ์มหาวิทยาลัย

REFERENCES

- [1] A.I.Y. Tok, F.Y.C. Boey, and X.L. Zhao Novel synthesis of Al₂O₃ nanoparticles by flame spray pyrolysis *J. Mater. Processing Technol.* (2006): 270-273.
- [2] R. Strobel, F. Krumeich, W.J. Stark, S.E. Pratsinis, and A. Baiker Flame spray synthesis of Pd/Al₂O₃ catalysts and their behavior in enantioselective hydrogenation *J. Catal.* 222 (2004): 307-314.
- [3] H.D. Jang, H. Chang, Y. Suh, and K. Okuyama Synthesis of SiO₂ nanoparticles from sprayed droplets of tetraethylorthosilicate by the flame spray pyrolysis *Curr. App. Phys.* (2006): 110-113.
- [4] R. Strobel, W.J. Stark, L. Madler, S.E. Pratsinis, and A. Baiker Flame-made platinum/alumina: structural properties and catalytic behaviour in enantioselective hydrogenation *J. Catal.* 213 (2003): 296-304.
- [5] M. Piacentini, R. Strobel, M. Maciejewski, S. E. Pratsinis, and A. Baiker, Flame-made Pt–Ba/Al₂O₃ catalysts: Structural properties and behavior in lean-NO_x storage-reduction. *J. Catal.* 243 (2006): 43–56.
- [6] R. Strobel, F. Krumeich, S. E. Pratsinis, and A. Baiker, Flame-derived Pt/Ba/Ce_xZr_{1-x}O₂: Influence of support on thermal deterioration and behavior as NO_x storage-reduction catalysts. *J. Catal.* 243 (2006): 229- 238.
- [7] M. J. Height, S. E. Pratsinis, O. Mekasuwandumsong, and P. Praserthdam Ag-ZnO catalysts for UV-photodegradation of methylene blue *Appl. Catal. B* 63 (2006): 305.
- [8] S. Hannemann, J. D. Grunwaldt, P. Lienemann, D. Günther, F. Krumeich, S. E. Pratsinis and A. Baiker Combination of flame synthesis and high-throughput experimentation: The preparation of alumina-supported noble metal particles and their application in the partial oxidation of methane. *App. Catal. A: General*, 316 (2007): 226-239.

- [9] Y. Li, B. Xua, Y. Fan, N. Feng, A. Qiu, J. Miao, J. He, H. Yang and Y. Chen
The effect of titania polymorph on the strong metal-support interaction of Pd/TiO₂ catalysts and their application in the liquid phase selective hydrogenation of long chain alkadienes. *J. Mol. Catal. A: Chemical*, 216 (2004): 107-114.
- [10] L. Madler, H.K. Kammler, R. Mueller, and S.E. Pratsinis Controlled synthesis of nanostructured particles by flame spray pyrolysis *Aerosol Sci.* 33 (2002): 369-389.
- [11] A. Fujishima, K. Hashimoto and T. Watanabe TiO₂ photocatalysis: Fundamental and applications, 1 st ed. Tokyo: BKC, (1999).
- [12] R. Mueller, Z. Madler, and S.E. Pratsinis Nanoparticles synthesis at high production rates by flame spray pyrolysis *Chem. Eng. Sci.* 58 (2003): 1969-1976.
- [13] W. Y. Teoh, L. Mädler, D. Beydoun, S. E. Pratsinis and R. Amal Direct (one-step) synthesis of TiO₂ and Pt/TiO₂ nanoparticles for photocatalytic mineralisation of sucrose. *Chem. Eng. Sci.* 60 (2005): 5852-5861.
- [14] A. Teleki, S.E. Pratsinis, K. Kalyanasundaram and P.I. Gouma Sensing of organic vapors by flame-made TiO₂ nanoparticles. *Sen. Act. B.* 119 (2006): 683-690.
- [15] W. Y. Teoh, R. Amal, L. Mädler and S. E. Pratsinis Flame sprayed visible light-active Fe-TiO₂ for photomineralisation of oxalic acid. *Catal. Today*, 120 (2007): 203-213.
- [16] R. Jossen, M. C. Heine, S. E. Pratsinis, S. M. Augustine and M. K. Akhtar
Thermal stability and catalytic activity of flame-made silica–vanadia–tungsten oxide–titania. *App. Catal. B*, 69 (2007): 181-188.
- [17] L. Mädler, W. J. Stark, S. E. Pratsinis Flame-made ceria nanoparticles. *J. Mat. Research*, 17 (2002): 1356-1362.
- [18] H. D. Jang, C. M. Seong, Y. J. Suh, H. C. Kim, C. K. Lee, Synthesis of lithium-cobalt oxide nanoparticles by flame spray pyrolysis. *Aero. Sci. and Technology*, 38 (2004): 1027-1032.

- [19] T. Sahn, L. Mädler, A. Gurlo, N. Barsan, S. E. Pratsinis and U. Weimar, Flame spray synthesis of tin dioxide nanoparticles for gas sensing. *Sen. and Actual. B: Chemical*, 98 (2004): 148-153.
- [20] Y. J. Jang, C. Simer and T. Ohm, Comparison of zinc oxide nanoparticles and its nano-crystalline particles on the photocatalytic degradation of methylene blue. *Materials Research Bulletin*, 41 (2006): 67-77.
- [21] R. Strobel, S. E. Pratsinis, A. Baiker, Flame-made Pd/La₂O₃/Al₂O₃ nanoparticles: Thermal stability and catalytic behavior in methane combustion. *J. Materials Chemistry*, 15 (2005): 605-610.
- [22] B. Schimmoeller, H. Schulz, S. E. Pratsinis, A. Bareiss, A. Reitzmann and B. Kraushaar-Czarnetzki, Ceramic foams directly-coated with flame-made V₂O₅/TiO₂ for synthesis of phthalic anhydride. *J. Cat.* 243 (2006): 82-92.
- [23] J. H. Kang, E. W. Shin, W. J. Kim, J. D. Park, and S. H. Moon, *J. Catal.*, 208 (2002): 310-320.
- [24] L. Nakkararuang, J. Panpranot, B. Ngamsom and P. Praserthdam, *Catal. Letter* (2005), *in press*.
- [25] A., P., Pietsch, J., and P., S. F., Poisoning and deactivation of palladium catalysts. *J. Mol. Catal. A*, 173 (2001): 275-286.
- [26] W. J. Kim, J. H. Kang, I. Y. Ahn, and S. H. Moon, *J. Catal. A*. 226 (2004): 226- 229.
- [27] H. Chang, S. J. Kim, H. D. Jang, J. W. Choi., Synthetic routes for titania nanoparticles in the flame spray pyrolysis. *Colloids and Surfaces A: Physicochem.* 313–314 (2008): 282–287.
- [28] J. Panpranot, K. Phandinthong, P. Praserthdam, M. Hasegawa, S. Fujita, and M. Arai, A comparative study of liquid-phase hydrogenation on Pd/SiO₂ in organic solvents and under pressurized carbon dioxide: Activity change and metal leaching/sintering *J. Mol. Cat. A* 253 (2006): 20-24.
- [29] J. Liu, and N. K. Nag, Atomic Resolution Electron Spectroscopy Investigation of Supported Catalysts: Pd/TiO₂ and Pd-Ni/TiO₂ *Proceeding of the 18th North American Catalysis Society Meeting* (2003): 225.
- [30] S. Somboonthanakij, O. Mekasuwandumrong, J. Panpranot, T. Nimmanwudtipong, R. Strobel, S.E. Pratsinis, and P. Praserthdam.

Characteristics and catalytic properties of Pd/SiO₂ synthesized by one-step flame spray pyrolysis in liquid phase hydrogenation of 1-heptyne. *Catal. Letters* 119 (2007): 346-352.

- [31] C.D. Wagner, W.M. Riggs, L.E. Davis, and J.F. Moulder, in: G.E. Muilenberg (Ed.), *Handbook of X-ray Photoelectron Spectroscopy*, Perkin-Elmer Corporation, Eden Prairie, MN, 1978.
- [32] K. Kontapakdee, J. Panpranot, and P. Praserthdam. Effect of Ag addition on the properties of Pd–Ag/TiO₂ catalysts containing different TiO₂ crystalline phases. *Cat. Comm.* 8 (2007): 2166–2170.
- [33] P. Weerachawanasak, P. Praserthdam, M. Arai, and J. Panpranot Effect of Ag addition on the properties of Pd–Ag/TiO₂ catalysts containing different TiO₂ crystalline phases. *Cat. Comm.* 8 (2007): 2166–2170.
- [34] J. K. and P. S. Anatase-phase titania: preparation by embedding silica and photocatalytic activity for the decomposition of trichloroethylene. *J. of Photochemistry and Photobiology A: Chemistry*, 127 (1999): 117-122.



APPENDICES

สถาบันวิทยบริการ
จุฬาลงกรณ์มหาวิทยาลัย

APPENDIX A

CALCULATION FOR CATALYST PREPARATION

A.1 Flame Spray Pyrolysis Method

Preparation of 0 – 10 wt%Pd/TiO₂ catalysts by flame spray pyrolysis (FSP) are shown as follows:

- Reagent:
- Palladium acetylacetonate [Pd(acac)₂]
Molecular weight = 304.62 g
 - Titanium(IV)tert-butoxide (TNB, Ti[O(CH₂)₃CH₃]₄)
Molecular weight = 340.32 g
Density = 1.0 g/ml
 - Acetonitrile
 - Xylene

Example calculation for the preparation of 0.5FSP

Based on 100 g for catalyst used, the composition of the catalyst will be as follows:

$$\begin{aligned} \text{Pd} &= 0.5 \text{ g} \\ \text{TiO}_2 &= 100 - 0.5 = 99.5 \text{ g} \end{aligned}$$

For 6 g of catalyst

$$\begin{aligned} \text{Pd required} &= 6 \times \frac{0.5}{100} = 0.03 \text{ g} \\ \text{TiO}_2 \text{ required} &= 6 - 0.03 = 5.97 \text{ g} \end{aligned}$$

Pd 0.03 g was prepared from Pd(acac)₂ and molecular weight of Pd is 106.4 as TiO₂ 5.97 g was prepared from TNB and molecular weight of TiO₂ is 79.9.

$$\begin{aligned} \text{Pd(acac)}_2 \text{ required} &= \frac{\text{MW of Pd(acac)}_2 \times \text{Pd required}}{\text{MW of Pd}} \\ &= \frac{304.62 \times 0.03}{106.4} = 0.0859 \text{ g} \end{aligned}$$

$$\begin{aligned} \text{TNB required} &= \frac{\text{MW of TNB} \times \text{TiO}_2 \text{ required}}{\text{MW of TiO}_2 \times \text{Density of TNB}} \\ &= \frac{340.32 \times 5.97}{79.9 \times 1.0} = 25.45 \text{ ml} \end{aligned}$$

Pd(acac)₂ and TNB were dissolved in xylene/acetonitrile mixture (70/30 % v/v). The total concentration of metal was always 0.5 M.

$$\text{mol of Pd required} = \frac{0.03}{106.4} = 2.82 \times 10^{-4} \text{ mol}$$

$$\text{mol of TiO}_2 \text{ required} = \frac{5.97}{79.9} = 0.075 \text{ mol}$$

$$\text{So, volume of solution} = \frac{(2.82 \times 10^{-4} + 0.075) \times 1000}{0.5} = 150 \text{ ml}$$

For 200 ml of solution

$$\text{Solvent required} = 150 - 25.45 = 124.55 \text{ ml}$$

$$\text{Xylene required} = \frac{70}{100} \times 124.55 = 87.18 \text{ ml}$$

$$\text{Acetonitrile} = 124.55 - 87.18 = 37.37 \text{ ml}$$

A.2 Incipient Wetness Impregnation Method

Preparation of 1 – 5 wt%Pd/TiO₂ catalysts by impregnation method are shown as follows:

- Reagent:
- Palladium acetylacetonate [Pd(acac)₂]
Molecular weight = 304.62 g
 - Support: TiO₂ prepared by flame spray pyrolysis.
 - Acetonitrile.

Example calculation for the preparation of 1Im-FSP

Based on 100 g for catalyst used, the composition of the catalyst will be as follows:

$$\begin{aligned} \text{Pd} &= 1 \text{ g} \\ \text{TiO}_2 &= 100 - 1 = 99 \text{ g} \end{aligned}$$

For 0.5 g of catalyst

$$\begin{aligned} \text{Pd required} &= 0.5 \times \frac{1}{100} = 0.005 \text{ g} \\ \text{TiO}_2 \text{ required} &= 0.5 - 0.005 = 0.495 \text{ g} \end{aligned}$$

Pd 0.005 g was prepared from Pd(acac)₂ and molecular weight of Pd is 106.4.

$$\begin{aligned} \text{Pd(acac)}_2 \text{ required} &= \frac{\text{MW of Pd(acac)}_2 \times \text{Pd required}}{\text{MW of Pd}} \\ &= \frac{304.62 \times 0.005}{106.4} = 0.0143 \text{ g} \end{aligned}$$

สถาบันวิทยบริการ
จุฬาลงกรณ์มหาวิทยาลัย

APPENDIX B

CALCULATION FOR METAL ACTIVE SITES AND DISPERSION

Calculation of the metal active sites and metal dispersion of the catalyst, a stoichiometry of CO/Pd = 1, measured by CO adsorption is as follows:

Let the weight of catalyst used	=	W	g
Integral area of CO peak after adsorption	=	A	unit
Integral area of 75 μ l of standard CO peak	=	B	unit
Amounts of CO adsorbed on catalyst	=	B-A	unit
Volume of CO adsorbed on catalyst	=	$75 \times \frac{(B - A)}{B}$	μ l
Volume of 1 mole of CO at 30°C	=	24.86×10^6	μ l
Mole of CO adsorbed on catalyst	=	$\frac{75}{24.86 \times 10^6} \times \frac{(B - A)}{B}$	μ mole
Molecule of CO adsorbed on catalyst	=	$[1.61 \times 10^{-6}] \times [6.02 \times 10^{23}] \times \frac{(B - A)}{B}$	molecules
Metal active sites catalyst	=	$[9.68 \times 10^{17}] \times \frac{(B - A)}{B} \times \frac{1}{W}$	molecules of CO/g of catalyst
Molecules of Pd loaded	=	$[6.02 \times 10^{23}] \times \frac{[\% \text{ wt of Pd}]}{[\text{MW of Pd}]}$	molecules/g of catalyst
Metal dispersion (%)	=	$100 \times \frac{\text{moleculod of Pd from CO adsorption}}{\text{molecules of Pd loaded}}$	

APPENDIX C

CALIBRATION CURVES

This appendix showed the calibration curve for calculation of composition of reactant and products in 1-heptyne hydrogenation. The reactant is 1-heptyne and products are 1-heptene and n-heptane.

The flame ionization detector (FID), gas chromatography Shimadzu modal 14B was used for analyzing the concentration of 1-heptyne, 1-heptene and n-heptane by using GS-alumina column.

The GS-alumina column was used with a gas chromatography equipped with a flame ionization detector (FID), Shimadzu modal 14B, for analyzing the concentration of 1-heptyne, 1-heptene and n-heptane. Condition uses in GC are illustrated in Table C.1.

Mole of reagent in y-axis and area, which was reported by gas chromatography, in x-axis is exhibited in the curves. The calibration curves of 1-heptyne and 1-heptene.

สถาบันวิทยบริการ
จุฬาลงกรณ์มหาวิทยาลัย

Table C.1 Conditions uses in Shimadzu modal GC-14B

Parameters	Conditions of Shimadzu GC-14B
Width	5
Slope	29
Drift	0
Min. area	20
T. DBL	2.7
Stop time	10
Atten.	0
Speed	2
Method	1
Format	1
SPL. WT	100
IS. WT	0

สถาบันวิทยบริการ
จุฬาลงกรณ์มหาวิทยาลัย

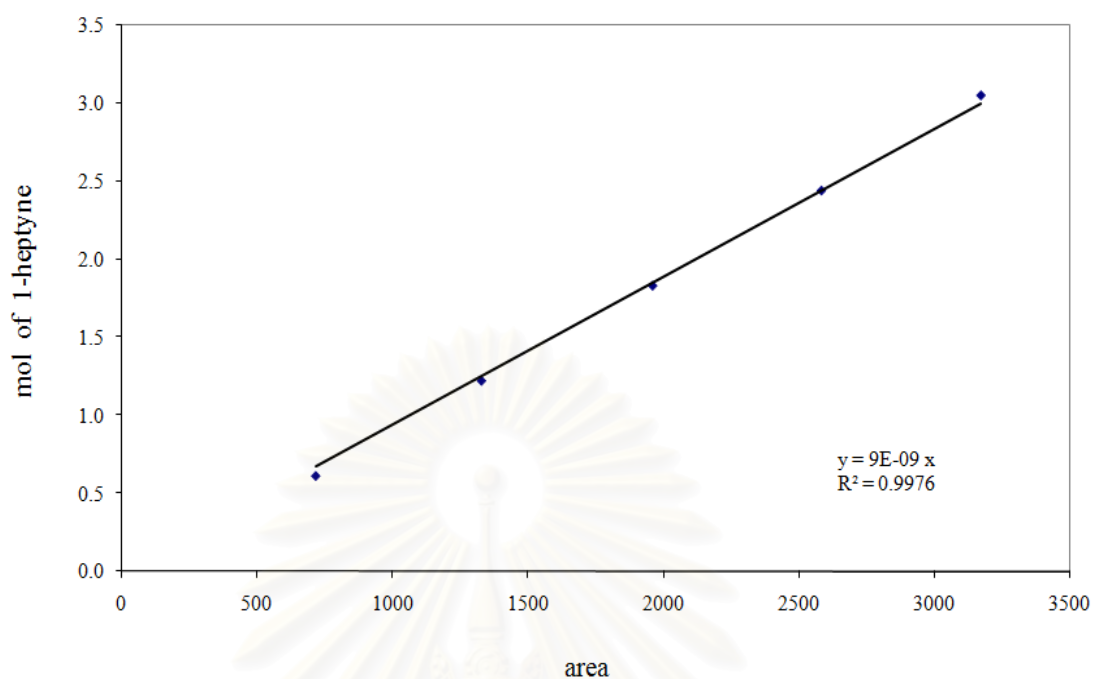


Figure C.1 The calibration curve of 1-heptyne

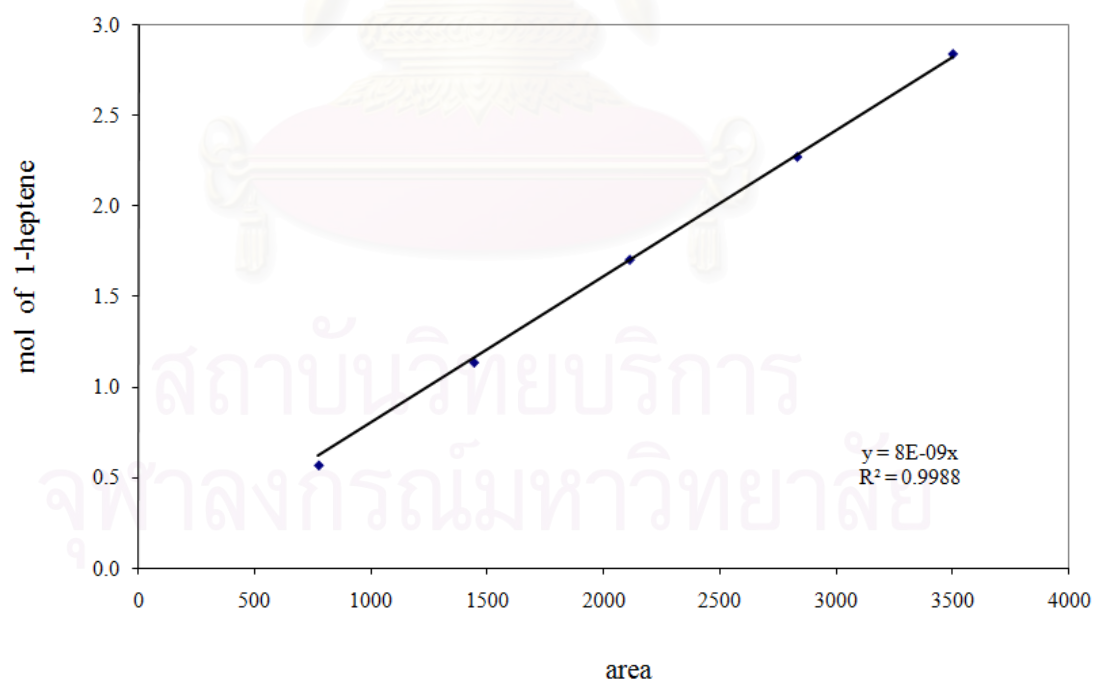


Figure C.2 The calibration curve of 1-heptene

APPENDIX D

CALCULATION OF 1-HEPTYNE CONVERSION AND 1-HEPTENE SELECTIVITY

The catalytic performance for the 1-heptyne hydrogenation was evaluated in terms of activity for 1-heptyne conversion and 1-heptene selectivity.

Activity of the catalyst performed in term of 1-heptyne conversion. 1-Heptyne conversion is defined as moles of 1-heptyne converted with respect to 1-heptyne in feed:

$$\text{1-heptyne conversion (\%)} = 100 \times \frac{\text{mole of 1-heptyne in (feed - product)}}{\text{mole of 1-heptyne in feed}} \quad (\text{D.1})$$

Where mole of 1-heptyne can be measured employing the calibration curve of 1-heptyne in Figure C.1, Appendix C.

$$\text{Mole of 1-heptyne} = \left(\frac{\text{Area of 1-heptyne peak}}{\text{from integrator plot on GC-14B}} \right) \times (9 \times 10^{-9}) \quad (\text{D.2})$$

Selectivity of product is defined as mole of 1-heptene formed with respect to mole of 1-heptyne converted:

$$\text{1-heptene selectivity (\%)} = 100 \times \frac{\text{mole of 1-heptene formed}}{\text{mole of total product}} \quad (\text{D.3})$$

Where mole of 1-heptene can be measured employing the calibration curve of 1-heptene in Figure C.2, Appendix C.

$$\text{Mole of 1-heptene} = \left(\begin{array}{l} \text{Area of 1-heptene peak} \\ \text{from integrator plot on GC-14B} \end{array} \right) \times (8 \times 10^{-9}) \quad (\text{D.2})$$



สถาบันวิทยบริการ
จุฬาลงกรณ์มหาวิทยาลัย

APPENDIX E

CALCULATION OF RUTILE PHASE COMPOSITION

The amount of rutile phase was calculated using the area of the major anatase and rutile XRD peaks according to the method described by Jung, K.Y. et al., 1999 [34] as follows:

$$\% \text{Rutile} = \frac{1}{\left[\left(\frac{A}{R} \right) 0.884 + 1 \right]} \times 100$$

Where A and R are the peak areas for major anatase ($2\theta = 25^\circ$) and rutile phase ($2\theta = 28^\circ$), respectively.

สถาบันวิทยบริการ
จุฬาลงกรณ์มหาวิทยาลัย

APPENDIX F

CALCULATION OF TURNOVER OF FREQUENCY

Metal active site = y molecule/g catalysts

TOF = $\frac{\text{rate}}{\text{(number of active site)}}$

= $\frac{[\text{molecule substrate converted}]}{[\text{g cat.}][\text{min}]}$ $\frac{[\text{g cat.}]}{y [\text{active site}]}$ $\frac{[\text{min}]}{[\text{s}]}$

= $[\text{s}^{-1}]$

สถาบันวิทยบริการ
จุฬาลงกรณ์มหาวิทยาลัย

APPENDIX G

LIST OF PUBLICATION

1. Songphon Phothakwanpracha, Joongjai Panpranot, Okorn Mekasuwandumrong and Piyasan Praserthdam. Characteristics and Catalytic Properties of Nano-Pd/TiO₂ Catalyst Prepared by Flame Spray Pyrolysis. *Proceedings of the 17th Thailand Chemical Engineering and Applied Chemistry Conference*, Chiang Mai Thailand, Oct. 29 – 30, 2007.



สถาบันวิทยบริการ
จุฬาลงกรณ์มหาวิทยาลัย

VITA

Mr. Songphon Phothakwanpracha was born in January 9th, 1984 in Ratchburi, Thailand. He finished high school from Phothawattanasenee School, Ratchburi in 2002, and received bachelor's degree in the department of Chemical Engineering from Faculty of Engineering, King Mongkut's Institute of Technology Ladkrabang, Bangkok, Thailand in 2006.



สถาบันวิทยบริการ
จุฬาลงกรณ์มหาวิทยาลัย